Changes to the Host Cell Proteome Induced by Expression of Hepatitis C Virus NS3/4A Open Reading Frames

by

Aileen Patterson

A Thesis submitted to the Faculty of Graduate Studies of

The University of Manitoba

in partial fulfilment of the requirements of the degree of

MASTER OF SCIENCE

Department of Medical Microbiology and Infectious Disease

Faculty of Medicine

University of Manitoba

Winnipeg, Manitoba, Canada

Copyright © 2013 by Aileen Patterson

Abstract

Hepatitis C virus (HCV) infects an estimated 200,000 people in Canada, and is the leading cause of liver transplants in North America. Viral infection usually leads to chronic infection, and complications include liver fibrosis, steatosis and hepatocellular carcinoma (HCC). The HCV non-structural proteins 3 and 4A (NS3/4A), is a multifunctional protein complex with roles in RNA replication and polyprotein processing. Additionally, *in vitro*, the NS3 protease on its own has been shown to induce advanced cellular transformation, and tumour formation in nude mice. However, the mechanism by which transformation occurs remains unknown. The objective of this study was to determine if the naturally occurring NS3/4A protein complex, rather than the NS3 protease domain on its own, could also induce cellular transformation and to determine the changes that NS3/4A expression had on the host cell protein content. To address these questions, stable cell lines were constructed expressing either NS3/4A or green fluorescent protein (GFP) as a control. Through measuring cell growth, it was determined that NS3/4A could not induce the transformation phenotype observed previously with NS3, suggesting a less clear role for authentic NS3/4A in HCC development than has been previously suggested.

In addition, changes to the host cell proteome during NS3/4A expression were evaluated by quantitative proteomics using stable isotope labeling of amino acids in cell culture (SILAC) in quadruplicate with reverse labeling. In total, over 6000 proteins were identified (>70,000 peptides), 23 of which were differentially

regulated by NS3/4A expression ($p<0.05$). These proteins included prostaglandin reductase 1 (PTGR1) and peripherin (PRPH). Despite clear evidence for the presence of a functional NS3/4A proteinase activity, protein level changes identified by mass spectrometry were not able to be confirmed by western blot analysis. Several possibilities to account for these discrepancies were explored using PTGR1 as a model protein. This included assessing the quality of antibodies used, possible protein isoforms, in depth analysis of the peptides identified by mass spectrometry, and examination of transcript levels by real time reverse transcriptase PCR. These analyses were unable to confirm the mass spectrometry results and highlight caution when interpreting protein abundance changes solely by mass spectrometry or western blotting alone.

Acknowledgements

I would first like to thank my supervisor Mike for his continued advice and support throughout my graduate degree, both professionally and personally. You've inspired me every step of the way with your ability to remain enthusiastic when it felt like every experiment was going nowhere.

To my advisory committee members, Drs Blake Ball and Julia Rempel – Thank you for your guidance and for your time and effort put into my thesis.

To my lab mates Xiaojie and Taeyo – Thank you for always offering help in the lab when I needed it and providing me with a great deal moral support through the years.

To the distinguished ladies and notable gentlemen of Teddy Bob's – Thank you for a great three years and many more to come. You have become so much more to me than friends, I consider you all to be one big dysfunctional family that I feel so lucky to be a part of.

And lastly, to my parents – Thank you for your enormous amount of support throughout my entire university career and time away from home. I can always count on both of you to be there when I need you. I couldn't have done it without you both.

Table of Contents

List of Tables

List of Figures

1.0. Introduction

1.1. Hepatitis C virus

Approximately 3% of the world's population is infected with hepatitis C virus (HCV), with 3-4 million new cases occurring each year (1). Canada has an infection rate of 0.8% with about 250 000 individuals infected (2). More than 350 000 infected individuals die each year due to HCV-related disease (3). There are currently no vaccines and treatment options, while improving, are still interferon/ribavirin based and have varying efficacies depending on the host and viral genotype (4).

1.1.1. Transmission

HCV is a bloodborne pathogen first documented as a non-A, non-B viral hepatitis transmitted through blood transfusions and organ transplants until it was isolated in 1989 by Michael Houghton's group (5). Since then, blood donors have been actively screened for HCV infection, an intervention that has dramatically reduced the number of new infections in most developed countries. Currently, the most common modes of transmission is through needle sharing during intravenous drug use, needle-stick injuries in healthcare settings, and being born to a HCV positive mother (3).

1.1.2. Clinical Outcomes

Of those individuals that are newly infected with HCV, up to 80% go on to develop a chronic infection, while the remaining individuals develop an acute infection and are able to clear the infection without treatment (6). Chronic infection leads to development of liver cirrhosis in up to 20% of patients, and development of end-stage liver disease or hepatocellular carcinoma in up to 5% of patients (6). Chronic liver disease caused by HCV infection include; hepatitis (inflammation of the liver), fibrosis (scarring of the liver), and steatosis (fatty deposits in the liver) (7, 8). While, for the most part, these effects are reversible if treated early, end-stage liver disease due to cirrhosis or hepatocellular carcinoma can only be treated with a liver transplant (9). Chronic HCV infection is the leading cause of liver transplantation in North America, however, in most cases, the new organ will become re-infected within a few years (9, 10).

1.1.3. Treatments

Although there is currently no vaccine for HCV, several treatment options are available, although they are not equally effective for all genotypes of the virus and the development of viral resistance is a concern. Until recently, the only treatment for HCV infection was pegylated interferon-alpha and ribavirin. Interferon alpha induces interferon-stimulated genes, generating an antiviral state within the cell. Ribavirin's mode of action is less well understood. As a nucleoside analogue, it may block viral replication by incorporation into nascent viral RNA, or it may act as a mutagen causing higher mutation rates in the RNA virus viability

(11, 12). The combination of these two therapies results in a sustained virological response (SVR) in approximately 56% of patients, defined as no detectable HCV RNA 6 months following therapy termination (13, 14). Unfortunately, about a third of chronic HCV patients do not respond to therapy at all, and the remainder relapse (15). SVR depends on the viral genotype, of which there are 7 for HCV (16, 17). HCV genotype 1 is most common in North America (approximately 70% of patients) and has a SVR of 42-46%, compared with genotypes 2 and 3 which have SVRs of 76-80% (13, 14, 18). As a therapeutic option, interferon and ribavirin are expensive, side effects are poorly tolerated, and many patients present contraindications to its use (15). The inclusion of first generation protease inhibitors telaprevir and boceprevir within the treatment regimen is improving the SVR (19).

1.1.4. HCV Virology

HCV is an enveloped, positive sense, single-stranded RNA virus in the genus *Hepacivirus* of the family *Flaviviridae* (20). The 9.6kb genome consists of a single open reading frame (ORF) of about 3000 amino acids flanked by 5' and 3' untranslated regions (Figure 1) (21, 22). The 5' UTR contains an internal ribosome entry site (IRES) that allows for cap-independent translation (23). The single ORF is translated into a polyprotein that is further processed by cellular and viral proteases into at least 10 proteins (21). The structural proteins include core, which forms the nucleocapsid, and the two envelope glycoproteins E1 and E2 (24, 25). The non-structural proteins include the p7 ion channel, non-structural protein 2 (NS2), NS3, NS4A, NS4B, NS5A, and NS5B (26). The NS2

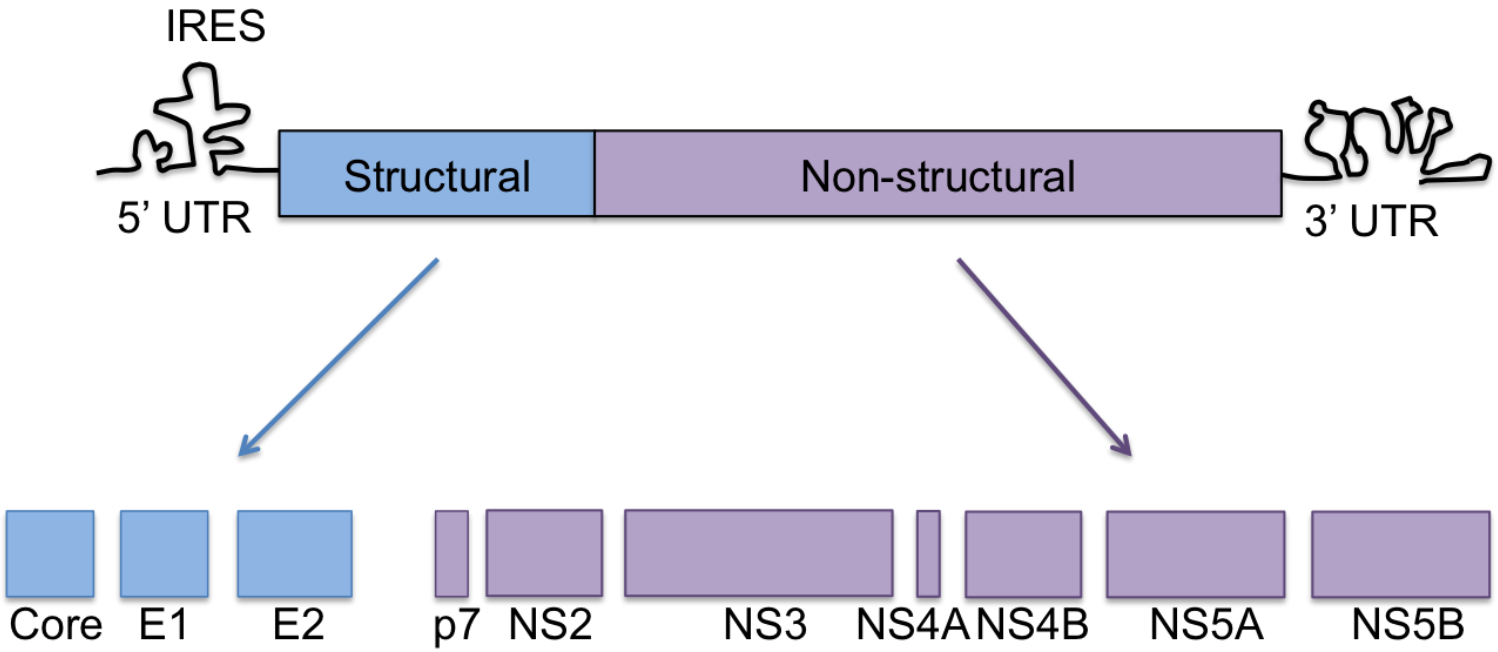

Figure 1. Hepatitis C virus genome. The 9.6kb single stranded, positive sense RNA genome is composed of 5' and 3' untranslated regions (UTR). The 5' UTR has an internal ribosome entry site (IRES) upstream of the open reading frame. The genome is translated as a single polyprotein which is proteolytically cleaved by host and viral proteases into structural proteins (Core, E1, and E2) and non-structural proteins (p7, NS2, NS3, NS4A, NS4B, NS5A, and NS5B). *Modified from Moradpour, D. et al. 2007. Nat. Rev. Microbiol.* ***5:****453- 463.*

protein, together with a portion of the NS3 protein, encode an autoprotease that cleaves NS2 from the rest of the non-structural polyprotein (the NS2/NS3 junction)(27). The NS3 protein contains a serine protease and an RNA helicase/NTPase essential for polyprotein processing and presumably RNA unwinding (28, 29). The NS4A protein serves as a protease co-factor for NS3 tethering the complex to the endoplasmic reticulum membrane (30). The NS4B protein is thought to induce the development of a “membranous web” within the cell, which serves as a site for HCV replication (31). NS5A is a phosphoprotein involved in viral replication and packaging, while NS5B is the RNA-dependant RNA polymerase (RdRp) (32, 33).

1.1.5. Life Cycle

The HCV life cycle is depicted in Figure 2. The receptors used by HCV to gain entry to the cell by receptor-mediated endocytosis have been intensively studied, and while only CD81 (34) and scavenger receptor class B type 1 (SR-B1) (35) have been shown to directly interact with E2, several other receptors appear to be involved. These include glycoamino glycans (GAGs) (36), low-density lipoprotein (LDL) receptor (37), claudin (38), and occludin (39). A current model suggests that HCV initially interacts with low affinity to GAGs and LDL receptors, placing them into proximity of CD81 and SR-B1 (22). Binding virions to the latter receptors localizes the virus to tight junctions where it can interact with claudin and occludin, allowing entry into the cell through endocytosis (22). Once the virus particle has been endocytosed by clathrin coated pits, the endosomes are acidified leading to fusion of the viral envelope to the endosomal membrane, and

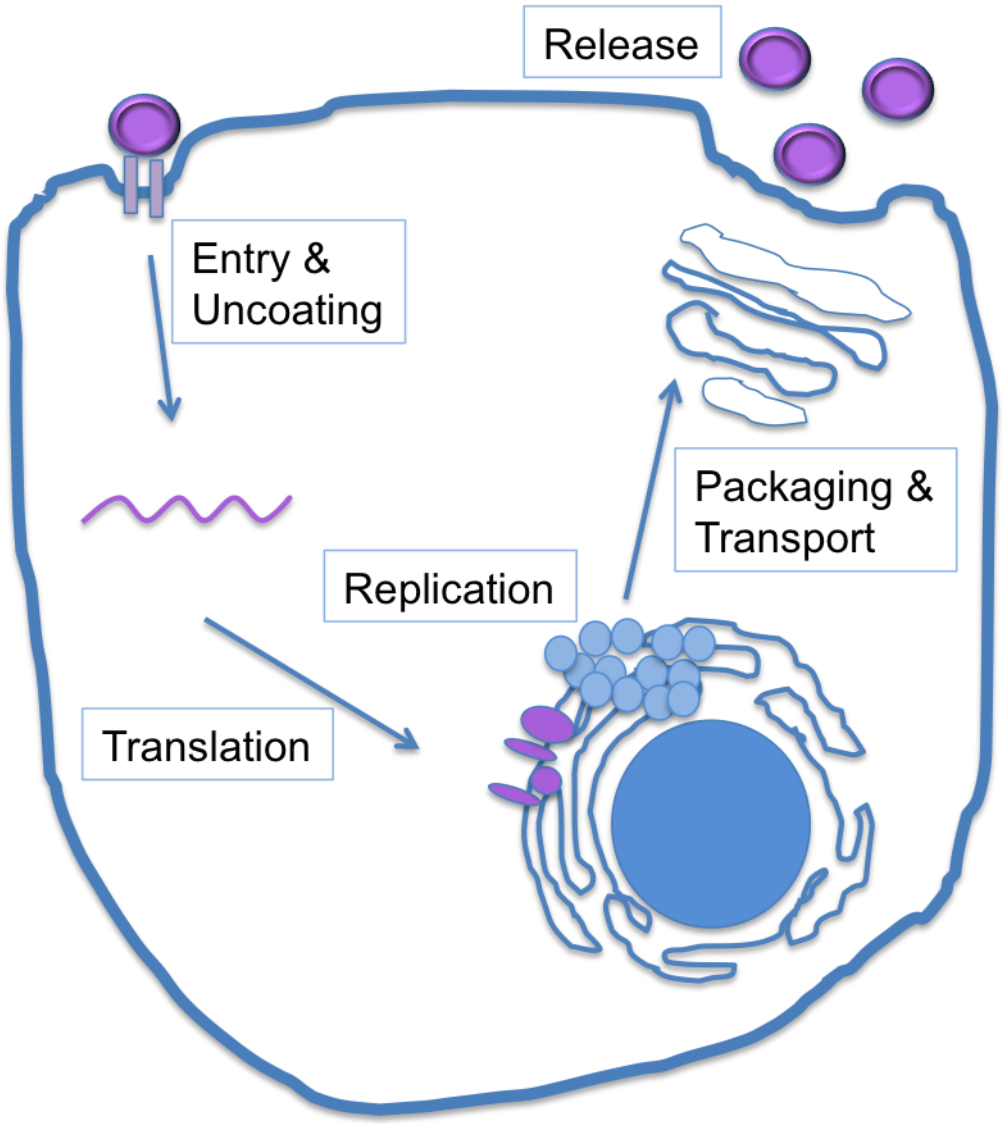

Figure 2. Generalized HCV life cycle. Viral entry into the cell occurs by receptor-mediated endocytosis, resulting in uncoating and release of the viral genome into the cytoplasm. The positive sense genome is translated on the endoplasmic reticulum (ER) as a polyprotein, which is then cleaved into individual proteins. Viral and host proteins generate replication complexes on a membranous web which serves as a site for negative and positive strand RNA synthesis. Viral RNA is packaged into viral nucleocapsids and released from the cell most likely through cellular lipid droplets. Modified from *Lindenbach BD and CM Rice. 2005. Nature. 436:933-938.*

release of the capsid into the cytosol (40, 41). The positive-sense RNA genome is translated via direct IRES interaction with host ribosomes and the polyprotein is cleaved by host and viral proteases into their individual components (42). RNA replication occurs on a specialized membranous web induced by the NS4B protein via reorganization of host intracellular membranes (43). The RNA genome is copied into a negative sense strand, which is then used as a template for synthesis of positive sense RNA. Although the mechanism is still poorly defined, HCV is known to utilize lipid droplet assembly and release as a means to release packaged infectious virus form the infected cell (44). There is also evidence supporting direct cell-to-cell virus transmission (45).

1.2. NS3/4A Viral Protein

1.2.1. Structure and Function

1.2.1.1. Helicase Domain

NS3 is an approximately 67kDa protein that serves multiple roles in the HCV life cycle. The N-terminal third harbours a protease, while the C-terminal two thirds contains an RNA helicase/nucleoside triphosphatase (NTPase). The helicase resembles a member of the superfamily 2 DExH/D-box helicases (46). Although the exact role for the helicase in the viral life cycle is unknown, it is essential for viral replication (47). dsRNA and dsDNA have been shown to be substrates for the NS3 helicase domain, however increased efficiency in RNA unwinding

required the full length NS3 proteins were assayed suggesting that the protease domain has some influence on this activity (48, 49).

There are currently two main models proposed for how the helicase unwinds RNA: the inchworm model and the Brownian ratchet model. The inchworm model proposes that the helicase moves down the strand of RNA at a rate of one nucleotide per ATP hydrolyzed through conformational changes which occur in the helicase domains upon ATP binding (46). Alternatively, the Brownian ratchet model suggests that the binding of ATP induces a conformational change in the helicase domain, which renders it less tightly bound to the RNA (50). As a result, Brownian motion, the random movement of particles, allows the helicase to slide down the RNA (50). Interestingly, the NS3 helicase can also use dsDNA, in addition to dsRNA, as a template. It is unclear whether this observation has any role in a natural infection.

While the protease and helicase domains are functionally independent of each other, full length NS3/4A has been found to bind RNA more tightly than with the helicase domain alone (51). This suggests that there is some interaction between the two domains, either through slight conformational changes, cellular protein recruitment, or an as yet undetermined mechanism.

1.2.1.2. Protease Domain

The N-terminal one third of the NS3 protein encodes a serine protease responsible for cleaving the viral non-structural proteins from the polyprotein (28,

52). The active site catalytic triad is composed of His57, Asp81, and Ser139 (53). A crystal structure for the protease domain indicates a chymotrypsin-like fold with two β-barrels stabilized by a zinc ion (53-55). The 54 amino acid NS4A protein binds the N-terminal region of NS3 and is required for proper folding of the protease domain and for tethering the protein complex to the membrane (55, 56). A consensus protease cleavage sequence has been determined: D/ExxxxC/T | S/Axxx (52). However, this sequence is not strict in its requirement since [1] many cellular proteins contain this consensus in their sequence but are not cleaved by NS3/4A, and [2] known cellular substrates of the NS3/4A protease do not strictly adhere to this sequence as each of MAVS, Trif, and TC-PTP cleavage sites differ in at least one of the required amino acids (57-59).

1.2.2. NS4A Cofactor and Localization

NS4A is a co-factor for the NS3 protease and is important for stabilizing the protease structure and increasing catalytic activity. To measure the protease activity of NS3, Failla et al used the NS5A-5B cleavage site as substrate in the presence or absence of NS4A (60). Only when NS4A was present was NS3 protease activity observed (60). Similar results were found using the NS4B-5A junction as a substrate (61). The N-terminal 21 residues of NS4A are mainly hydrophobic, forming a transmembrane α-helix, which tethers the protein to cellular ER membranes (30). NS3 has also been shown to localize to the mitochondrial membrane in chronic HCV infected patients (62) and in HCV replicon expressing cells (63). Recently, NS3/4A was found to localize even more specifically to the mitochondrial associated membrane (MAM) (64). While

NS3/4A is known to be a cytoplasmic protein, it has been reported that NS3 can localize to the nucleus, and that a putative nuclear localization signal in the N-terminus of NS3 was found through bioinformatics analysis (65). Co-expression of NS4A inhibited NS3 nuclear localization (65).

1.3. NS3/4A Host Interactions

1.3.1. Innate Immunity

Human cells have developed pathways to recognize pathogens and respond to infection; however, HCV has evolved means to persist as a chronic infection. In a typical virus infection, pathogen associated molecular patterns (PAMPs) such as dsRNA, which occur during viral replication, are recognized by the cell via pattern recognition receptors (PRRs) (66). There are two main cellular innate antiviral immune pathways that induce an interferon response: the retinoic acid-inducible gene I (RIG-I) pathway and the Toll-like receptor 3 pathway (Figure 3) (67, 68). RIG-I is a cytosolic protein that binds dsRNA. Upon substrate interaction, RIG-I activates the mitochondrial antiviral signaling (MAVS) protein, also known as IPS-1, VISA, and Cardif. MAVS is located on the mitochondrial membrane and, through a series of signaling molecules, phosphorylates and thus activates the interferon regulatory transcription factor 3 and 7 (IRF3/7), or nuclear factor kappa-light-chain-enhancer of activated B cells (NF-κB)(67). The TLR3 pathway can also recognize dsRNA, however, it is located on the endosomal membrane and senses extracellular dsRNA (68). Once the dsRNA is recognized, it activates

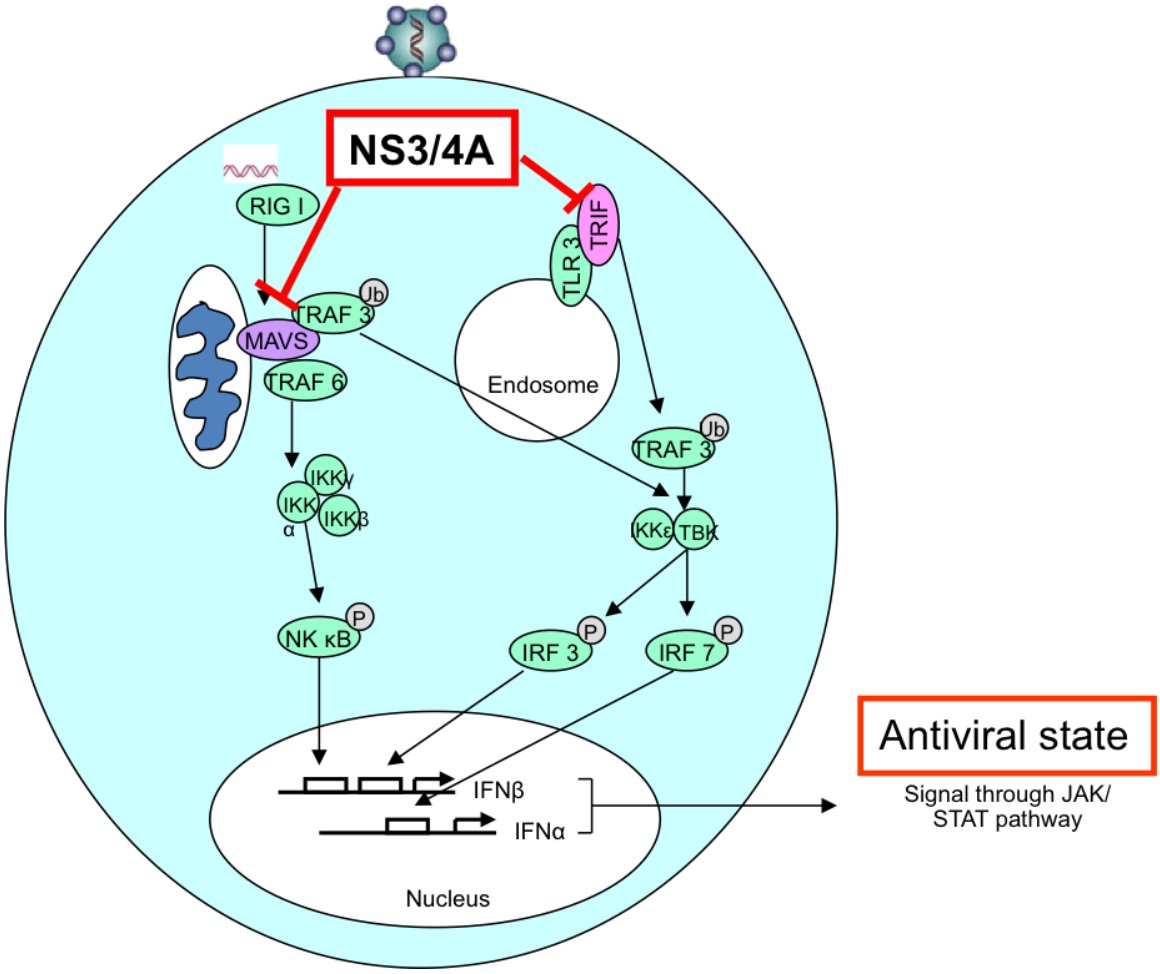

Figure 3. Innate immune signaling pathways associated with HCV NS3/4A. Upon infection of a cell, the innate immune signaling molecules RIG I and TLR3 detect dsRNA and initiate a signaling cascade that ultimately results in interferon production. The resulting interferon is able to stimulate surrounding cells, as well as the producing cell, to induce an antiviral state through the JAK/STAT pathway. NS3/4A is able to cleave both MAVS and Trif, downstream signaling molecules of RIG I and TLR3 respectively, thus inhibiting interferon production. *Modified from Joyce MA and DLJ Tyrrell. 2010. Microbes and Infect. 12:263-271.*

the adaptor molecule Toll-IL-1 receptor domain-containing adaptor inducing interferon beta (Trif) to phosphorylate and activate the IRFs (68). Activation of these pathways leads to the transcription of interferon α and β, which are secreted and serve to stimulate the producing cell and to activate adjacent cells. Interferon receptor binding activates the Janus kinase-signal transducer and activator of transcription (Jak-STAT) pathway to induce interferon-stimulated genes (ISGs), leading to an antiviral state in the cell (22).

1.3.1.1. Trif Substrate

Since over 75% of HCV infected patients go on to develop a chronic infection, it was hypothesized that the endogenous interferon signaling pathways must be affected by the virus. When NS3/4A was expressed in cells, IRF3 phosphorylation was suppressed and nuclear localization was reduced (69). This was not the result when NS3 or NS4A were expressed individually, or when the active site of NS3 was mutated or blocked, implicating protease activity as the important factor in IRF3 inactivation (69). In 2005 Li et al. demonstrated that the adaptor protein for TLR3, Trif, was enzymatically cleaved by the NS3/4A protease, suppressing its ability to further transduce the TLR signal (58).

1.3.1.2. MAVS Substrate

While the discovery of Trif cleavage certainly contributes to the dampening of the immune system, it could not be the only target as RIG-I signaling is a somewhat redundant pathway to stimulate IRF3. Moreover, it seemed more likely that the viral dsRNA would be detected in the cytosol and not in an extracellular space as

this is where viral replication occurs. It was subsequently determined that the RIG-I adaptor protein, MAVS, was also cleaved by the NS3/4A protease (57). Cleavage occurs at Cys-508, which releases the protein from the mitochondrial membrane into the cytosol where it is no longer in proximity to the rest of the signaling molecules (57). This also strongly suggests that cellular localization is an important aspect of NS3/4A function.

While MAVS cleavage by NS34A provides insight as to how the innate immune response is dampened by HCV infection, it may not be the sole reason for viral persistence. In one study, 129 liver biopsies from chronic HCV patients were analyzed and only 48% exhibited cleaved MAVS (controlled against 39 liver biopsies from non-HCV liver disease)(70). As well, strong interferon responses were detected in many patients along with a large variation in ISG expression. It was shown that if there was a strong interferon response in chronic HCV patients prior to interferon therapy (presumably due to lack of cleaved MAVS), therapy outcomes were poor, while a weak interferon response correlated with a good response to therapy (70). This suggests that MAVS cleavage is not the only determinant to the development of a chronic HCV infection.

1.3.2. Oncogenesis via Inflammation

As well as dampening the immune system, HCV is associated with liver cancer. Up to 5% of chronically infected HCV patients develop hepatocellular carcinoma, and approximately 25% of HCC cases are caused by HCV, globally (71). While some DNA viruses have been linked to cancer, how a ssRNA virus that

replicates in the cytoplasm is able to cause this remains unknown (72). There are at least two prominent explanations that may explain this: indirectly via inflammation of the liver, or directly whereby HCV proteins play a more specific role.

The inflammation model suggests that proinflammatory cells are recruited to the liver when the innate immune system is triggered, and if the infection cannot be effectively cleared, chronic inflammation leads to damage to neighboring tissues, possibly through oxidative stress (73). HCV, and several of its structural and non-structural proteins expressed individually, have been shown to increase reactive oxygen species (ROS) in infected cells (74). Interestingly, NS3 has been shown to activate Nox2, a membrane protein of liver macrophages (Kuppfer cells). Nox2 increases lead to ROS production that targets neighboring cells to undergo oxidative stress (75, 76). As well, a potent antioxidant, glutathione, is produced predominantly in the liver therefore liver damage caused by HCV may result in reduced production thus also contributing to oxidative stress (74). Oxidative stress also stimulates the production of TGF-β and collagen in the liver, which eventually leads to fibrosis (77). Therefore, the body's response to HCV infection may be detrimental to the liver.

1.3.3. Oncogenesis via NS3/4A

There may also be direct interactions between viral proteins and cellular proteins that deregulate signalling pathways involved in cellular growth and repair leading to liver cancer. It was shown that HCV core and NS3 proteins induced cellular

transformation when expressed individually in cells (78, 79). While both proteins are linked to cellular transformation, NS3 appeared to induce advanced cellular transformation more quickly compared to core (79). Regulation of p53 was suggested as the source of this difference, whereby NS3 repressed p53 and core activated p53 transactivation as measured by a luciferase reporter assay.

Sakamuro et al. transfected a non-tumorigenic murine fibroblast cell line, NIH 3T3, with the protease and helicase domains of NS3 separately to determine which region was involved in cellular transformation (80). The doubling time of cells transfected with the protease domain had a decreased doubling time (11.3-12.7h) compared to those transfected with the helicase domain (19.7-21.1h) or the NIH 3T3 cells alone (21.2h), meaning the protease domain was required for increased cell growth (80). As well, cells with the NS3 protease domain were able to grow on soft agar, indicating they had lost anchorage independent growth, one of the hallmarks of cancerous cells. Subcutaneous infection of BALB/c nude mice with cells expressing either the protease or helicase domain demonstrated that 100% (5/5) of the mice transfected with the NS3 protease domain developed tumours, while 20% (1/5) of the mice transfected with the helicase domain developed a tumour (80). Additionally, the tumour in this helicase domain transfected mouse was of a smaller size. This data suggested that the protease domain was sufficient for cellular transformation and tumour development, at least in mice.

Similarly, Zemel et al revisited this phenomenon, but instead used a different cell line. Non-tumourigenic rat fibroblasts (RF) transfected with the NS3 protease or helicase domains demonstrated that, similar to the results seen in mouse fibroblasts, the protease domain alone was solely responsible for an increased growth rate, anchorage independent growth, and the ability to grow under limited growth factors supplemented in the media (81). Additional experiments using the serine protease inhibitor TPCK disabled the transforming abilities of NS3 (81).

The transformation phenotype imparted by NS3 was also seen in a human cell line QSG7701 which are liver cells taken from tissue 6 cm from hepatocarcinoma cells (82). In these studies NS3 expression shortened cell doubling time, allowed anchorage independent growth, and produced tumours when these cells were injected in nude mice (82). These results demonstrate that advanced cellular transformation was not restricted to rodent cells and may be relevant in human cancer development.

1.3.3.1. NS3 Internal Cleavage

Most of the above studies detailed above were performed by expressing only the NS3 protease domain, but the relevance of these observations that did not use NS3 as a full-length form or when expressed without the NS4A cofactor is unclear. During expression of the full length NS3 open reading frame, Shoji et al demonstrated that antibodies directed to NS3 detected two bands: one at 72kDa, which represented the full length NS3, as well as one at 49kDa (83). Site directed mutagenesis determined that the NS3 protein was being cut in the helicase

domain (83). In contrast, another study showed that NS4A was required for NS3 internal cleavage and that the products were 44 and 41kDa (the 49kDa fragment could not be detected) (84). The 44kDa product was able to grow 2 fold more colonies on soft agar than NS3 alone (84). As well, mutation of the serines in the protease catalytic triad abolished cleavage products, indicating again that protease activity was involved (84). Even though the two studies showed different internal NS3 cleavage sites, all were located in the helicase domain (83, 84). Whether disrupting the helicase function is beneficial for the virus, perhaps by allowing less productive viral replication leading to a chronic infection, is unclear. It should still be pointed out that these studies were performed in the absence of other viral proteins or viral replication and therefore further studies are required to determine the importance in an authentic viral infection.

1.3.3.2. NS3–Host Protein Interactions

Since p53 plays a major role in cell growth regulation and can direct the cell to survive or die through apoptosis, studies determining if NS3 affected p53 expression or activity were conducted. Ishido et al found that p53 co-immunoprecipitated with NS3, in the presence or absence of NS4A, and that the protease domain was involved in this complex formation (85). It was also shown that the NS3-p53 complex lead to increased cell growth through transcriptional repression of the cyclin dependent kinase (CDK) inhibitor $p21^{WAF1}$, a transcriptionally activated target of p53 (86).

Several other proteins have also been found to interact with NS3. Through an interaction in the helicase domain of NS3, it was found that protein kinase A (PKA) was no longer able to translocate to the nucleus, inhibiting its function in carbohydrate and lipid metabolism (87). At the same time, NS3 was found to be a substrate for protein kinase C (PKC) which acted as a competitive substrate for PKC thereby inhibiting its ability to serve as a signal transducer for many pathways, including the immune response and cell growth (88). As well, the helicase domain of NS3 was found to interact with histones H2B and H4 and was suggested to disrupt their function by masking the DNA binding site of the histones and preventing nucleosome formation (89).

1.3.3.3. Additional NS34/A Protease Substrates

Besides Trif and MAVS, NS3 protease activity has also been shown to target additional host proteins. In 2009, Brenndorfer et al. determined that HCV altered the epidermal growth factor (EGF) signalling pathway T cell protein tyrosine phosphatase (TC-PTP) such that protein levels, but not mRNA levels, were decreased (59). They found that the NS3/4A protease cleaves TC-PTP at two sites (59). They suggested that down regulating TC-PTP can leave the EGF receptor in a constitutively active phosphorylated (active) state, signalling continued cell growth (59).

Recently, another NS3/4A protease substrate was identified, the DNA damage-binding protein 1 (DDB1) (90). DDB1 is a major subunit of the Cullin 4 (Cul4)-DDB1 ubiquitin ligase complex that functions to recruit substrate for ubiquitination

(91). Targets of the complex include proteins involved in DNA repair, replication, and transcription (91). Upon NS3/4A expression, DDB1 was found to be cleaved, however when the protease was mutated or a protease inhibitor was used, DDB1 was no longer affected. Furthermore, DDB1 cleavage seemed to be important for HCV replication since overexpression of a non-cleavable mutant inhibited viral replication (90). Interestingly, work previous to this demonstrated that the loss of DDB1 in mouse hepatocytes led to liver tumour development (92). Therefore, cleavage of DDB1 by NS3/4A may aid in replication of the virus, and increase the potential for HCC.

Through quantitative proteomics, glutathione peroxidase 8 (GPx8) was also found to be a substrate for the NS3/4A protease (93). Cleaved GPx8 was also found in liver biopsies of chronic HCV patients, and was determined to be involved in viral particle formation (93). GPx8 is a membrane bound protein that may be involved in sequestering harmful hydrogen peroxide that is thought to be produced through disufide bond formation (94). While the function of cleaved GPx8 has not yet been determined, reduced activity of this protein may provide another link to the increase in oxidative stress observed upon HCV infection, and thus development of hepatocellular carcinoma.

1.4. Studying Host Genomic/Proteomic Changes

The effects of NS3/4A on a host cell can provide invaluable insight into how this viral protein is able to cause pathogenesis or assist the virus in its replication

program. Looking at these changes one target at a time is time consuming and deciding which target to study is often impractical. Therefore, studying these effects at a global genomic or proteomic level is favoured. Genomic microarray studies on HCV infection or following HCV open reading frame expression has been performed and the data suggests many affected cellular pathways. Core biopsy samples of cirrhotic livers from chronic HCV patients were compared to non-diseased liver samples to discover marker(s) of liver disease progression by microarray analysis (95). Approximately 1% of gene targets (132/13600) were found to be deregulated and were involved in pathways such as interferon response and the anti-apoptotic pathway. Many other studies looking at the cellular gene transcription profile upon HCV infection have found an increase in protein targets involved in proapoptotic and proinflammatory responses, and a decrease in protein targets involved in the antioxidant response (96-100).

While the genome is the blueprint for cellular activities, the proteins that are encoded by these genes are the predominant effectors in the cell. Moreover, results at the mRNA level are not necessarily representative of what happens at the protein level. In fact, current studies suggest a poor correlation between gene and protein quantitation. Studies in human liver and lung cancer (101, 102) as well as in the yeast *Saccharomyces cervisiae* (103) suggest less than a 50% correlation between mRNA levels seen by microarray and mass spectrometry-based analysis. This is not surprising, however, since there are [1] many post-transcriptional processes that occur including alternative splicing, small

interfering RNAs (siRNAs), and micro RNAs (miRNA), and [2] varying half-lives for proteins and mRNAs. As well, transcriptional data cannot provide functional information about the protein, such as post-translational modifications or subcellular localization. Therefore, changes that occur at the transcriptional level are not always indicative of the functional changes in the cell, and a proteomic approach of identifying NS34A effects in the cell could provide valuable functional information.

1.4.1. Global Proteomic Profiling

Several methods are available to study protein abundance changes in a cell population including western blot analysis, enzyme-linked immunosorbent assays (ELISAs), antibody arrays, and mass spectrometry. While most of these approaches require known and validated antibodies, mass spectrometry (MS) allows high throughput identification of thousands of peptides without specific detection reagents (104).

There are two main approaches to mass spectrometry, the bottom-up approach in which proteins are identified based on which peptides are seen by the mass spectrometer, and the top-down approach that analyzes intact proteins. Currently, top down methods are limited because of the limited mass ranges and the general requirement for less complicated samples (ie. less protein). As such, this approach is limited to samples of purified proteins or those that contain very simple protein mixtures. The most common utilization of mass spectrometry is a bottom up approach where information about the identified proteins is made

based on their peptide constituents (Figure 4A). Here, cellular proteins are digested into peptides by site-specific proteases, most commonly trypsin (105). Following digestion, peptides are ionized and injected into a mass spectrometer where the corresponding mass to charge (m/z) ratio is measured for each peptide sampled over a predetermined mass window (105). Each MS peak represents an individual peptide from the original mixture. To obtain more specific information about each of these MS1 peptide peaks, data dependent acquisition methods select and isolate sequentially the most abundant peptides (those with a high MS peak intensity) for limited fragmentation (105). Fragmentation occurs in a limited and random fashion along the peptide backbone yielding spectra mostly comprised of a specific pattern of ions (typically y and/or b). The resulting spacing associated with the MS/MS spectral peaks corresponds to amino acid molecular weights and can be used to identify the peptide sequence by comparing the fragmentation pattern to an *in silico* database of digested proteins using statistical analysis (105).

1.4.2. Quantitative Proteomics

There are two main relative quantification methods following identification, label-free and label-based approaches. The label-free method allows for peptides between different experimental MS runs to be compared by their m/z ratio and peak intensities (106). However, this method can be sensitive to experimental bias as a lack of multiplexing leads to differences between each sample run not necessarily due to different experimental conditions. Label based methods circumvent this by labeling the peptides with various isotopic affinity tags such

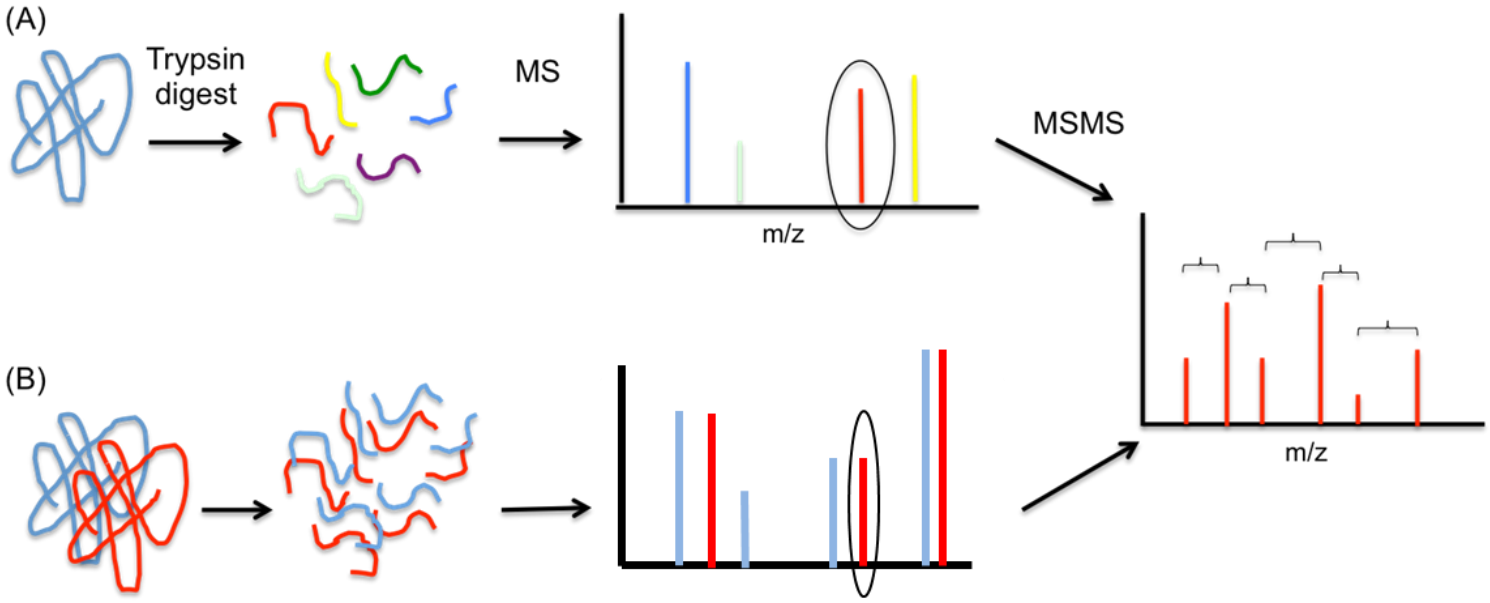

Figure 4. Protein identification by mass spectromtery. (A) Proteins are digested into peptides by the enzyme trypsin and analyzed by mass spectrometry. Peaks in the first scan (MS) represent each of the peptides arranged by their mass over charge ratio (m/z). The top 10 intense peaks over a period of time are then subsequently subjected to a second round of analysis (MS2) whereby the peptide is subjected to limited fragmentation at peptide bonds by high energy and collision gas. The resulting spectra can be used to determine the amino acid sequence based on the known molecular weight separation masses for the amino acids. MS2 spectra are then analyzed by software that matches peptide sequences to a human protein database to identify the parent protein. (B) SILAC proteins are processed the same way with the exceptions that two experimental protein mixtures are multiplexed and characteristic SILAC pairs, either 6 (lysine) or 10 (arginine) Th apart, are apparent during the MS scan.

as: isotope-coded affinity tags (iCAT)(107), isobaric tags for relative and absolute quantitation (iTRAQ)(108), or stable isotope labels by amino acids in cell culture (SILAC)(109). SILAC has the advantage that the isotopically coded amino acids are metabolically integrated into the growing cells and cell lysates are mixed 1:1 prior to sample processing. All downstream sample processing is therefore performed equally to the test and control samples. SILAC involves replacing standard cell culture media with leucine and arginine. In this case, carbon-12 (C_{12}) is replaced with C_{13} at each carbon position in the leucine molecule and C_{13} and N_{15} replace Carbon-12 and Nitrogen-14 in the arginine molecule. This labeling affects only the mass, increasing the leucine mass by 6 Th and the arginine by 10 Th, and no other properties of the amino acids (109). As well, labeling of these amino acids has the added benefit that during trypsin digestion, most peptides will incorporate at least one heavy lysine or heavy arginine label as trypsin cleaves after lysine and arginine.

In SILAC, two or more experimental conditions are defined and cells are grown in normal media or media supplemented with isotopically ‘heavy’ amino acids. As the cells grow and divide, the ‘heavy’ leucine and arginine are metabolically incorporated into new proteins. In order to get near full incorporation, cells must grow in the media for at least 10 days, depending on the doubling time of the cell line used. Following labeling, the two cell populations are equally mixed and digested for MS analysis (109). Because the label has been metabolically

integrated into the proteins, there is no chance of label transferring between samples and as such ratios are maintained.

Once SILAC samples are mixed, digested, and analyzed by the mass spectrometer, specific signatures in the MS spectra are looked for. These signatures are called SILAC pairs, which represent the same peptide but from the two separate experimental conditions (Figure 4B). The distance between the SILAC pairs depends upon which lysine and arginine labels are used and which amino acid is at the peptide terminus; lysine-6 results in SILAC pairs 6Da apart, while arginine-10 results in SILAC pairs 10Da apart (109). Software has been developed that interrogates the MS data for SILAC pairs, identifies the peptide, and quantifies the peptide based on relative peak abundances (110, 111). The resulting data can be statistically evaluated for significant protein abundance differences between conditions.

1.5. Research Aims

NS34A is an important, multifunctional protein complex of HCV that plays a major role in viral replication, dampening the innate immune response, and potentially in the development of liver cancer. However, the exact mechanism(s) by which this viral protein is involved in the above roles remains unclear. Specifically, its role in hepatocellular carcinoma has been heavily studied in the context of NS3 expression, and not the naturally occurring NS3/4A complex, which is localized to the ER and mitochondrial membranes. There has been no systems wide analysis

of the alterations to host protein physiology following NS3/4A expression. Identifying cellular proteins and pathways that NS34A interacts with at a global proteomic level will provide important insight into these mechanisms and potentially uncover novel therapeutic host targets. I hypothesize that by applying a combination of biochemical fractionation and mass spectrometry, the identity of proteins altered by NS3/4A expression can be identified. The aims of this study were to [1] stably express NS3/4A in cells and confirm its presence and function, [2] evaluate the cellular transformation event in the context of NS3/4A expression, [3] determine differentially regulated proteins upon NS3/4A expression by quantitative proteomics through isoelectric focusing fractionation and SILAC, and [4] confirm differentially regulated proteins.

2.0. Materials & Methods

2.1. Cells and Cell Line Maintenance

Cell line GP2-293 (Clontech, cat# 613505) is a human embryonic cell line derived from the prototypic HEK 293 cell line. Cells were maintained in Dulbecco's Modified Eagle Media (DMEM, Life Technologies, cat# 11995-065) with 10% Fetal Calf Serum (Life Technologies, cat# 10082-147) and 1x Penicillin Streptomycin (Life Technologies, cat#15070-063). When cells reached 70-80% confluency, they were split with trypsin (Life Technologies, cat# 12605-010), leaving 10% for reseeding.

2.2. Cloning

2.2.1. PCR

Polymerase chain reaction (PCR) was performed using the BioRad iProof High Fidelity PCR reagents (BioRad, cat#172-5301). The PCR mixture was made up of 10ul 5xiProof buffer, 2.5ul of each 10mM primer stock, 1ul of 10mM dNTP stock, approximately 1ng DNA template and 0.5ul iProof polymerase and brought to a final volume of 50ul with sterile water. Nucleotide sequences of the primers are shown in Appendix Table A1. PCR was performed using an Eppendorf Mastercycler ep Gradient S thermocycler with an initial 30 second denaturing step at 98°C, followed by 36 cycles of 30 seconds denaturing (98°C), 30 seconds annealing (55°C), 2 minute elongation (72°C), followed by a final 7 minute elongation at 72°C. Amplicons were left at 4°C for short term storage or at -20°C

for long-term storage following purification with a QIAquick PCR Purification Kit (Qiagen cat#28108). Amplicons that were constructed are: NS3/4A 1b, NS3/4A 2a, PTGR1, and PRPH.

2.2.2. DNA Digestion

pQCXIN vector (Clontech) and amplicons were digested with restriction enzymes detailed in Table A1. Digestions involving BsiWI were performed sequentially with the BamHI or NotI (Table A1) at 37°C for 1.5 hours, then BsiWI was added and digestion was continued at 55°C for an additional 1.5 hours. For vector digestion, 500 ng was digested in a total volume of 40 ul. Amplicons were similarly digested by mixing approximately 200-500 ng of purified amplicon with 1x NEB Buffer 3, 0.4ul BSA, 30ul DNA, and 1.5ul of each restriction enzyme together and digested as stated above.

2.2.3. DNA Purification

Digested reaction mixtures were supplemented with 6x DNA loading dye (30% glycerol and 0.00025% bromophenol blue in water) to a 1X concentration then electrophoresed on a 1% agarose gel, containing 0.0001% ethidium bromide, for 1 hour at 100V in a 1x Tris/borate/EDTA (TBE) buffer. The gel was then placed on a UV tray and DNA bands corresponding to the correct molecular weight of the vector or insert were excised and placed in Eppendorf tubes. DNA was purified from the agarose gel slices using a QIAEX II Gel Extraction Kit (Qiagen, cat#20051). 300ul of Buffer QX1 and 10 ul of QIAEX II slurry was added to each 100mg of gel and incubated at 50°C for 10 minutes, vortexing briefly every 2

minutes. Samples were centrifuged, supernatant removed, and the pellet was washed once with Buffer QX1 and twice with Buffer PE. DNA was then eluted from the resulting pellet by adding 20ul of 10mM Tris-Cl, pH 8.5, incubating at 50°C for 5 minutes, then centrifuging and transferring the supernatant to a fresh tube. Purified samples were then either used immediately for ligation or stored at -20°C.

2.2.4. Ligation

A ligation ratio of 1:1 molar ratio (vector:insert) was normally used. Ligations were performed in a 20 ul volume containing 1X T4 ligase buffer (New England Biolabs, cat#B0202S), 1ul T4 DNA ligase (New England Biolabs, cat#M0202L) and no more than 20-100 ng insert + vector DNA. Ligation was performed at room temperature for approximately 1 hour.

2.2.5. Bacterial Transformation

Following ligation, samples were transformed into OneShot® Top10 *Escherichia coli* cells (Life Technologies, cat#C4040). 50ul of bacteria was thawed on ice for each transformation, and 4ul of the ligation reaction was added and incubated on ice for 30 minutes. Cells were then placed in a 42°C water bath for 30 seconds then returned to ice for two minutes. 250ul of S.O.C. media (Invitrogen, cat#15544-034) was then added to each vial, the mixture was transferred to a 15ml culture tube and incubated at 37°C for 40 minutes with shaking (225rpm). 10 and 100ul of each mixture was then spread on LB agar plates containing 100ug/ml ampicillin and incubated overnight at 37°C.

2.2.6. Plasmid DNA Miniprep Isolation

6-12 colonies were selected from the transformation plates and grown overnight at 37°C in 3ml LB broth containing 100ug/ml ampicillin at 280rpm. Bacteria were pelleted (13,000xg, 15 min, 4^{o}C), supernatant removed, and DNA purified from the pellet using the Qiaprep Spin Miniprep Kit (Qiagen, cat#27106). DNA was eluted from the column with 50ul Buffer EB (10mM Tris-Cl, pH 8.5), and stored at -20°C until further use. DNA concentrations were determined using a Nanodrop Spectrophotomoeter (Thermo Scientific, Nanodrop 2000).

2.2.7. Diagnostic Restriction Digest/DNA Sequencing

Insertion of gene into vector was confirmed by diagnostic DNA digests where 400ng of DNA was digested with 0.5ul of the same restriction enzymes as were used for initial cloning, followed by electrophoresis on a 1% agarose gel at 100V for 30 minutes. For each clone, 5ul of plasmid (150ng/ml) was sequenced with 5ul of forward or reverse primers (1uM) by Sanger dideoxy sequencing (sequencing was performed by the NML DNA Core Services). Sequencing traces were evaluated using the modules Seqman and Editseq in the Lasergene 7 DNAStar software (Lasergene Corp).

2.2.8. Endofree Plasmid DNA Maxiprep

In order to purify DNA for cell culture transfections, transformed bacteria were grown up overnight at 37°C in 100ml LB broth and 100ug/ml ampicillin at

280rpm. Bacteria was then spun down and plasmid DNA was purified from the pellet by using the Endofree Plasmid Maxiprep Kit (Qiagen, cat#12362). The only change to the protocol was centrifuging the precipitated DNA at 5000xg for 60 minutes at 4°C after addition of isopropanol and ethanol. The resulting DNA pellet was dissolved in 500ul of endotoxin-free TE Buffer (QIagen) and stored at -20°C until further use. DNA concentrations were determined using a Nanodrop spectrophotometer.

2.3. Stable Cell Lines

2.3.1. Cell Culture Transfections

Transfecting DNA into cells was done using the Effectene Transfection Reagent (Qiagen, cat#301427). 100ul of EC buffer, 1ug DNA, and 8ul of enhancer were mixed together in an Eppendorf tube and left to sit 2-5 minutes. 10ul of Effectene was then added to the mixtures and left to sit for another 10 minutes. Meanwhile, media from the cells in a six well plate, at about 70% confluence, was removed and replaced with 1.5ml fresh DMEM. 500ul of fresh DMEM was added to the transfection mixtures and then carefully added to the cell culture wells. Transfected cells were left for 48 hours at 37°C before protein harvest/lysis. GFP was used as a monitor of transfection efficiency.

2.3.2. Retrovirus Production

The packaging cell line GP2 293 (Clontech, cat#631458) was plated on 10cm plates at $3.2x10^6$ cells/well, resulting in a 70% monolayer the following morning.

Transfections were performed as described above except that plasmid pVSV-G expressing the vesicular stomatitis virus glycoprotein (VSVG) was included in the DNA mixture. Additionally, the amounts of reagents were scaled up for a 10cm dish. 300ul of EC buffer, 2ug DNA, 2ug VSVG, and 32ul of enhancer were mixed together. Next, 50ul of Effectene (Qiagen) was added and the mixtures incubated for 10 min at room temperature. While incubating, cell media was removed and replaced with 7 ml fresh media. 3ml of fresh DMEM was added to the DNA mixture, which was then added to the cell culture plates. Cells were incubated for 48 hours at 37°C. Following 48 h incubation, retrovirus was isolated from the cell culture supernatant, filtered through a 0.45um filter and stored in aliquots at -80^{o}C.

2.3.3. Retrovirus Infection of Cells in Cell Culture

Cells were seeded in a 12-well cell culture plate at 1.5x10^{5} cell/well (50% confluency the next morning). Approximately 350ul of concentrated virus was carefully added to cells, which were rocked every hour for 4 hours post infection. 1ml of DMEM was then added to wells. The following day, cells were selected with 500ug/ml of G418 for 10 days. Cells not harbouring a selective marker (without retrovirus) died within 5 days. Retrovirus expressing a Green Fluorescent Protein GFP (Clontech) was used to monitor infection and selection efficacy. Cells were typically maintained in a T75 flask and split as needed upon reaching 80-90% confluency.

2.3.4. Lentivirus shRNA Infection

shRNAs targeting the HCV NS34A protein were designed by inserting the NS34A sequence into the Public TRC Portal (The RNAi Consortium, http://www.broadinstitute.org/rnai/public/seq/search) and five target sequences were picked from the top of the list, such that they did not overlap. Forward and reverse primers were also provided with each target sequence. shRNAi sequences were cloned into the pLKO TRC2 vector (Sigma, cat#SHC201). 2.8uM of forward and reverse oligos were mixed with 1.4X NEB2 Buffer (New England Biolabs) up to 35ul in water. Samples were placed in a beaker of boiling water for 10 minutes, after which the heat was turned off and water was left to cool slowly to room temperature over 4 hours for the oligos to anneal. Meanwhile, 0.5ug of TRC2-pLKO-Stuffer Cloning Vector (Carpenter, unpublished) was digested with AgeI and EcoRI in NEB4 Buffer for 1 hour at 37°C. Digestions were electrophoresed on a 1% agarose gel, and the 7.5 kb vector band was excised using a Qiagen gel extraction kit as above. 10-12ng of vector and 20-50ng of annealed oligos were ligated together for 2 hours at room temperature. Top10 cells were transformed and DNA isolated as per above. 300ng of cloned DNA was screened by digesting with BamHI and XhoI for 45 minutes, followed by electrophoresis on a 1% agarose gel. Appearance of a 233 bp band indicated successful cloning. shRNA was the sequenced with the pLKO vector primers 791F and 792R (Appendix Table 1) using a Hi GC reaction mix and evaluated using the modules Seqman and Editseq in the Lasergene 7 DNAStar software. DNA from the clones with shRNA correctly inserted with

proper sequence was isolated for cell culture using the Endofree Maxiprep as above.

A derivative of the HEK 293 cell line known as 293TN (SBI, cat# LV900A-1) was used for shRNA vector transfection at a density of $3.0x10^5$ cells/well in a 6-well plate for approximately 70% confluency next day. For transfection, X-tremeGene HP Transfection Reagent (Roche, cat#06366244001) was used. 0.2mL of serum and antibiotic free DMEM was mixed with 0.34ug of the shRNA vector, 0.56ug of the gag/pol packaging plasmid, 0.56ug of the rev packaging plasmid, and 0.54ug of the VSV-G packaging plasmid. 6ul of the X-tremeGene reagent was added to each reaction mix and incubated for 15 minutes at room temperature. After the incubation, the media on the cells was replaced and the DNA mixture was added drop wise to the cells and incubated at 37°C for 48 hours. Supernatant containing virus was filtered and stored at -80°C.

For lentivirus infection, GP2 293 cells stably expressing NS3/4A 1b or HBH-GFP were plated in a 24-well dish at $5.5x10^4$cells/well for 50% confluency the next day. Approximately 6 hours after plating cells, 8 ug/ml polybrene was mixed with 100ul of filtered virus inoculum and up to 200ul with DMEM and replaced with media on cells. The next day, the polybrene was replaced with 1ml of DMEM. After 72 hours, cell stably expressing the shRNA vector (which contains a puro resistance gene) were selected with DMEM containing 1 ug/ml of puromycin for

approximately 4 days, when cells containing no vector died. Cells were then passaged to desired amounts for further testing.

2.3.5. Cell Lysate Preparation

Cells were removed from the plate with a cell scraper and transferred to a 15ml tube then spun at 500xg for 10 minutes at 4°C and supernatant discarded. Pellet was then resuspended in 1-10ml PBS, spun again for 10 minutes to remove abundant proteins present in the fetal bovine serum in the media. This wash was repeated twice. Pellets were resuspended in 350ul-2ml 4% SDS in PBS and transferred to a 1.7ml Eppendorf tube. Lysates were then boiled for 10 minutes, and stored overnight at -80°C. The next day, lysates were thawed and passaged through a QIAshredder (Qiagen, cat#79656) to shear DNA. Samples were stored at -80°C until further analysis.

2.4. Protein Concentration Determination

Protein concentrations were determined through a BCA (bicinchorinic acid) Protein Assay (Pierce, cat#23227) using a modified protocol from the Janes Lab at the University of Virginia (http://bme.virginia.edu/janes/protocols/index.html). In this protocol, the albumin standard was diluted to construct a standard curve consisting of 4, 2, 1, 0.5, and 0.25 mg/ml. In a 96-well plate, 7.5ul of standard was added to 2.5ul water in each well, except where 7.5ul water was used for the 0mg/ml point, to form the standard curve. 2.5ul of diluted and/or undiluted protein lysate was added to 7.5ul of water per well. Next, BCA solution was prepared

consisting of 50 parts Solution A to 1 part Solution B, and 200ul was added per well and incubated at 37 ºC for 15 minutes. The plate was read in a SpectraMax Plus spectrophotometer (Molecular Devices) at A_{562} and protein concentrations were calculated from the standard curve.

2.5. SDS-PAGE and Western Blot Analysis

Approximately 40ug of cell lysate was electrophoresed on a 4-20% SDS-PAGE gradient gel (Life Technologies, cat#NP0302BOX) for 1.5 hours at 150V on an Xcell SureLock Mini-Cell Electrophoresis System (Life Technologies). Protein was then transferred to a nitrocellulose membrane (Invitrogen, cat# IB3010-02) using an iBlot semidry transfer system (Life Technologies) for 7 minutes. For chemiluminsescent blotting, membranes were then blocked in 5% skim milk in TBST (Tris Buffered Saline with 0.1% Tween 20) for at least 1 hour. Primary antibody to NS3 (Millipore, cat#MAB8691, used at 1:1000) or MAVS/Cardif (Epitomics, cat#ALX-210-929, used at 1:2000) was applied to the blocked membrane and incubation was continued overnight at 4°C. The following day, blots were washed in TBST for 10 minutes three times, and then incubated in appropriate HRP secondary antibody in TBST for 1.5 hours. After washing the membranes again, chemiluminescent detection reagent (Millipore, cat# WBKLS0500) was applied for HRP detection and then developed by x-ray.

For fluorescent western analysis, membranes were incubated in a 1:1 solution of LiCor Odyssey blocking buffer:PBS for at least an hour. Primary antibody in LiCor blocking buffer:PBS supplemented with 0.1% Tween-20 was added to the blots, and incubated overnight with gentle shaking at 4°C. Blots were washed 3 times in TBST for 10 minutes, and 4ul of appropriate LiCor secondary antibody was incubated with a 1:1 mixture of Odyssey blocking buffer and PBS, 0.1% Tween-20, and 0.01% SDS in the dark for 1 hour. The membranes were washed again, but in the dark, and left to dry overnight at 4°C covered in tinfoil. Once fully dried, membranes were imaged using the Odyssey Infrared Imaging System scanner (LiCor Biosciences, Mandel Scientific, cat#LIC-9201-00). All other antibodies used are in appendix Table A2.

2.6. Transformation Phenotype

2.6.1. Alamar Blue Assay

To test the proliferation of stably or transiently transfected cells, an Alamar Blue assay was performed (Invitrogen). NIH 3T3 cells were plated at a density of 3000 cells/well to provide a complete cell monolayer 5 days later. Set up of this experiment was on a 96-well plate, with cells plated at densities mentioned above and DMEM added to a final volume of 100ul per well. Each cell line, as well as cell control and vector control lines, were plated in 6 wells/day (30 wells total), with 30 wells of DMEM also plated as a blank for the assay. The day after seeding the wells, the media was replaced with 100ul of fresh, pre-warmed DMEM along with 10 ul of Alamar Blue to 6 media only wells, and 6 wells for

each tested cell line. Wells were mixed by pipetting up and down twice, and then incubated at 37°C for 4h. Plates were read at 570nm and 600nm using a SpectraMax Plus spectrometer every day at the same time for 5 days. Media of all wells was replaced every day.

2.6.2. Cell Proliferation Assay

Stable NIH 3T3 cells (containing pQCXIN vector only, NS3/4A1b,and NS3/4A 2a) were plated at $5.5x10^4$ cells/ml in a 6-well dish, in duplicate, to give approximately 10% confluency the next day. Cells were allowed to grow for 15-17 days, splitting them all when any of them reached 70% confluency. Splitting these cells went as follows; cells were washed with 1ml PBS and incubated at 37°C for 5 minutes with 350ul of trypsin. 1.65ml of fresh media was added to trypsinized cells, and 300ul of this was plated in a new 6-well dish and made up to 3ml with fresh media. Cells were counted at the end of the experiment, and the experiment was repeated.

2.7. Proteomics

2.7.1. Stable Isotopic Labeling of Amino Acids in Cell Culture (SILAC)

2.7.1.1. Growing cells

Stable GP2 293 cells containing GFP and NS3/4A were used in SILAC experiments. These cells were plated into T25 flasks at a cell density of $1.0x10^6$ cells/flask. Approximately 6 hours later, cells were washed in PBS and media was replaced with SILAC media. Cells were left in SILAC media for at least 10

days, splitting as needed, and transferred to a T75 before cell lysis. Each cell line was grown in one flask containing “heavy” SILAC DMEM, consisting of $^{13}C_6$ Lys (Sigma, cat# 605239) and $^{13}C_6{}^{15}N_4$ Arg (Sigma, cat# 608033), and another flask containing “light” SILAC DMEM ($^{12}C_6$Lys, $^{12}C_6{}^{14}N_4$ Arg).

2.7.1.2. Cell lysis

Cells to were washed twice with 10mL of ice cold PBS then removed from the plate by aspiration into a 50mL tube with 10mL of ice cold PBS. Cells were pelleted at 800xg for 5 minutes at 4 ºC. Supernatant was removed, and cells were lysed in 1mL of SDS Lysis Buffer (4% SDS in PBS). Samples were denatured at 95 ºC for 5 minutes, cooled then the DNA was sheared by passing sample through a Qiashredder cartridge at 10 000xg for 2 minutes. DTT was added to a final concentration of 100mM and aliquots were stored at -80 ºC until further use.

2.7.2. Sample Preparation and Cartridge trypsin digestion

Samples were digested using a modified FASP method as detailed below (112). Approximately 150 ug cell lysates were mixed with 1 volume of Urea Exchange Buffer (UEB, 8M urea, 50mM Tris-HCl, pH 8.0) and left on the bench for 10 minutes. Meanwhile, Nanosep 30K cartridges (Pall, cat# OD030C34) were prepared by spinning 200uL water through the cartridges at 10,000xg for 1 minute, followed by spinning 200uL of UEB through the column for 2 minutes. Samples with UEB were then passed through the cartridges 300uL at a time, spinning at 10,000xg for 10 minutes. Cartridges were washed twice with 250uL

UEB, spinning for 15 minutes each time. In order to alkylate the reduced proteins, 100uL iodoacetoamide (IAA) Buffer (50mM IAA in UEB) was added to the cartridges, shaken at 600rpm for 1 minute, then covered with tinfoil and incubated at room temperature. After 20 minutes, samples were spun for 10 minutes and washed three times with 100uL of UEB, centrifuging for 10 minutes each time. Next, samples are washed twice with 150uL of Ammonium Bicarbonate (AB) Buffer (50mM Ammonium Bicarbonate) and centrifuged for 10 minutes. Then, 50uL of Benzonase Solution (2mM $MgCl_2$ in 50mM AB buffer, 500U of benzonase) was added and mixed at 600rpm for 30 minutes. Washing samples with 100uL of AB Buffer three times followed incubation. Cartridges were transferred to fresh 1.5mL Eppendorf tubes. 50uL of Trypsin Solution (2ug Promega trypsin gold mass spectrometry grade, cat#V5280 in 50uL AB) buffer was placed directly on the cartridge membrane and, tubes were placed inside 50mL tubes filled with 2mL water, and incubated overnight at 37 ºC. The next morning, 50ul of AB buffer was added to each cartridge and shaken for 2 minutes Liquid was collected by inverting the column and spinning at 10 000xg for 3 minutes. 50ul of 0.5M NaCl was added to the column for 3 minutes with shaking, and extract was pooled as before. Finally, 50uL of AB buffer was added for 3 minutes, with shaking, and liquid pooled with the pervious samples.

Eluted peptides were then brought up to 240ul with water and acidified to 2% trifluoric acid (TFA) in preparation for desalting before use in isoelectric focusing (IEF). A 3ml 3M Varian Empore C18 cartridge (Sigma, cat#4215SD) was placed

in a 15ml tube. Using a syringe plunger, the cartridge was equilibrated by pushing through 1ml of methanol, then 0.5ml 0.1%TFA in 70% acetonitrile (ACN), and finally 0.5ml of 0.1% TFA in water. Sample was then loaded into the cartridge and slowly pushed through the membrane. The cartridge was washed by pushing through 0.5ml of 0.1% TFA in water twice and desalted peptides were eluted into an Eppendorf tube by gravity flow of 0.5ml of 70% ACN through the cartridge, twice. Eluted peptides were dried down in a SpeedVac and stored at -80 ºC until further processing.

2.7.3. Off-gel IEF fractionation

24 cm 3-10NL IPG strips (GE Healthcare) were placed in an Agilent Off-Gel IEF focusing cassette and 40ul of Rehydration Solution (5% glycerol and 2% 3-10 IPG buffer in water) was added to each well. While the strip was left for 20 minutes to rehydrate, peptide sample was resuspended in 720ul water and brought up to 3.6ml with the Rehydration Solution. Two wicks coated in rehydration solution were added to the ends of the strip and mineral oil was added to each end of the assembly (200ul to anode, and 1.3ml to cathode). Once the strip was rehydrated, 150ul of peptide solution was added to each well and 200ul of additional mineral oil was added to the each end. The assembly was sealed and placed into the Off gel fractionator (3100 Off gel fractionator, Agilent Technologies) and run according to the following program: focusing at 50kVh, 4500V, 50uA, and 200mW for 100 minutes. Fractions were harvested pooled into 12 fractions as follows:1, 2, 3, 4, 5, 6+7+8, 9+10, 11+12+13, 14, 15, 16+17+18+19+20, 21+22+23+24, and stored at -80 ºC until further processing.

2.7.4. Peptide purification

Dried down, desalted peptides were acidified with 50ul of 10% Acid Solution I (30% ACN, 5% acetic acid, 5% formic acid) in water. Tips were made in-house that consisted of five C18 disks in a pipette tip. Tips were equilibrated first with 80ul of 0.5% formic acid (FA) in 80% ACN, then 80ul of 0.5% FA. 50ul of peptide sample was bound to the resin at a time until all sample was used. Tips were washed twice with 50ul of 0.5% FA, then eluted into a new Eppendorf tube with 50ul 0.5% FA in 80% ACN, twice. These samples were again dried down in the Speed Vac and resuspended in 25ul of 0.1% FA in 2% ACN and transferred to HPLC loading vials for mass spectrometry analysis.

2.8. Mass Spectrometry

Desalted fractions were injected into an LTQ Orbitrap-Velos mass spectrometer (Thermo Fisher) through a nano-flow HPLC (Proxeon). 15 ul of sample (~1.5 ug) was concentrated onto a 2.0cm C18 pre-column prior to injection onto a 10cm C18 analytical column. Peptides were eluted using a 2h linear gradient from 2-40% acetonitrile in 0.1% formic acid. Following a 1s MS analysis in the Orbitrap, the top 10 precursors were selected for fragmentation analysis in the linear ion trap. Chosen m/z signals were excluded from subsequent re-analysis for 2 minutes.

2.9. Real-Time Reverse Transcriptase PCR (RT^2-PCR)

GP2 293 stable cell lines were each seeded in 6 well plates at $5.5x10^5$ cells/well (70% confluency the next day) for RNA extraction. Using the RNeasy Plus Mini Kit (Qiagen, cat#74134), cells were lysed and homogenized with 350ul of Buffer RLT Plus. Genomic DNA was removed by adding the sample to a gDNA Eliminator column centrifuged for 30s at 8000xg (all centrifugation steps were done at this speed unless otherwise noted). 1 volume of 70% ethanol was then added to the flow through, transferred to an RNeasy spin column, and centrifuged for 15s. Columns were washed with 700ul of Buffer RW1, centrifuged for 15s, then washed twice with 500ul of Buffer RPE and centrifuged for 30s and 2min, respectively. The spin columns were placed in new collection tubes (supplied), and RNA was eluted with 50ul of RNase-free water centrifuged for 1 min. RNA samples were stored at -20ºC until further processing. The amount of RNA isolated was determined by reading the A_{260} from 2ul of sample on the nanodrop (with an A_{260}:A_{280} reading greater than 2.0).

The RT^2 First Strand Kit (SABiosciences, cat#330401) was used to make cDNA from RNA samples so that RT^2 PCR could be performed. For each sample, 1ug of RNA was mixed with 1X GE Buffer (gDNA Elimination Buffer) and water to a final volume of 10ul and incubated at 42ºC for 5 minutes. After heating, samples were chilled on ice immediately for at least 1 min, then mixed with 2X BC3 (RT Buffer 3), 10% P2 (Primer and External Control Mix), 20% RE3 (RT Enzyme Mix 3), and RNase-free water up to 10ul. This mixture was heated at 42ºC for 15

minutes then stopped by boiling samples at 95ºC for 5min. 91ul of RNase-free water was added to samples and stored at -20ºC until further use. A no reverse transcriptase control (NRT) was done for each sample where the reverse transcriptase was replaced with water.

Real-time PCR was performed using RT^2 qPCR Primer Assays (ACTB #PPH00073G, GAPDH #PPH00150F, PTGR1 #PPH16323A, BNIP1 #PPH00308C, PRPH #PPH09060A, and PSMD5 #PPH14088A) and RT^2 SYBR Green Mastermixes (cat#330500) from SABiosystems. For each reaction, the following components were mixed together in a total volume of 25ul with RNase-free water; 50% RT^2 SYBR Green Mastermix (12.5ul), 4% cDNA synthesis reaction (1ul), and 4% RT^2 qPCR Primer Assay (1ul). Each reaction was pipetted into a well of a 96 well plate (Life Technologies/Applied Biosystems, cat#4346906), covered with a protective film (Life Technologies/Applied Biosystems, cat#4311971), and placed into a StepOnePlus Real-Time PCR System (Applied Biosystems/Life Technologies). The cycling conditions were as follows; 1 cycle at 95ºC for 10 min, followed by 40 cycles of 95ºC for 15 seconds and 60ºC for 1 minute, finishing with a melting curve (95ºC for 1 minute, 65ºC for 2 minutes, then 65ºC to 95ºC at 2ºC/minute). For each Primer Assay, a no template control (NTC) reaction was prepared with water in place of template. Each reaction was done in triplicate.

2.10. Data Analysis

2.10.1. MaxQuant/raw data

All Thermo ".raw" files were loaded into MaxQuant version 1.3.0.5 (110). MaxQuant enables high peptide identification rates, individualized p.p.b.-range mass accuracies and proteome-wide protein quantification (111) which was used to generate peak lists from the MS and MS/MS spectra for database searching. The search algorithm in Andromeda (113) was set to allow 2 missed trypsin cleavages. Carbamidomethylation of cysteines was set as a fixed modification whereas methionine oxidation and N-terminal protein acetylation were set as variable modifications. For protein identification, 2 peptides were required with one being unique to that protein group. Searches prior to recalibration were set at 10 ppm MS and 0.2 Da MS/MS. The IPI Human database (version 3.87) was used along with the amino acid sequences for NS3 and GFP. In addition, common contaminants including keratin and trypsin were included. Peptide and protein false discovery rates were set to 0.01. Ratios were determined by MaxQuant. Resulting output ".txt" files were used for further statistical and graphing analysis as described below.

2.10.2. Perseus

Resulting MaxQuant data from all four experiments (ProteinGroup.txt files) were loaded into the statistical software Perseus (www.maxquant.org). Filters were applied to remove reverses and contaminants, and to retain only those proteins observed in at least three experiments. Protein ratios from experiments where

NS3/4A was expressed in “light” SILAC media were inverted so that all four experiments displayed normalized ratios of NS3/4A/GFP rather than “heavy”/”light”. The resulting ratios were transformed to $\log_2$ and proteins with a Benjamini-Hochberg corrected p-value < 0.05 and a greater than 30% difference in $\log_2$ ratios were chosen as differentially regulated candidate proteins.

3.0. Results

3.1. Production of stable cell lines expressing functional NS3/4A

In order to study the effects of NS3/4A on host cell oncogenesis and potential role in HCV pathogenesis, the NS3/4A gene was cloned into an expression vector to make stable cell lines that expressed this protein. The first aim of this study was to replicate previous studies showing that NS3 protease expression in NIH 3T3 cells (a mouse fibroblast cell line) induced advanced cellular transformation (79, 80). To do this, the NS3/4A coding region from the HCV genotypes 1b and 2a were individually cloned into the retroviral vector pQCXIN (Figure 5). The pQCXIN vector encodes ampicillin (for plasmid selection in bacteria), neomycin resistance markers (for selection in human cells), and packaging sequences flanked by retroviral long terminal repeats (LTRs). As the open reading frame of interest is under a cytomegalovirus (CMV) promoter, pQCXIN constructs can be used as isolated DNA for transient transfections or, when packaged in a suitable cell line, as a retroviral particle for stable cell line production. Constructs were transiently transfected into GP2 293 cells, lysed after 48 hours, and the expression of NS3 evaluated by western blot analysis. As a negative control, mock-infected Huh7.5 cells detected no 70kDa band (Figure 6A lane 1). JFH1 infected Huh7.5 cells were used as a positive NS3 control as it expresses the full viral genome, and NS3 was detected at 70kDa (Figure 6A, lane 2). Further negative controls included the original GP2 293 cell line, and GP2 293 cells expressing GFP, neither demonstrated NS3 expression (Figure 6A, lanes 3 and 4). The NS3 protein was detected in GP2 293 cells expressing

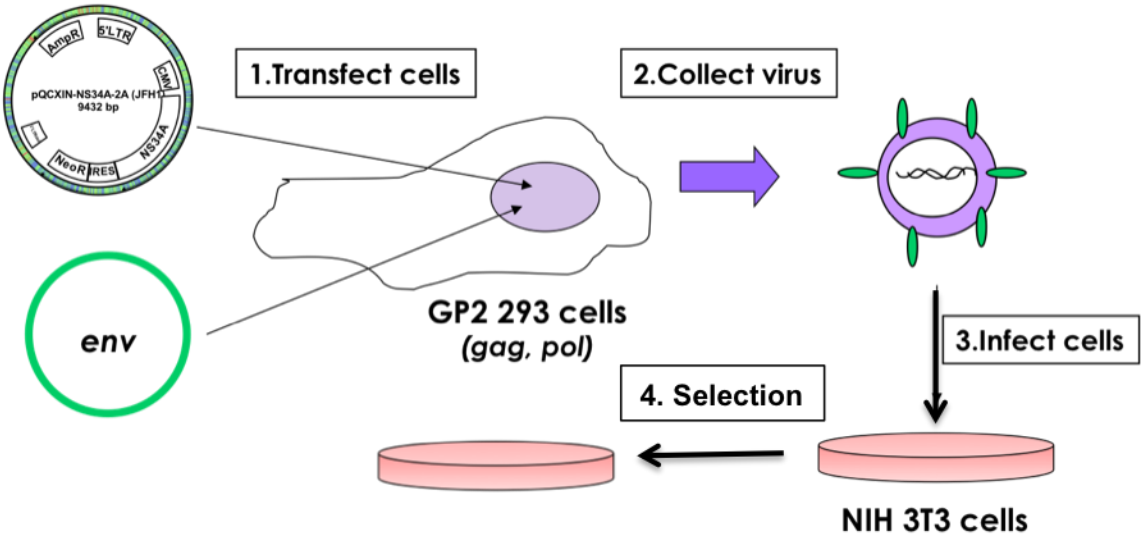

Figure 5. Retrovirus and stable cell line production. (1) The retroviral pQXCIN vector containing the NS3/4A 1b, 2a, GFP, or vector only sequences were transfected into GP2 293 cells with a plasmid expressing vesicular stomatitis virus glycoprotein (VSVG). (2) Forty eight hours post transfection, the cell supernatant containing packaged retrovirus was harvested. (3) The resulting retroviruses were used to infect target cells (NIH 3T3 or 293), and (4) cells were selected for 10 days with media containing G418 (neomycin).

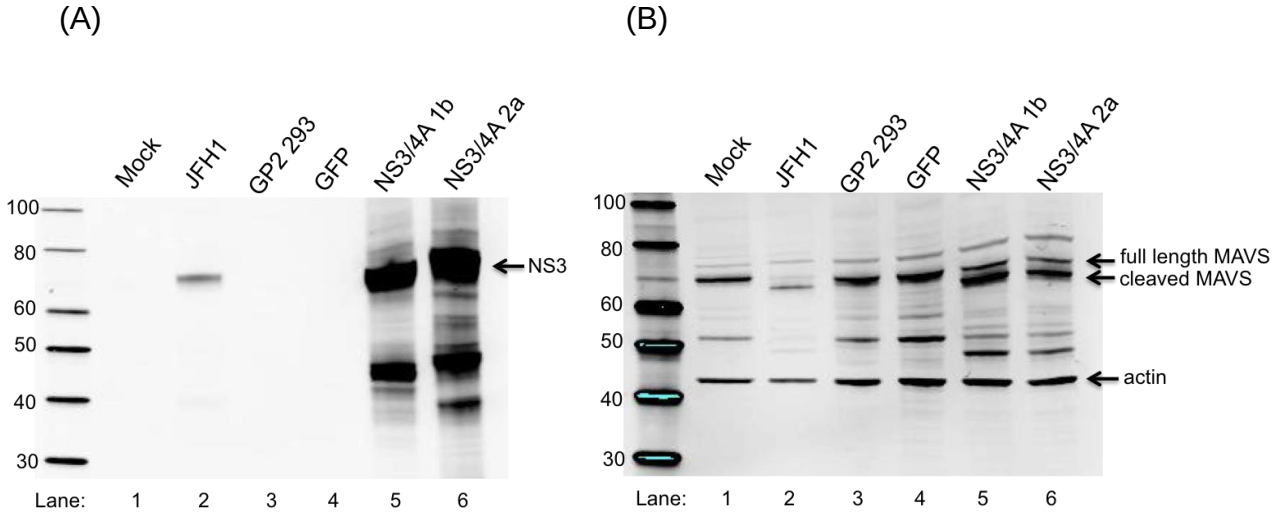

Figure 6. Transient NS3/4A expression and function in GP2 293 cells. Protein lysate was loaded in each well of an SDS-PAGE gel. Huh7.5 cells that were mock (lane 1) or JFH1 infected (lane 2) were added as negative and positive controls, respectively. GP2 293 cells were transiently transfected with the DNA constructs GFP (lane 4), NS3/4A 1b (lane 5), or NS3/4A 2a (lane 6). The gel was transferred to a nitrocellulose membrane and probed with (A) an HCV NS3 antibody, which detects a band of 70kDa (arrow), (B) a MAVS antibody, which detects full-length MAVS protein also at 70kDa (top arrow) and a 68kDa cleaved protein band (middle arrow). The blots were imaged by LiCor infrared imaging, and molecular weight markers are indicated in kDa. Actin was used as a load control (bottom arrow).

the NS3/4A genotypes 1b and 2a (Figure 6A, lanes 5 and 6). Although these results indicated presence of NS3, the presence of NS4A was still unknown.

Due to the lack of a good NS4A antibody, NS3 protease activity was measured as a surrogate marker since NS4A regulates this activity. MAVS was chosen as an endogenous indicator of protease activity as it is an authentic cellular target of NS3/4A. Western blot analysis was performed using antibodies against the endogenous MAVS. Mock infected Huh7.5 cell extracts contained full length MAVS at 70 kDa (Figure 6B, lane 1), whereas MAVS was present mostly in a cleaved form, 68 kDa, in the positive JFH1 infected cells (Figure 6B, lane 2). The GP2 293 and GFP controls also demonstrated only full length MAVS (Figure 6B, lanes 3 and 4). In cells transfected with the NS3/4A 1b and 2a genotypes, full length and cleaved MAVS were both detected at 70 and 68 kDa, respectively (Figure 6B, lanes 5 and 6). The amount of cleavage and amount of NS3/4A is not directly comparable between the JFH1 and transiently transfected NS3/4A constructs as the NS3 genotypes are not identical (and therefore antibody affinity may be different). Additionally, the cell lines used were different. Nonetheless, it demonstrates that the NS3/4A construct was present and functional against an authentic substrate, and could be used for further study.

3.2. Phenotypic study of NS3/4A oncogenic potential

Previous results had demonstrated that NS3 expression was directly linked to increased cellular proliferation in NIH 3T3 cells (79, 80). To test the transformation potential of NS3/4A in NIH 3T3 cells, cellular proliferation was measured by an Alamar Blue assay. This assay monitors cell growth through a reduction/oxidization indicator dye that changes colour upon cellular metabolic reduction; increased cell numbers leads to more dye metabolism. NIH 3T3 cells stably expressing NS3/4A 1b, NS3/4A 2a, the pQCXIN vector, and an untransfected control were plated at 3000 cells per well in a 96-well plate in sextuplate for each of 5 days. Media was replaced with fresh media and 10ul of Alamar Blue every 24 hours. Four hours post dye addition, the absorbance ratio of 570nm/600nm (metabolized dye/unmetabolized dye) was calculated. At 5 days, cells reached monolayer and the experiment was terminated. The amount of dye metabolized between cells expressing NS3/4A, vector control, and NIH 3T3 cells showed no significant change at any time point (Figure 7).

As the Alamar Blue assay was performed only up to only five days duration, it was hypothesized that increased cell growth might be visible only after a longer time period. Therefore, a cellular growth assay was used to monitor cell growth over a two-week period. NIH 3T3 cells expressing NS3/4A genotypes 1b and 2a and vector alone were plated in duplicate in a 6-well dish and were split simultaneously and identically (as cells approached 80% monolayer) with

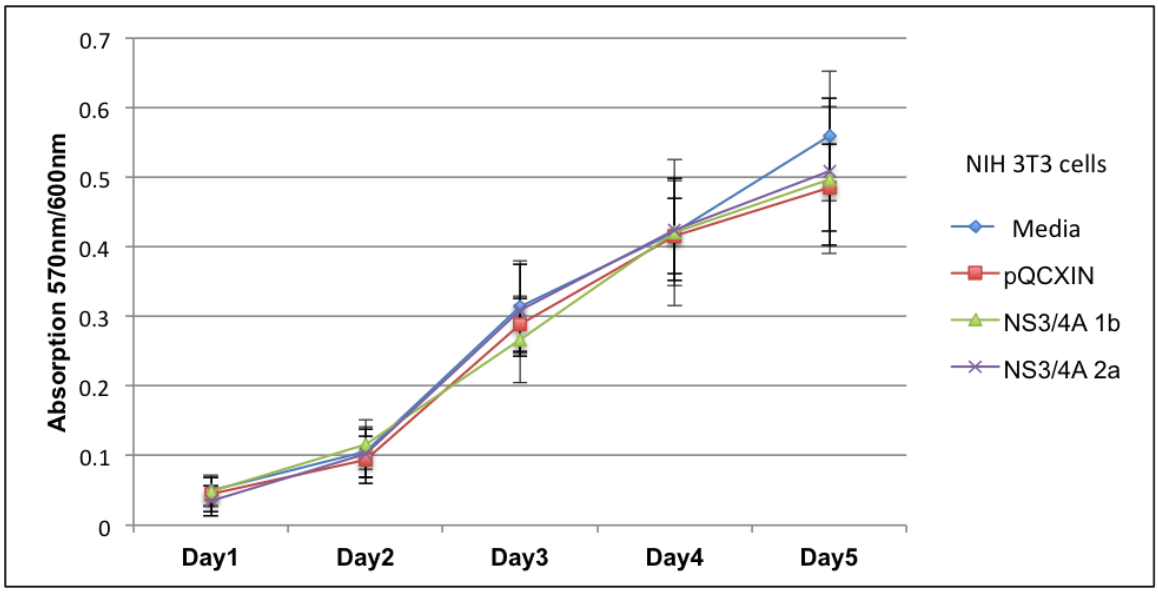

Figure 7. Alamar blue assay. NIH 3T3 cells stably expressing NS3/4A 1b, 2a, vector control, and cells only were plated at 3000 cells per well in a 96-well plate. Alamar blue was added to the cells and measured by absorbance at 570nm and 600nm four hours later. The ratio of emitted light at 570/600nm was calculated and plotted for each of five days. Error bars indicate standard deviation for six replicate wells.

the same total volume of liquid transferred to new plates. After two weeks, NIH 3T3 cells containing vector only averaged $1.2x10^6$ cells, NS3/4A 1b expressing cells averaged $1.3x10^6$ cells, and the NS3/4A 2a expressing cells averaged $2.0x10^6$ cells (Figure 8). Although NIH 3T3 cells expressing NS3/4A 2a trended towards an increase in cell proliferation over the two-week period, cells expressing NS3/4A 1b did not. These results suggested that NS3/4A 1b did not induce the advanced cellular transformation as previously reported with NS3 1b.

3.3. Stable Isotopic Labeling of Amino acids in Cell culture (SILAC)

Proliferation data from both the short term and long term experiments for the NS3/4A 1b genotype did not show changes although the literature suggested it should. When NS4A was complexed with NS3 no advanced cellular transformation was induced, possibly due to cellular localization of the protein complex, as NS4A tethers it to cellular membranes. Therefore, the project focus shifted to evaluating global proteomic changes upon NS3/4A 1b expression in a human cell line (HEK 293 cells). SILAC paired with mass spectrometry was used to compare differentially regulated proteins between NS3/4A 1b expressing cells and control cells. For this experiment, GFP was used as a control for proteomic expression changes in an effort to control for the over-expression of any gene (in this case and irrelevant one) stably integrated into the genome. In this way, proteomic expression changes due to the presence of NS3/4A 1b could be inferred from those involved in other phenomena such as endoplasmic reticulum stress or the mere act of translating large amounts of a protein. The stable

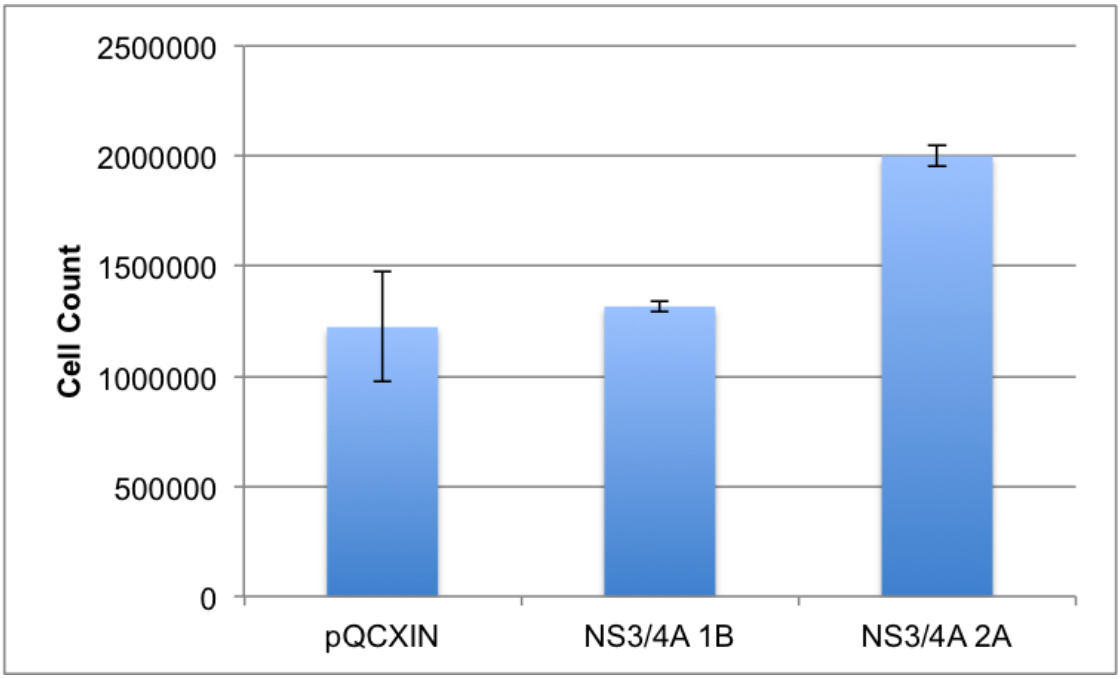

Figure 8. Cellular transformation potential of NS3/4A in NIH 3T3 cells. NIH 3T3 cells expressing NS3/4A genotypes 1b and 2a and vector control were plated in a 6-well dish in duplicate and split simultaneously every 3-4 days as at least one of the plates of cells was nearing monolayer. At the end of 2 weeks, cell numbers were counted. Bars represent average of duplicate cell counts, and bars representing the cell count range.

NS3/4A 1b cell lines constructed earlier, along with the GFP control, were chosen for analysis. Stable cell lines were selected with neomycin for two weeks, and then transferred into ‘light’ or ‘heavy’ SILAC media for 10 days to ensure complete incorporation. ‘Light’ media was supplemented with lysine and arginine of monoisptopic carbon-12 and nitrogen-14 (normal media), whereas the ‘heavy’ media was supplemented with lysine containing of carbon-13 and arginine containing of carbon-13 and nitrogen-15. This SILAC experiment was performed in quadruplicate and included label swapping such that two light label and two heavy label experiments were performed for each of the NS3/4A and GFP expressing cell lines. After 10 days of growth in labeled media, protein was harvested from cells for western blot and for mass spectrometry analysis. In two replicates, NS3/4A 1b expressing cells were grown in ‘light’ SILAC media while GFP expressing cells were grown in ‘heavy’ SILAC media (Figure 9). To control for potential differences in media, NS3/4 1b expressing cells were also grown in ‘heavy’ SILAC media and GFP expressing cells were grown in ‘light’ SILAC media for the remaining two replicates.

To ensure expression and function of the NS3/4A 1b protein, Western blots were performed on SILAC cell lysates and probed for the NS3/4A and MAVS proteins. As expected, NS3 (70kDa) was detected only in NS3/4A expressing cells, and the MAVS cleavage product (68kDa) was detected only in NS3/4A expressing cells (Figure 10A and B). GFP expression was measured directly from cells

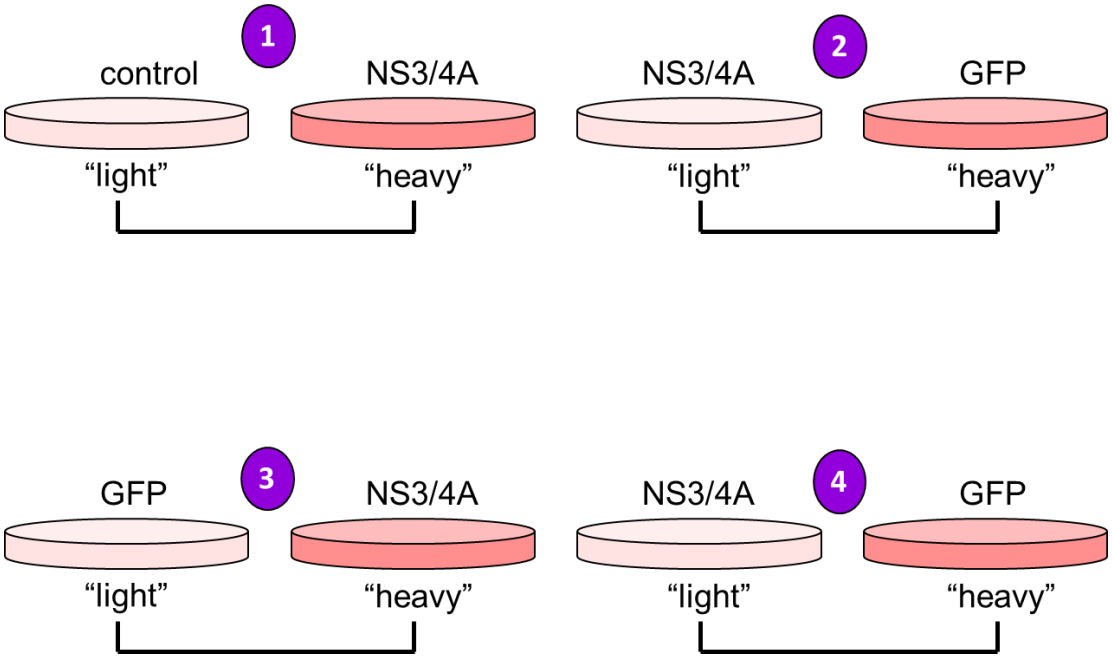

Figure 9. Experimental replicate design for NS3/4A proteomic analysis. A total of four SILAC replicates were analyzed, two replicates in which GFP expressing cells were grown in 'light' SILAC media and NS3/4A expressing cells were grown in 'heavy' SILAC media (1 and 3). The other two replicates were label swapped so GFP expressing cells were grown in 'heavy' SILAC media and NS3/4A expressing cells were grown in 'light' SILAC media (2 and 4).

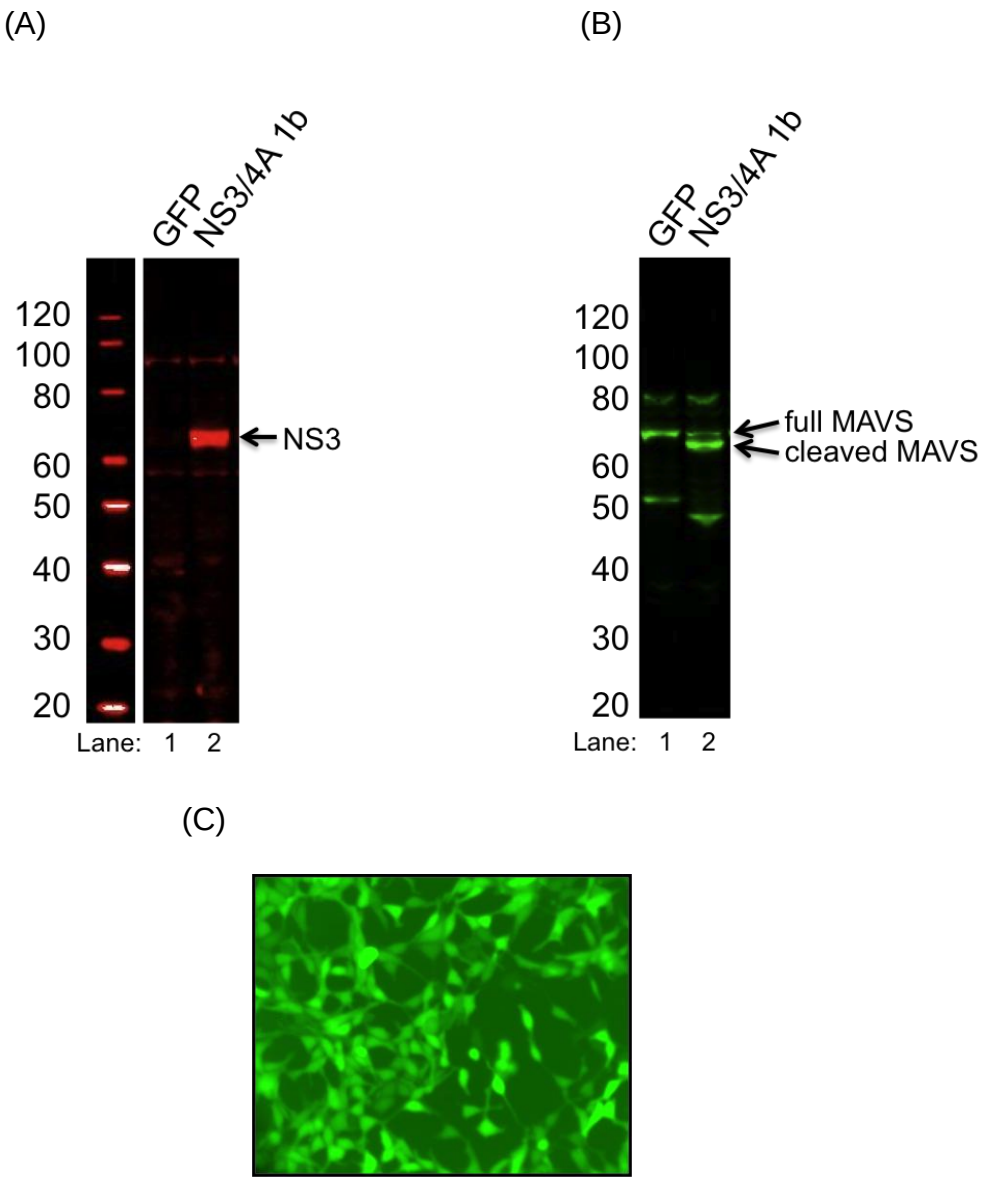

Figure 10. Stable NS3/4A and GFP protein expression. Protein lysates from GP2 293 cells expressing GFP and NS3/4A, used in subsequent SILAC experiments, were electrophoresed on an SDS-PAGE gel, transferred to nitrocellulose, and subjected to western blot analysis. Proteins were detected by primary antibodies to NS3 or MAVS and detected by secondary infrared labeled antibodies and imaged by LiCor infrared imaging. Western blots were probed with (A) an NS3 antibody (70 kDa) and (B) a MAVS antibody (70kDa full length, 68 kDa cleaved). (C) GP2 293 stable cells expressing GFP were imaged by fluorescent microscopy using a fluorescent filter set for GFP excitation/emission. Molecular weight markers are indicated in kDa.

before harvest, and all cell lines expressing GFP demonstrated green fluorescence when observed by fluorescence microscopy compared to cells not expressing GFP (Figure 10C).

Once it was determined that NS3/4A 1b was functional and that GFP was expressed in GP2 293 cells, lysates were mixed at a 1:1 ratio of total protein and digested into peptides by the serine protease trypsin (Figure 11). Peptides were then separated into 24 fractions via isoelectric focusing (IEF) in order to decrease sample complexity (Figure 11). Previously it was observed that unique peptides appear to concentrate in certain fractions rather than others (112). To see if this occurred in the GP2 293 cell line, a 1:1 mixed sample of NS3/4A and GFP SILAC peptides were separated by IEF and the number of total and unique peptides for each fraction was determined by mass spectrometry (Table 1). While typically over 1000 total peptides were detected in each fraction, they were not all unique to that fraction (Figure 12). More than 60% of peptides found in F01 to F05, F15, and F16 were identified as unique to each fraction, while the remaining fractions contained fewer than 40% unique peptides. To decrease the number of samples processed and machine time required the 24 fractions from each experiment were pooled into 12 fractions containing comparable amounts of unique peptides, between 690 and 1400 peptides (Table 1). F06, F07, and F08 were pooled into PF06; F09 and F10 were pooled into PF0 7; F11, F12, F13, and F14 were pooled into PF08; F17, F18, F19, F20, and F21 were pooled into PF11; and F22, F23,

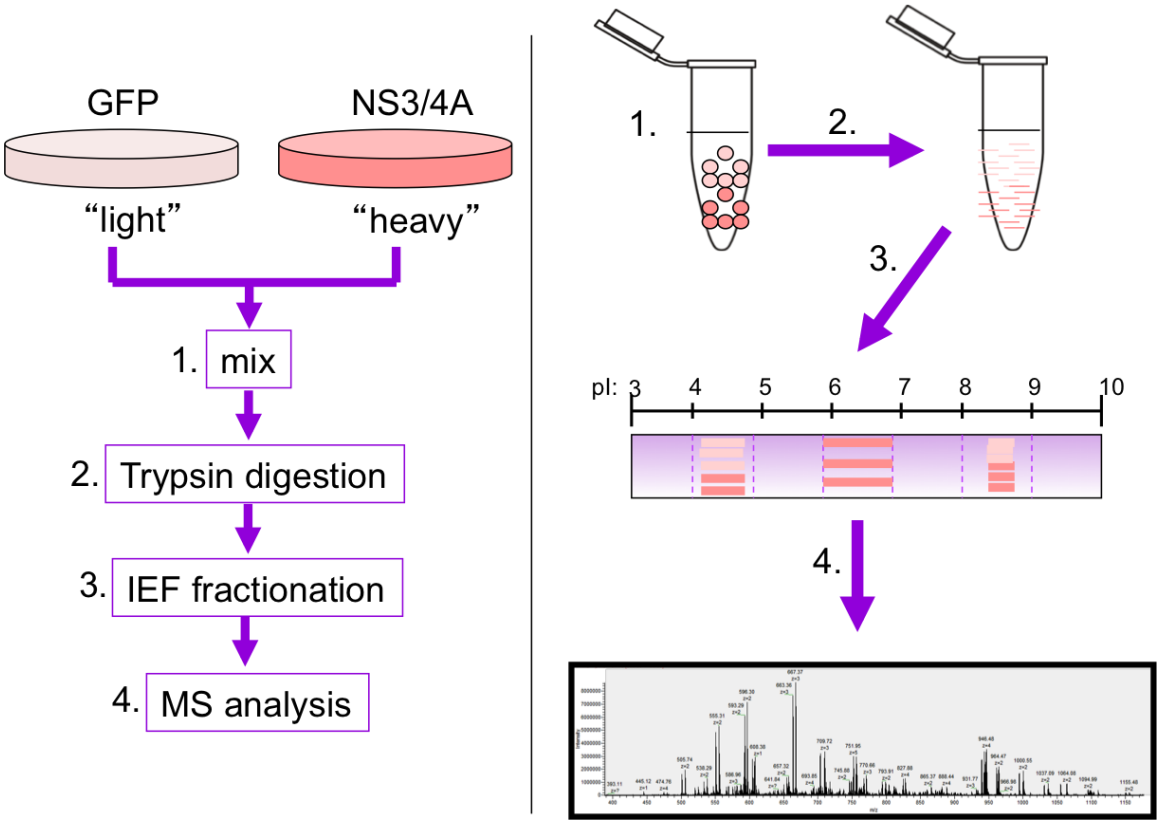

Figure 11. Flowchart and pictoral representation of SILAC methodology. GP2 293 cells stably expressing NS3/4A 1b and GFP were grown in “light” and “heavy” SILAC media for 10 days. Cells were then (1) lysed and mixed, (2) digested into peptides by trypsin, (3) fractionated by isoelectric focusing, and then (4) each fraction was analyzed by mass spectroscopy to identify and quantify SILAC peptides.

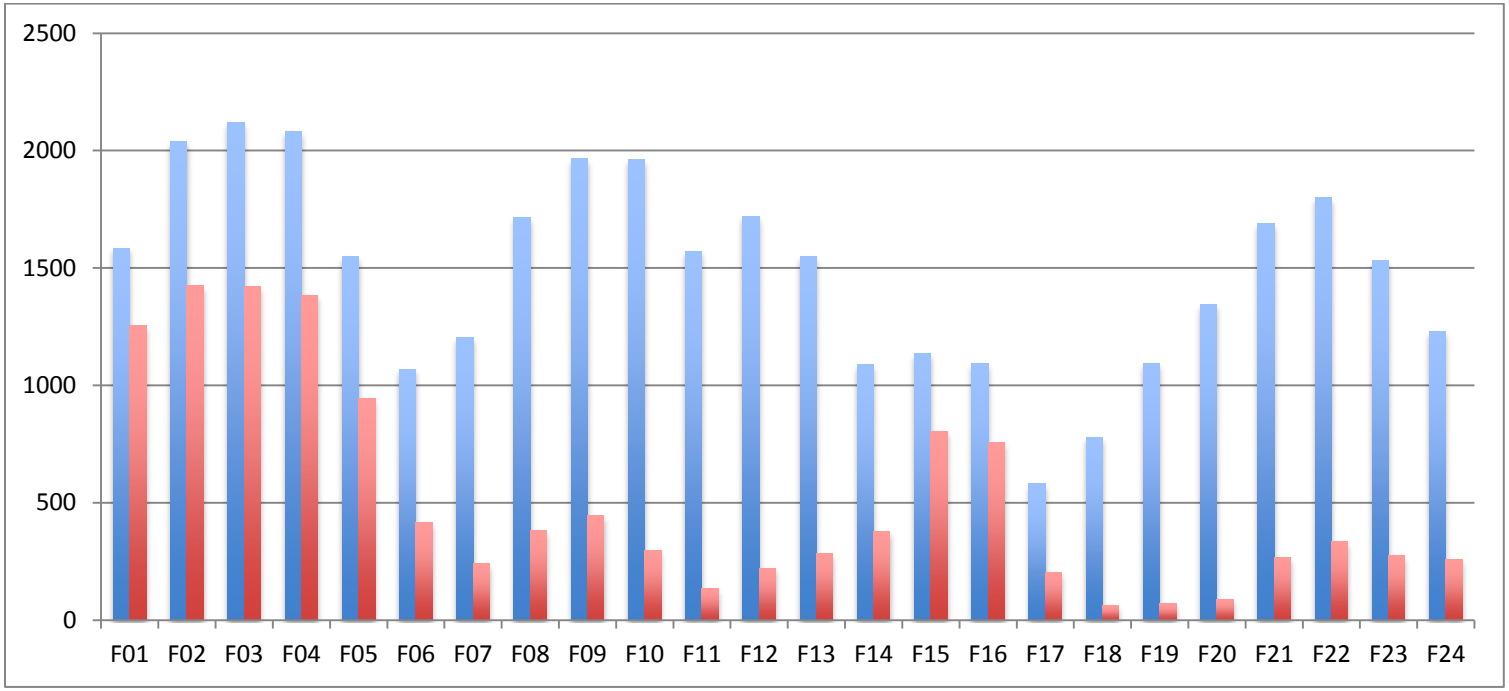

Figure 12. Distribution of total and unique peptides identified by MaxQuant following isoelectric focusing (IEF) and mass spectrometry. Each bar indicates the amount of peptides detected in each of 24 fractions; blue bars represent total peptides detected in that fraction, while red bars represent the unique peptides detected solely in that fraction.

Table 1. Distribution of peptides by IEF. The number of total and unique peptides found in each of 24 IEF fractions were determined and pooled into 12 fractions to give approximately 1000 unique peptides per fraction.

Fraction	Total Peptides	Unique Peptides	% Unique	Pooled Unique Peptides	
F01	1585	1257	79	(PF01)	1257
F02	2038	1427	70	(PF02)	1427
F03	2121	1423	67	(PF03)	1423
F04	2083	1384	66	(PF04)	1384
F05	1549	944	61	(PF05)	944
F06	1069	417	39	(PF06)	1042
F07	1205	242	20		
F08	1713	383	22		
F09	1965	445	23	(PF07)	740
F10	1960	295	15		
F11	1572	136	9	(PF08)	1021
F12	1719	222	13		
F13	1550	285	18		
F14	1088	378	35		
F15	1135	805	71	(PF09)	805
F16	1094	758	69	(PF10)	758
F17	581	205	35	(PF11)	694
F18	777	64	8		
F19	1094	70	6		
F20	1343	89	7		
F21	1690	266	16		
F22	1801	336	19	(PF12)	869
F23	1530	275	18		
F24	1231	258	21		

and F24 were pooled into the PF12 (Table 1). All other fractions were left unchanged.

3.4. Differentially Regulated Proteins

Following mass spectrometry of all four experiments, the resulting data was analyzed using the quantitative proteomics software MaxQuant, which was specifically designed for SILAC-based proteomics experiments. MaxQuant takes the initial spectra (MS1) to detect SILAC pairs and then matches the corresponding MS2 peptide fragment spectra to a database of all known human proteins sequences. The resulting identified peptides were then assembled into protein identifications, and protein ratios were determined for SILAC pairs.

After combining the four experiments, a total of 74,224 peptides were detected at a false discovery rate (FDR) of 0.01, resulting in 6133 protein identifications also at an FDR of 0.01. Protein identifications were accepted when at least two peptides matched a reference protein sequence in the IPI database, with at least one of those peptides being unique to that protein. One hundred and thirty four of these identified proteins were considered common contaminants (keratin and trypsin for instance) or reverses (matched to the IPI database reversed sequences), and were therefore discarded. In total, 3820 of the identified proteins were seen in at least three of the four experiments and these were used for further statistical analysis. Appendix Table A3 contains experimental ratios. The data distribution was analyzed to determine whether parametric or non-

parametric testing was possible. The $\log_2$ ratios of the normalized total identified proteins were plotted against the frequency of each ratio for each of the four experiments (Figure 13). Each experiment demonstrated a normal distribution; therefore a Student's t-test was applied to compare the protein abundances from NS3/4A expressing cells and control GFP expressing cells. A Benjamini-Hochberg false discovery rate of 0.15 was also applied to the data. Proteins that had corrected p-value less than 0.05 and greater than a 30% ratio change were deemed of interest. A 30% ratio change was used since this ratio could be detected by confirmation by western blot analysis. Of the 3820 proteins, 23 fit these criteria including 10 upregulated proteins and 13 downregulated proteins in NS3/4A versus GFP expressing cells (Figure 14). The proteins identified included PTGR1, PSMD5, OXCT, PRPH, BNIP1, DHCR24, and others (Tables 2 and 3).

Candidates for further study were chosen from the list of differentially regulated proteins (Tables 2 and 3). The proteins were ranked by $\log_2$ ratios, and the top 2 upregulated proteins and the top downregulated protein were chosen for further analysis. From the list of upregulated proteins, 15-oxoprostaglandin 13-reductase (PTGR1) had the highest ratio of 1.53 with an associated corrected p-value of 3.11×10^{-3}, and 26S protease subunit S5 basic (PSMD5) had the second highest fold change of 1.21 with a corrected p-value of 1.78×10^{-3} (Table 2). From the list of downregulated proteins, peripherin (PRPH) had a fold change of -0.86 with a corrected p-value of 4.25×10^{-2} (Table 3). The majority of identified proteins were not deregulated, however GFP and NS3/4A were detected in all experimental

(A) (B)

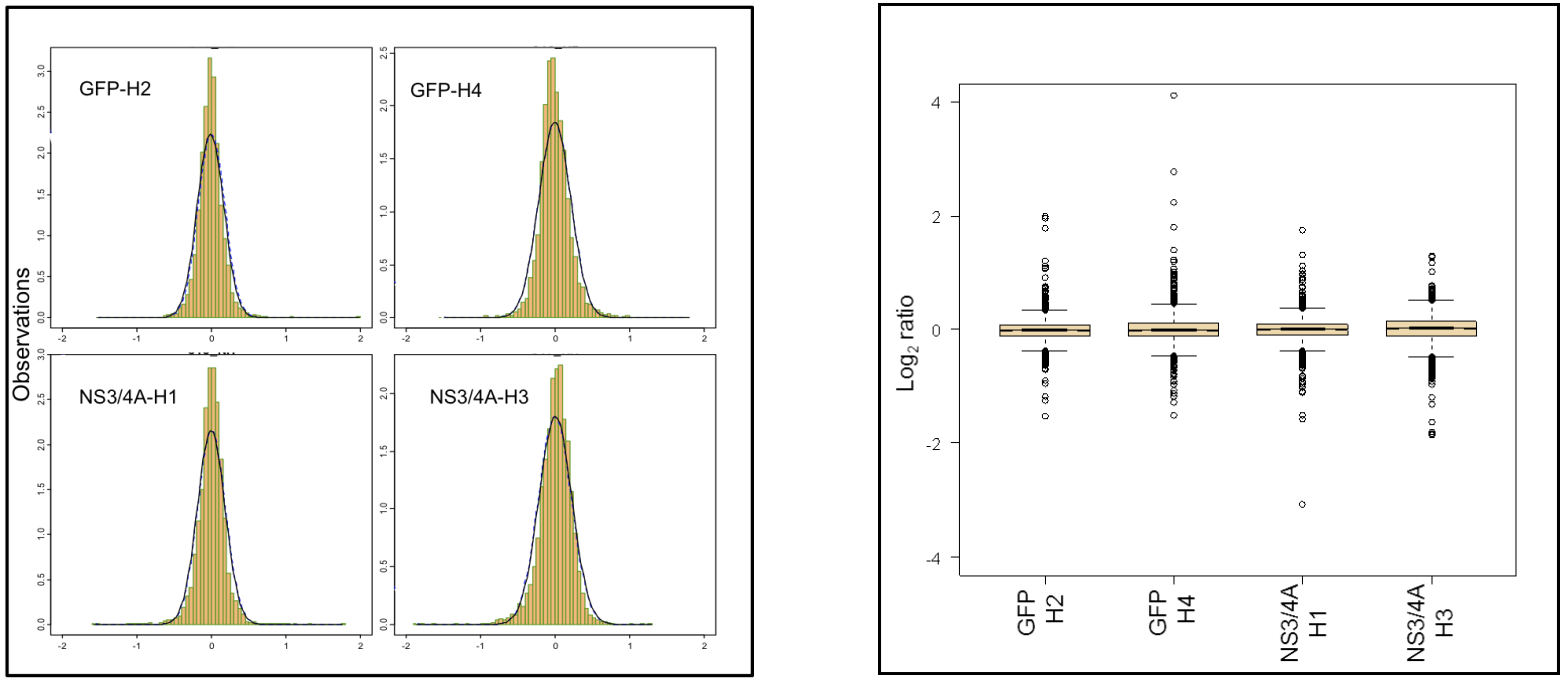

Figure 13. Distribution of protein ratios for SILAC experiments. Log_2 ratios (NS3/4A/GFP) for digested proteins from all four replicates were calculated and normalized. (A) Resulting protein ratio observations were binned with a normal distribution curve drawn for comparison. (B) Peptide ratios were also plotted with box plots with each experimental replicate along the x-axis and log_2 ratios along the y-axis. NS3/4A was heavy labeled in experiments 1 and 3, and light labeled in experiments 2 and 4.

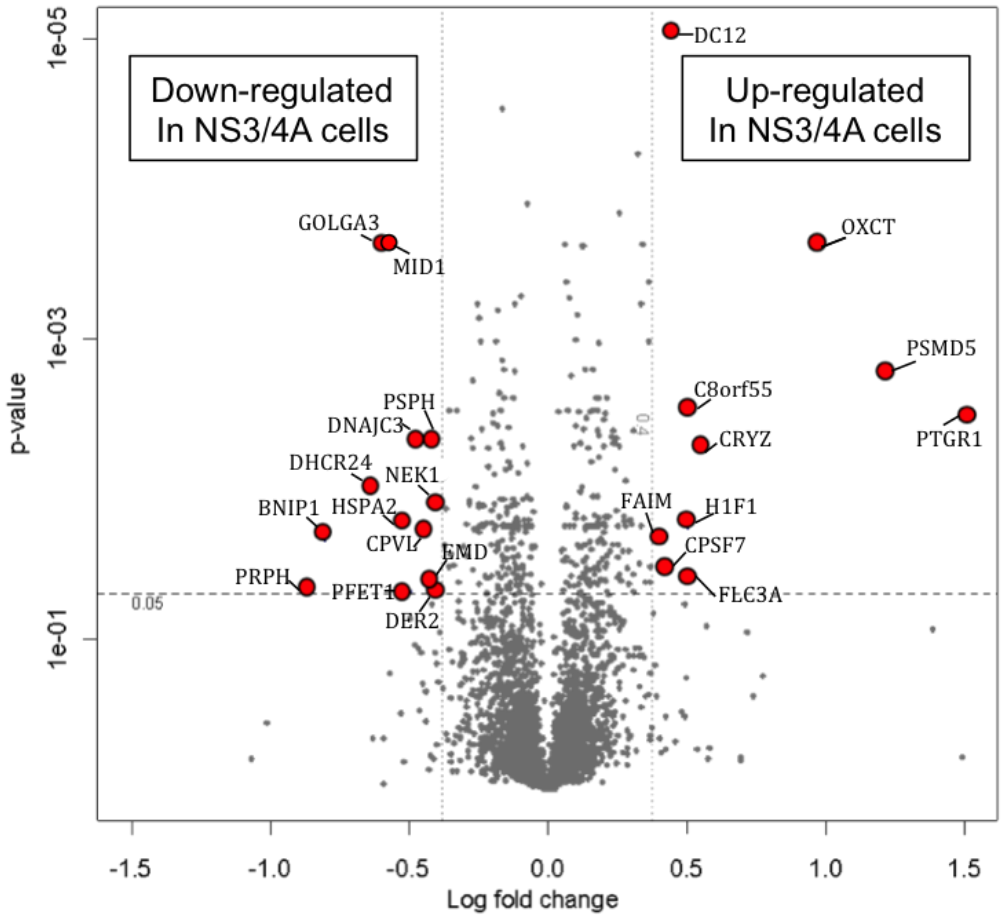

Figure 14. Volcano plot of ratios for NS3/4A/GFP expressing cell line proteins. Identified proteins with ratios from at least three replicates were combined and plotted with $\log_2$ ratios along the x-axis and p-values along the y-axis. Proteins with a $\log_2$ fold change above 0.4 or below -0.4 and a p-value less than 0.5 are plotted in red and considered differentially regulated upon NS3/4A expression. Gene names are indicated.

Table 2. Differentially up-regulated proteins upon NS3/4A expression. Gene name, protein name, function, number of experiments seen in, log_2 ratio, and p-value of up-regulated proteins in GP2 293 cells expressing NS3/4A.

Gene Name	Protein Name	Function	Count	Ratio (Log_2)	p-value
PTGR1	15-oxoprostaglandin 13-reductase	Leukotriene metabolism	4	1.53	3.11E-03
PSMD5	26S protease subunit S5 basic	Proteasome chaperone	3	1.22	1.78E-03
OXCT	3-oxoacid-CoA transferase 1	Ketone catabolism	4	0.98	2.43E-04
CRYZ	NADPH:quinone reductase	Cellular respiration	4	0.55	4.96E-03
H1F1	Histone H1.1	Nucleosome condensation	4	0.51	1.77E-02
C8orf55	Mesenchymal stem cell protein DSCD75	Thioesterase	4	0.49	3.01E-03
FLC3A	GABA(A) receptor-associated protein-like 2	Intra-golgi transport	4	0.49	3.72E-02
DC12	UPF0361 protein C3orf37	Uncharacterized	3	0.45	8.78E-06
CPSF7	Cleavage and polyadenylation specificity factor 59 kDa subunit	Pre-mRNA processing	4	0.43	3.31E-02
FAIM	Fas apoptotic inhibitory molecule 1	Anti-apoptotic	4	0.4	2.17E-02

Table 3. Differentially down-regulated proteins upon NS3/4A expression. Gene name, protein name, function, number of experiments seen in, log_2 ratio, and p-value of down-regulated proteins in GP2 293 cells expressing NS3/4A.

Gene Name	Protein Name	Function	Count	Ratio (Log_2)	p-value
PRPH	Peripherin	Intermediate filament	4	-0.86	4.25E-02
BNIP1	BCL2/adenovirus E1B 19 kDa protein-interacting protein 1	Anti-apoptotic	4	-0.8	2.16E-02
DHCR24	24-dehydrocholesterol reductase	Cholesterol biosynthesis	3	-0.64	9.52E-03
GOLGA3	Golgi complex-associated protein of 170 kDa	Golgi structure	4	-0.6	2.43E-04
MID1	Midin	E3 ubiquitin ligase activity	3	-0.59	2.43E-04
HSPA2	Heat shock-related 70 kDa protein 2	Stress-induced chaperone	4	-0.51	1.65E-02
PFET1	Pfetin	G-protein signalling	4	-0.5	4.89E-02
DNAJC3	DnaJ homolog subfamily C member 3	ER stress	4	-0.44	4.71E-03
CPVL	Carboxypeptidase, vitellogenic-like	Peptidase	4	-0.44	1.79E-02
PSPH	L-3-phosphoserine phosphatase	Serine biosynthesis	4	-0.42	4.71E-03
NEK1	Never in mitosis A-related kinase 1	Cell cycle regulation	3	-0.4	1.34E-02
EMD	Emerin	Membrane anchorage	4	-0.4	3.93E-02
DER2	Degradation in endoplasmic reticulum protein 2	Glycoprotein degradation	3	-0.39	4.39E-02

sets in which they were expressed at the appropriate deregulation, but were excluded from the comparison list.

3.5. Confirmation of Mass Spectrometry Data

3.5.1. Western Blot

Although mass spectrometry data has been shown to produce good relative quantification, it is based on peptide not protein data. Abundance changes of the candidate proteins were analyzed by western blot in an attempt to confirm the mass spectrometry data at the protein level. Figure 15 shows a typical result of testing these antibodies against NS3/4A 1b expressing cells, GFP expressing control cells, and GP2 293 control cells. One PTGR1 antibody detected multiple bands in all cell lysates, but did not detect the expected ~36kDa protein (Figure 15A, lanes 1-3). A peripherin (PRPH) antibody was expected to detect a band ~57kDa; however no feature was visible (Figure 15B, lanes 1-3). Multiple bands were also detected with the PSMD5 antibody, but not at the expected ~56kDa protein size (Figure 15C, lanes 1-3). Antibodies to actin and GAPDH were used as loading and quality controls and the 42kDa and 37kDa proteins were detected in all lanes in equal amounts, respectively (Figure 15D and E, lanes 1-3). Several antibodies targeting PTGR1 were evaluated, and finally one was found that detected a 36kDa band, however, there was no apparent fold change in this protein expression between NS3/4A 1b expressing cells and GFP expressing cells in comparison to the actin load control (Figure 16).

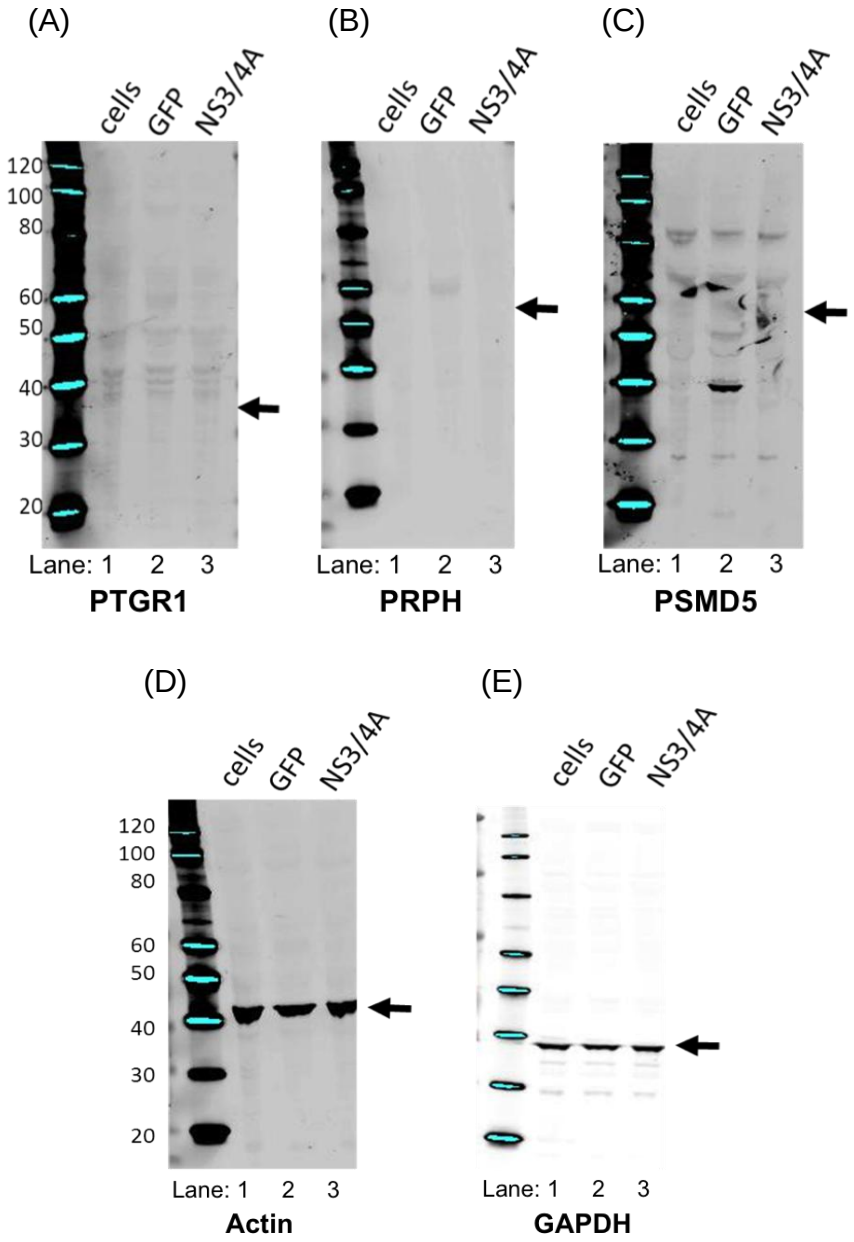

Figure 15. Western blot analysis of candidate protein expression from SILAC experiments. Protein lysate from GP2 293 cells, cells expressing GFP, and cells expressing NS3/4A 1b were electrophoresed on an SDS-PAGE gel, transferred to nitrocellulose, and probed with antibodies to the following candidate proteins: (A) PTGR1 (36 kDa), (B) PRPH (54 kDa), (C) PSMD5 (56 kDa), and the load controls (D) actin (42 kDa), and (E) GAPDH (37kDa). Indirect detections were performed with the LiCor infrared imager. Arrows indicate expected positions for each protein. Molecular weight markers are indicated in kDa.

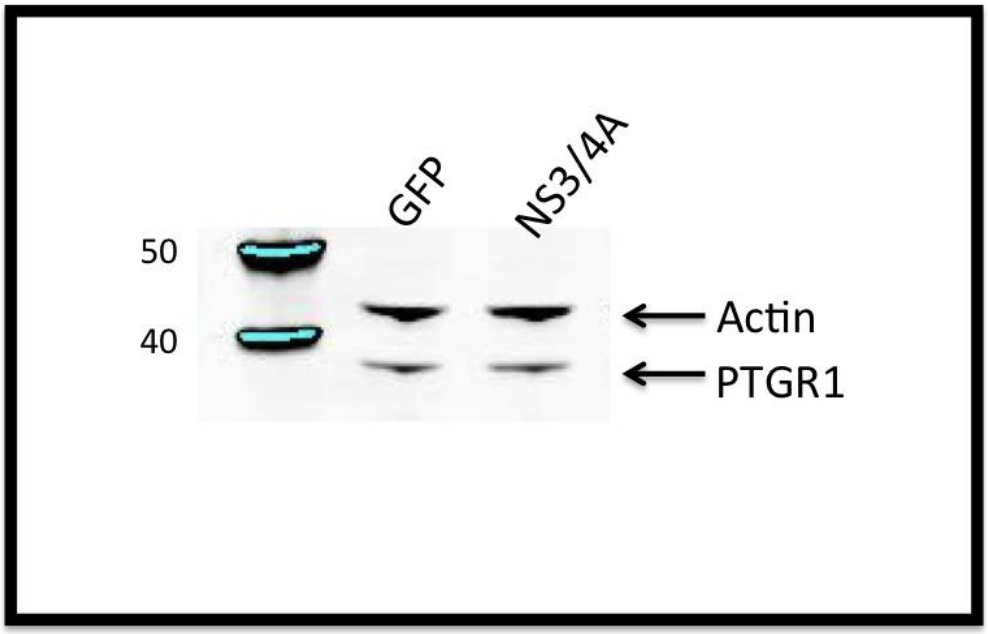

Figure 16. PTGR1 protein amounts as evaluated by western blot. Cell lysate from GP2 293 cells expressing GFP and NS3/4A were electrophoresed through an SDS-PAGE gel, transferred to nitrocellulose, probed with an actin antibody and an antibody against PTGR1, and imaged through LiCor infrared imaging. Molecular weight markers are indicated in kDa.

3.5.1.1. Antibody Quality

Unexpectedly, the western blot did not confirm the most degregulated protein found by mass spectrometry, PTGR1. Using PTGR1 as a model, we set to investigate why there were differences in the western blot data as compared to the mass spectrometry data. To ensure the PTGR1 antibody detection was emitting in a linear fashion, a series of protein lysate dilutions were run on SDS-PAGE and probed with the PTGR1 (36kDa) and actin (42kDa) antibody (Figure 17A). The blot was imaged and bands were quantified by the LiCor software and then plotted against amount of total protein in each band (Figure 17B). Fluorescent units for each dilution are as follows: $5.0x10^5$ and $3.4x10^5$ at 10ug/ul, $1.3x10^6$ and $6.0x10^5$ at 20ug/ul, $3.4x10^6$ and $1.1x10^6$ at 40ug/ul, and $4.2x10^6$ and $1.5x10^6$ at 50ug/ul for actin and PTGR1, respectively (Figure 17B). Both antibodies behaved linearly and did not reach saturation at the concentrations used in previous western blots, therefore, the antibody detection was not masking a true protein deregulation.

3.5.1.2. Candidate Protein Overexpression

Next, given the problems previously assessed, to ensure the antibodies used were targeting the correct proteins, expression constructs were made for either PTGR1 or peripherin (PRPH). These plasmids were transiently transfected into GP2 293 cells, protein lysate was harvested 48 hours later, and western blots probed for with the appropriate antibody. Figure 18A presents the resulting

(A)

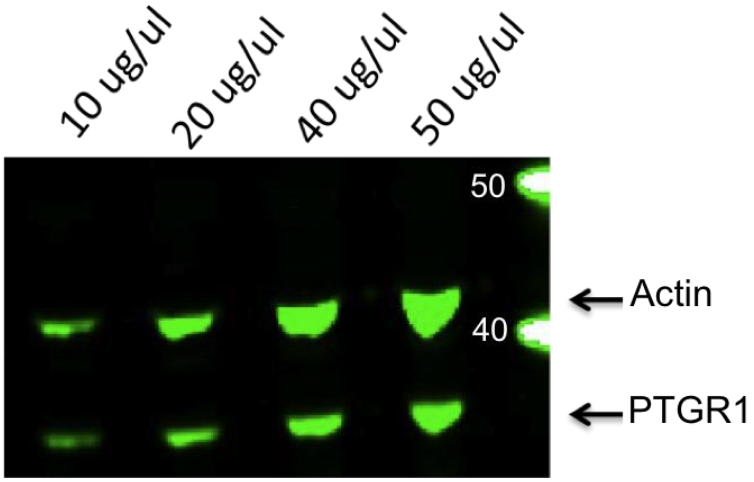

(B)

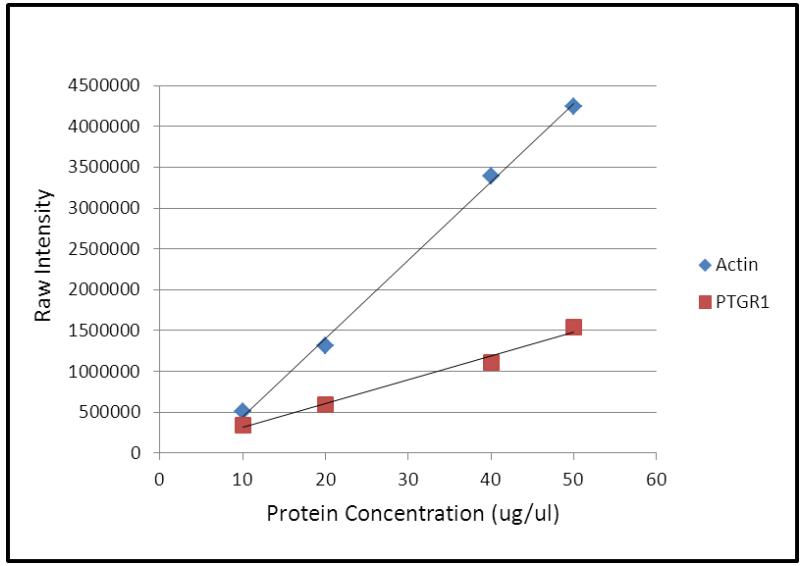

Figure 17. Actin and PTGR1 antibody western blot analysis for linearity. GP2 293 protein lysates were loaded onto an SDS-PAGE gel in varying dilutions (50 ug, 40 ug, 20 ug, and 10 ug total lysate), transferred to nitrocellulose, probed with actin and PTGR1 antibodies, and imaged by LiCor infrared imaging. (A) Actin and PTGR1 antibodies detected bands at 42kDa and 36kDa as expected. (B) The intensity of each band was plotted within the dilution series; blue diamonds representing actin, and red squares representing PTGR1. Molecular weight marker is shown to the right of (A) in kDa.

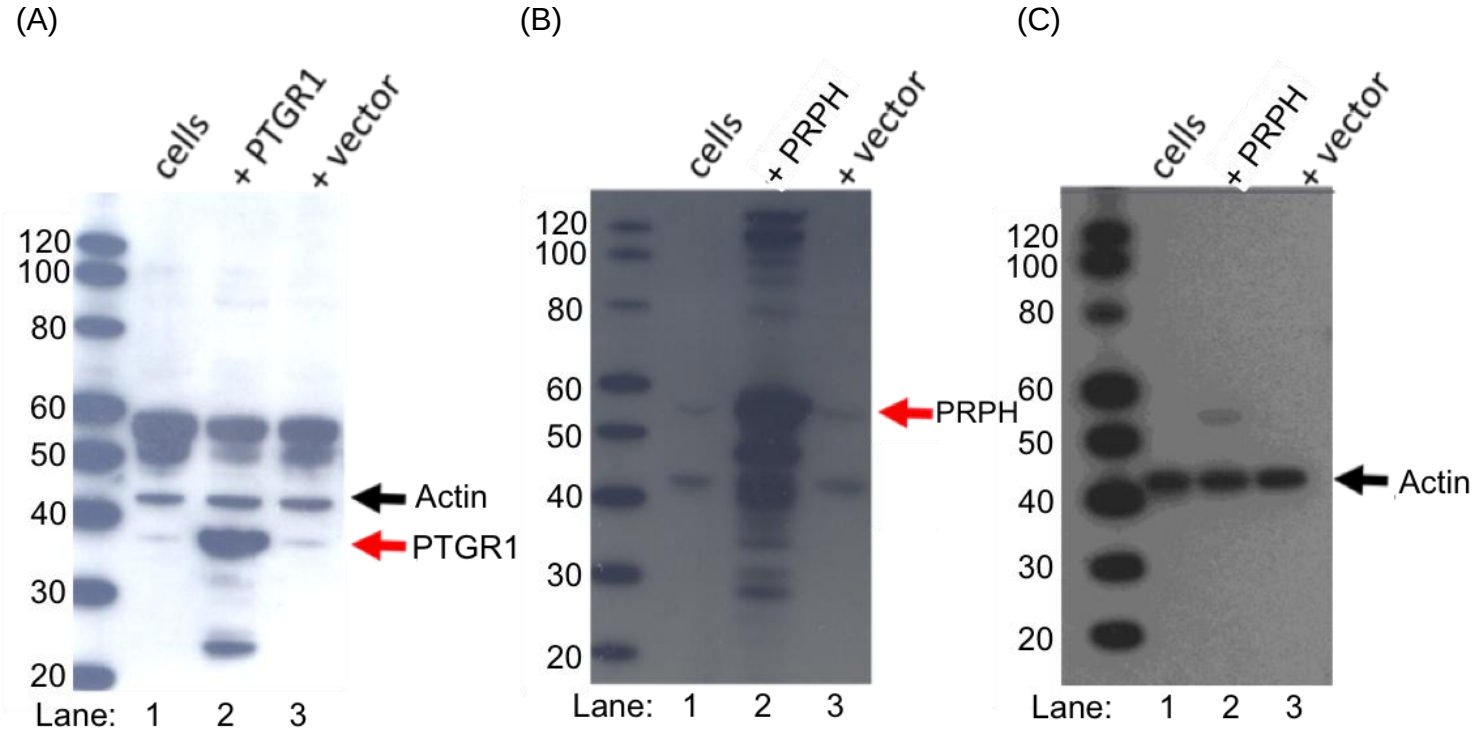

Figure 18. Overexpression of PTGR1 and peripherin (PRPH) proteins. PTGR1 and PRPH genes were cloned into pQCXIH vectors and transiently transfected into GP2 293 cells. 48 hours post transfection, cell lysate was loaded on an SDS-PAGE gel. (A) GP2 293 cell lysates, along with lysates from cells transfected with PTGR1 and vector control were probed with a PTGR1 and actin antibody and imaged on X-ray film. Actin was detected at 42kDa (black arrow) and PTGR1 was detected at 36kDa (red arrow). As well, GP2 293 cell lysates and lysates from cells transfected with PRPH and vector alone were probed with (B) a PRPH antibody and (C) an actin antibody then imaged by horseradish peroxidase (HRP) with X-ray film. PRPH was detected at 56kDa (red arrow), while actin was detected at 42kDa (black arrow). Molecular weight markers are indicated in kDa.

western blot when cell lysates from GP2 293 cells transfected with the PTGR1 construct, vector alone, or cells only were probed with a PTGR1 and actin antibody. The actin band at 42kDa demonstrates equal loading, and while a band at 36kDa, which is the predicted size for PTGR1, was seen in all lanes, it was markedly increased in the PTGR1 transfected lane (Figure 18A, lane 2) but not in cells only (lane 1) or vector only (lane 3). Similarly, GP2 293 cells transfected with the peripherin construct displayed a 56kDa band compared to lanes containing the vector control and cells only (Figure 18B, lane 2). Because of the potential for overload, the actin band at 42kDa shows equal loading (Figure 18C). Endogenous peripherin was also faintly detected in cell and vector control lanes (Figure 18B, lanes 1 and 3). These results suggest that both the PTGR1 and peripherin antibodies could detect the correct expressed proteins and differences in expression levels should be apparent if present.

3.5.2. PTGR1 Sequence Data Analysis

To ensure the mass spectrometry data was correct, all the peptide data on the PTGR1 protein identification and quantification was manually reassessed in depth. One possibility was that the protein was truncated or differentially degraded and that the mass spectrometry data corresponded to only one portion of the protein. Therefore, the peptide sequences identified for PTGR1 by mass spectrometry were mapped to the total protein sequence of PTGR1. However, the peptides were distributed throughout the entire protein, therefore this was

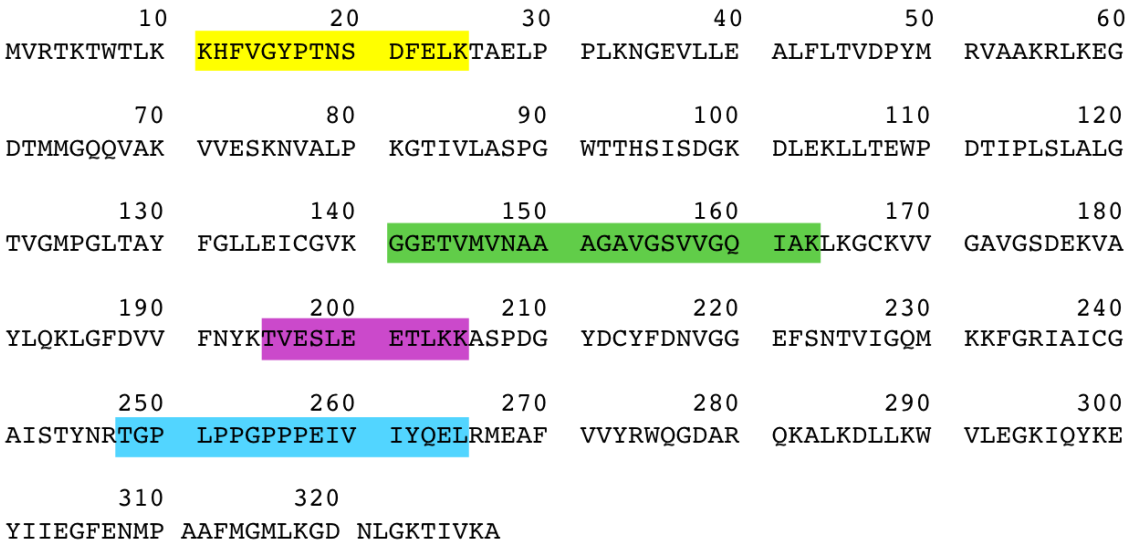

Figure 19. Peptides identified by MaxQuant for the PTGR1 sequence. PTGR1 peptides identified by mass spectrometry are highlighted. Four peptide sequences were identified in total, each being identified various times in each replicate. Yellow and blue peptides were detected once; the green peptide was seen four times; and the purple peptide was seen 11 times.

probably not the case (Figure 19). Another possibility was that the identified peptides had a large variance in measured ratios and the presented average was not representative. To check this, each PTGR1 peptide identified in all four SILAC experiments were graphed with their $\log_2$ ratios of NS3/4A expressing cells/GFP-expressing cells. In total, four peptide sequences for PTGR1 were identified 17 times, each in varying amounts (Figure 20). The peptides were distributed with a $\log_2$ ratio above 0.84 or below -1.06, with the former belonging to experiments in which NS3/4A was 'heavy' labeled and the latter belonging to experiments where NS3/4A was 'light' labeled. This led us to believe that the variance was not the reason for the discrepancy.

Although all peptides and proteins were only accepted with an FDR of 0.01, we wished to determine if another possibility for the discrepancy between the protein and peptide data was that the peptide-spectrum was matched to a protein incorrectly. Therefore we examined the posterior error probability (PEP). The PEP indicates a statistical measure of the identification bias error. The peptide KHFVGYPTNSDFELK was seen once with a $\log_2$ ratio of 1.65, a PEP score of 0.37 and seen only when NS3/4A was 'heavy' labeled. The peptide GGETVMVNAAAGAVGSVVGQIAK was seen three times in experiments where NS3/4A was 'light' labeled with $\log_2$ ratios of -1.73, -1.83, and -2.02, corresponding to PEP scores of 3.2×10^{-46}, 1.3×10^{-18}, and 6.7×10^{-22}, respectively. This peptide was also seen once in an NS34/A 'heavy' labeled experiment with a

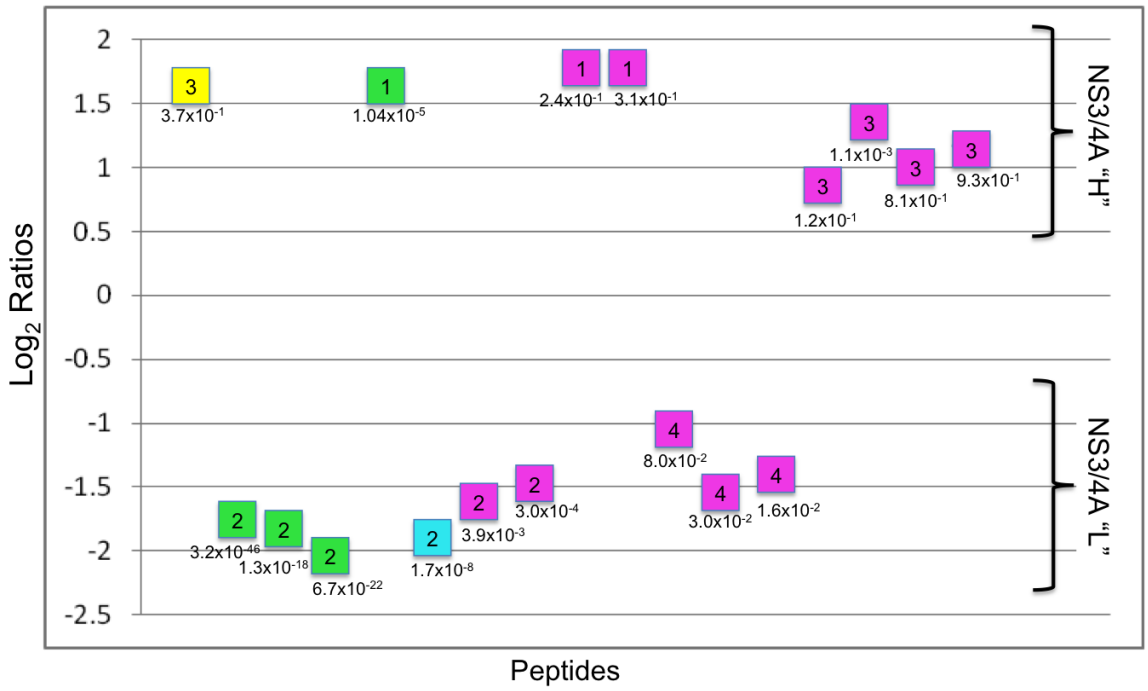

Figure 20. Distribution of PTGR1 peptide $\log_2$ ratios. Each observation of the four identified PTGR1 peptides were plotted with respective $\log_2$ ratios along with posterior error probability (PEP) scores. Peptides with a positive $\log_2$ ratio were found in experiments where NS3/4A expressing cells were grown in "heavy" SILAC media, and those with a negative $\log_2$ ratio were found when NS3/4A expressing cells were grown in "light" SILAC media. Experiments from which peptides were seen are indicated in corresponding squares, with the number inside each box corresponding to the experiment number. Individual colours correspond to peptide sequences indicated in Figure 19.

$\log_2$ ratio of 1.60 and a PEP score of 1.04×10^{-5}. The peptide TGPLPPGPPPEIVIYQEL was seen once in an NS34/A 'light' labeled experiment with a $\log_2$ ratio of -1.87 and an associated PEP score of 1.7×10^{-8}. The peptide TVESLEETLK was observed a total of 11 times, 6 times in the NS3/4A 'heavy' experiments, and 5 times in the NS3/4A 'light' experiments. Those from the 'heavy' experiments had ratios of 1.77, 1.75, 0.84, 1.36, 0.97, and 1.18, with associated PEP scores of 0.24, 0.31, 0.12, 1.1×10^{-3}, 0.81, and 0.93, respectively. Those found in the 'light' experiment had ratios of -1.63, -1.44, -1.06, -1.56, and -1.40, with PEP scores of 3.9×10^{-3}, 3.0×10^{-4}, 0.08, 0.03, and 0.016, respectively. This was the expected ratio distribution of peptides identified in experiments where NS3/4A was "light" and "heavy" labeled, and therefore did not suggest difficulties with the overall mass spectrometry data.

3.5.3. PTGR1 Isoforms

A common concern with mass spectrometer data is that it identifies peptides, while western blots measure intact proteins. In the MaxQuant software, identified peptides are matched to one or more protein sequences containing that peptide, and the listed protein identification is actually the top match of a list of homologous proteins. To determine if there were PTGR1 isoforms, a list of other proteins matched with the peptides seen for PTGR1 was generated and shown in Figure 21 with colour coded peptides matched to Figure 19. PTGR1 (IPI00292657) was the top hit, however PTGR1 and PTGR1 isoform 2 (IPI00642248) contained all four of the identified proteins (Figure 21). An

IPI00292657 = PTGR1
SQ SEQUENCE 329 AA; 35870 MW; E121ADB7C5BD9CF8 CRC64;

MVRTKTWTLKKHFVGYPTNSDFELKTAELPPLKNGEVLLEALFLTVDPYMRVAAKRLKEGDTMMGQQVAKVVESKNV
ALPKGTIVLASPGWTTHSISDGKDLEKLLTEWPDTIPLSLALGTVGMPGLTAYFGLLEICGVKGGETVMVNAAAGAV
GSVVGQIAKLKGCKVVGAVGSDEKVAYLQKLGFDVVFNYKTVESLEETLKKASPDGYDCYFDNVGGEFSNTVIGQMK
KFGRIAICGAISTYNRTGPLPPGPPPEIVIYQELRMEAFVVYRWQGDARQKALKDLLKWVLEGKIQYKEYIIEGFEN
MPAAFMGMLKGDNLGKTIVKA

IPI00642248 = PTGR1 isoform 2
SQ SEQUENCE 301 AA; 32895 MW; BD24D01FD752BE62 CRC64;

MVRTKTWTLKKHFVGYPTNSDFELKTAELPPLKNGEVLLEALFLTVDPYMRVAAKRLKEGDTMMGQQVAKVVESKNV
ALPKGTIVLASPGWTTHSISDGKDLEKLLTEWPDTIPLSLALGTVGMPGLTAYFGLLEICGVKGGETVMVNAAAGAV
GSVVGQIAKLKGCKVVGAVGSDEKVAYLQKLGFDVVFNYKTVESLEETLKKASPDGYDCYFDNVGGEFSNTVIGQMK
KFGRIAICGAISTYNRTGPLPPGPPPEIVIYQELRMEAFVVYRWQGDARQKALKDLLKWVLEIKRENEED

IPI01013515 = Uncharacterized Protein
SQ SEQUENCE 177 AA; 19225 MW; ED970379BAD7D3E3 CRC64;

MPGLTAYFGLLEICGVKGGETVMVNAAAGAVGSVVGQIAKLKGCKVVGAVGSDEKVAYLQKLGFDVVFNYKTVESLE
ETLKKASPDGYDCYFDNVGGEFSNTVIGQMKKFGRIAICGAISTYNRTGPLPPGPPPEIVIYQELRMEAFVVYRWQG
DARQKALKDLLKWVLELPYFVID

IPI00164901 = Uncharacterized Protein
SQ SEQUENCE 119 AA; 13045 MW; 044F1B57F5A0E8DA CRC64;

MVRTKTWTLKKHFVGYPTNSDFELKTAELPPLKNGEVLLEALFLTVDPYMRVVESKNVALPKGTIVLASPGWTTHSI
SDGKDLEKLLTEWPDTIPLSLALGTVGMPGLTAYFGLLEICG

IPI00643630 = Uncharacterized Protein
SQ SEQUENCE 70 AA; 7983 MW; E77FF1214CF13142 CRC64;

MVRTKTWTLKKHFVGYPTNSDFELKTAELPPLKNGEVLLEALFLTVDPYMRVAAKRLKEGDTMMGQQVAK

Figure 21. PTGR1 protein group identified by MaxQuant software. The sequences of five proteins rolled up under the PTGR1 protein identification are shown with identified peptides highlighted. IPI numbers, as well as protein name, number of amino acids (AA), molecular weight (MW) are shown. Colours correspond to peptides seen in Figure 19.

uncharacterized protein (IPI01013515) was also identified as having three of the four peptides, and two other uncharacterized proteins (IPI00164901 and IPI00643630) contained one of the four peptides (Figure 21), therefore the mass spectrometer may be detecting the peptides of one of these other proteins. To determine if the lack of agreement between mass spectrometry to western blot was due to this possible isoform issue, an immunoprecipitation was attempted in order to enrich for the potential isoforms to see if there were any abundance changes in PTGR1 isoforms, as the epitope recognized by the antibody contained the purple peptide.

A resin containing immobilized protein A/G was used to enrich for proteins that bound the PTGR1 antibody, and the resulting elution is shown in Figure 22. The input protein, starting protein lysate prior to addition of antibody, contained PTGR1 as indicated by a band ~36kDa (Figure 22). However, isoforms of PTGR1 were not detected in the elution sample (Figure 22). The elution sample also had a large amount of band smearing primarily due to the presence of heavy and light chains detected by the secondary antibody, which impeded the interpretation of the blot. Therefore, this was not useful to enrich for isoforms and the mass spectrometer may have detected one of the other proteins and not PTGR1.

3.5.4. RT^2-PCR Candidate Transcript Analysis

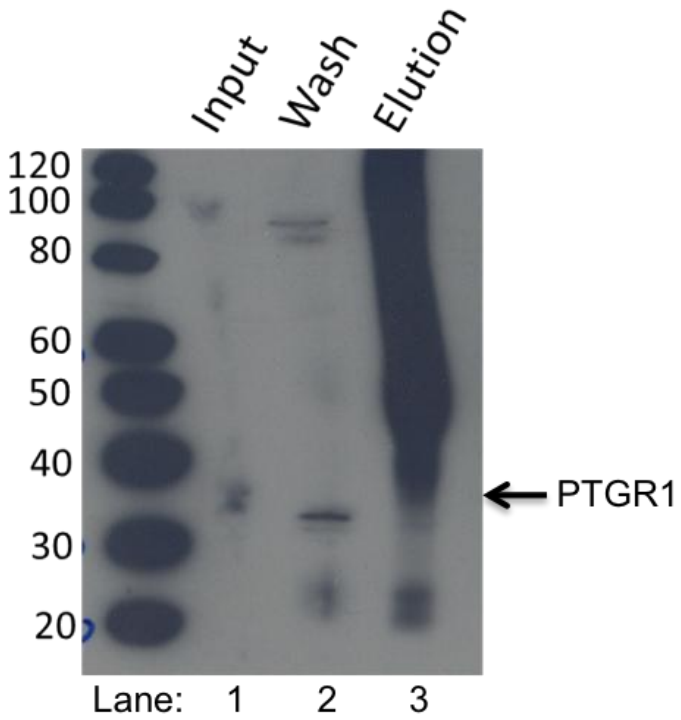

Figure 22. Immunoprecipitation of PTGR1 to identify isoforms. Protein lysate from GP2 293 cells expressing NS3/4A 1b was mixed with PTGR1 antibody and incubated with immobilized protein A/G resin. Resin was washed then protein was eluted with SDS. Input protein, protein removed by first wash, and eluted protein were loaded on an acrylamide gel, transferred to a nitrocellulose membrane, probed with the same PTGR1 antibody, and imaged by x-ray film. PTGR1 should be detected at 36kDa (arrow). Input (lane 1): starting material before complexed with antibody. Wash (lane 2): eluted material after first wash of resin bound with protein-antibody complex. Elution (lane 3): eluted protein with SDS. Arrow indicates expected migration of protein. Molecular weight markers are indicated in kDa.

Because of the difficulties in obtaining quality antibodies, real-time reverse transcriptase PCR (RT^2-PCR) was chosen as a secondary method of evaluating changes induced by NS3/4A with the caveat that there is often poor correlation between mRNA and protein data. Transcript levels for the top two up-regulated and top two down-regulated proteins were measured in NS3/4A expressing cell lines, GFP expressing cell lines, and control GP2 293 cell lines. The gene targets were PTGR1, PSMD5, NEF4, and BNIP1. Genomic DNA was monitored in each sample by omitting the reverse transcriptase, creating a no reverse transcriptase (NRT) control. As well, each primer set was processed without template cDNA to monitor DNA contamination, a no template control (NTC). No contamination was detected in the NRT or NTC controls.

The resulting data for each of the target genes in each cell line are presented in Figure 23, where the $\log_2$RQ (relative quantitation) was plotted for each target gene in each cell line with GAPDH used as an endogenous control and the GP2 293 cell sample used as the reference sample. In GFP expressing cells, PTGR1 had a $\log_2$RQ of -2.014, compared to a $\log_2$RQ of -1.95 for PTGR1 in NS3/4A expressing cells. Cells expressing GFP had a $\log_2$RQ of 0.467 for PRPH, compared to a $\log_2$RQ of 0.294 in NS3/4A expressing cells. For BNIP1, cells expressing GFP had a $\log_2$RQ of -0.825, while NS3/4A expressing cells had a $\log_2$RQ of -0.392. Cells expressing GFP had a $\log_2$RQ of -1.922 for PSMD5, compared to a $\log_2$RQ of -1.786 in NS3/4A expressing cells. There were no

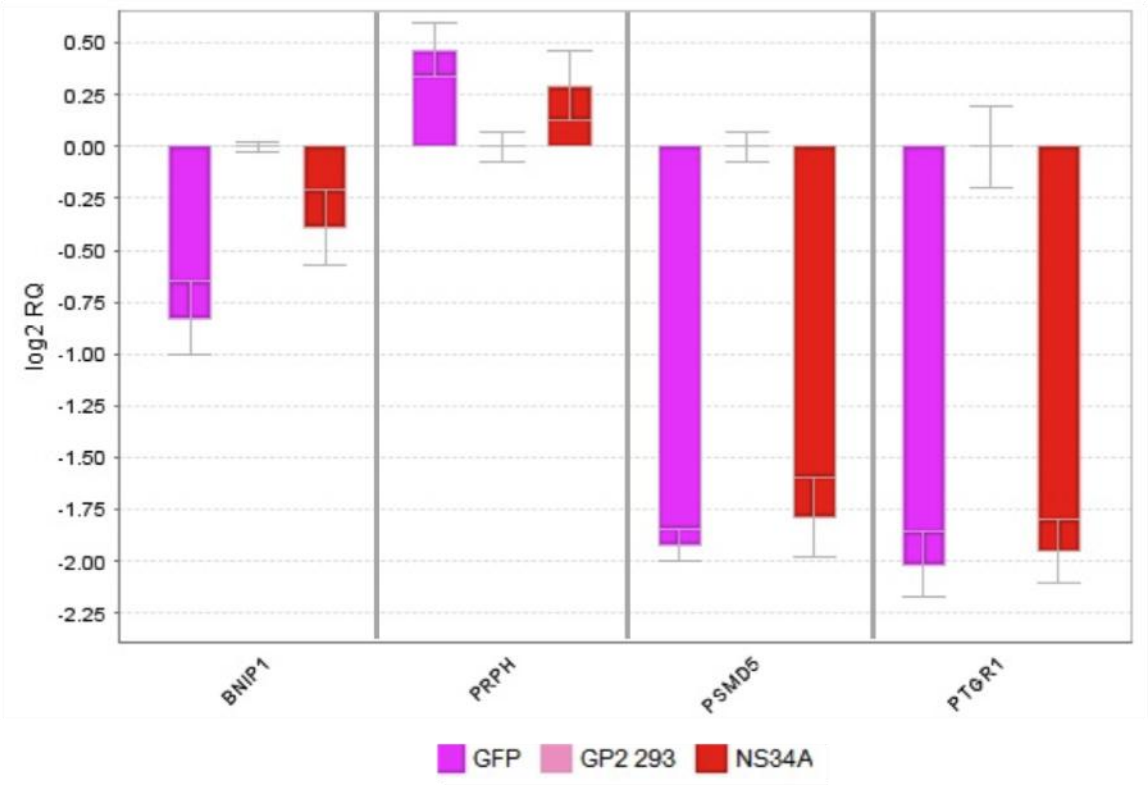

Figure 23. Graphical representation of $\log_2$ relative quantitation (RQ) for each target gene. Results are expressed as $\log_2$RQ from triplicate experiments. Dark pink bars represent results from GP2 293 cells expressing GFP; light pink bars represent results from GP2 293 cells; red bars represent results from GP2 293 cells expressing NS3/4A. GAPDH was used as an endogenous control, and GP2 293 as the reference sample.

significant changes in transcript level of the targets PRPH, PTGR1, and PSMD5 in GFP and NS3/4A expressing cells when compared to GP2 293 cells (Figure 23). However, for the BNIP1 target there was a slight decrease in transcript levels from NS3/4A expressing cells relative to GFP expressing cells, compared to GP2 293 cells. While this data did not corroborate the mass spectrometry data, it provided an important learning point to include many controls before interpreting data.

3.5.5. shRNA Expression Knock Down of NS3

Because the stable cell lines generated in this study have typically one integrated expression cassette per genome, we wondered if the level of NS3/4A expression was significantly lower than with transiently generated cell lines. As such, this could account for the lower level of protein deregulation seen with previous studies. Therefore, to gain a better understanding of the expression levels seen in NS3/4A and GFP expressing cells, knock down constructs targeting NS3/4A 1b were made. NS3 amounts were evaluated by western blot for each of the constructs. GP2 293 cells (Figure 24A, lanes 1 and 4) and GFP expressing cells (lanes 2 and 5) were used as negative controls, and demonstrated no NS3 expression (Figure 24A). NS3/4A expressing cells were shown to have a band at 70kDa (Figure 24A, lanes 3 and 6). NS3/4A expressing cells with the shRNA lentivirus vector (Figure 24A, lane 7) or NS3/4A cells with a shRNA targeting GFP (lane 8) did not effect NS3 expression. However, two shRNAs targeted to different regions of NS3/4A were able to markedly reduce NS3 levels (Figure

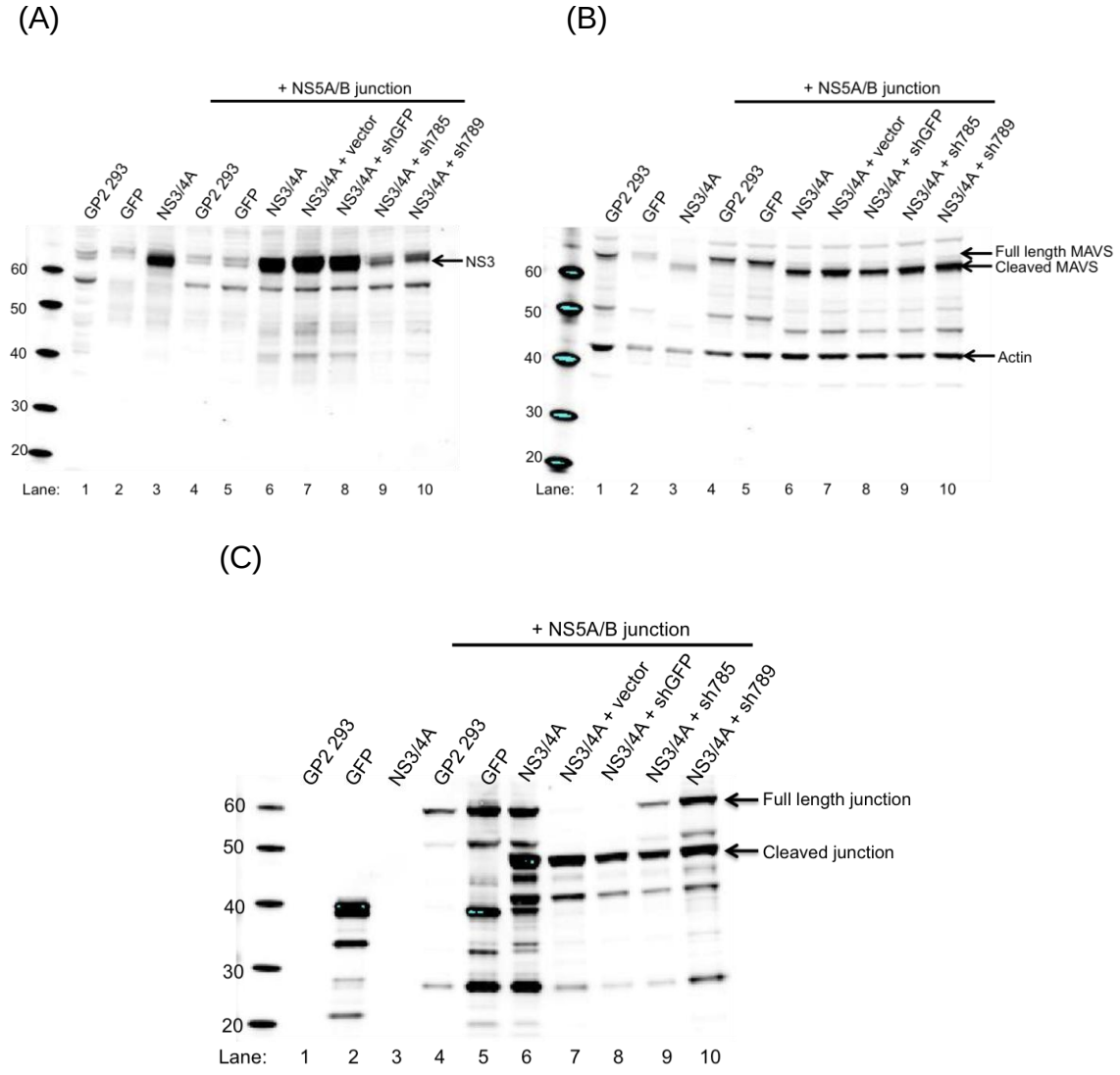

Figure 24. NS3/4A expression and function upon NS3 silencing. Western blots of protein lysates from GP2 293 cells, cells expressing GFP, cells expressing NS3/4A 1b, and cells expressing NS3/4A 1b with shRNAs targeted to NS3. Western blots were probed with antibodies to (A) NS3 at 70kDa, (B) MAVS at 70kDa or 68kDa for cleaved product with actin load control at 42kDa. Cells from lanes 4-10 were also transfected with the NS5A/B junction sequence, targeted by the NS3/4A protease, N-terminally tagged with GFP. (A) and (B) are the same western blot imaged in different infrared channels. (C) Western blot analysis probed with antibodies to GFP at 54kDa for full-length construct and 44kDa for cleaved product. Arrows indicate expected migration pattern for each protein.

24A, lanes 9 and 10). Therefore, these two shRNAs could be used for further study. MAVS expression was also monitored to determine whether reducing NS3 expression similarly reduced its proteolytic activity. Full length MAVS was seen in the negative controls GP2 293 and GFP (Figure 24B, lanes 1+4 and 2+5), while cleaved MAVS was detected in NS3/4A expressing cells (lanes 3+6). NS3/4A cells infected with the shRNA vector and the shRNA targeting GFP also demonstrated MAVS cleavage (Figure 24B, lanes 7 and 8). However, in NS3/4A expressing cells in which NS3 protein expression was greatly reduced, MAVS cleavage was still observed to similar levels as to the original NS3/4A expressing cells (Figure 24B, lanes 9 and 10).

It was unknown whether the continued MAVS cleavage with reduced amounts of NS3/4A was due to continued protease activity or the permanent stimulation of an NS3/4A induced pathway leading to constitutive MAVS cleavage. In order to test this possibility, the NS5A/B junction site from the HCV polyprotein was used as a substrate to monitor protease activity specific to NS3/4A. This construct was N-terminally tagged with GFP for detection by western blot analysis. Figure 24C demonstrates the results of transfection of cells with this construct. Full length NS5A/B was seen in the negative controls GP2 293 and GFP (Figure 24C, lanes 4 and 5), while cleaved NS5A/B was detected in NS3/4A expressing cells (lane 6), NS3/4A cells infected with the shRNA vector and the shRNA targeting GFP also demonstrated NS5A/B junction cleavage (Figure 24C, lanes 7 and 8).

However, NS5A/B junction cleavage was still maintained in NS3/4A expressing cells with greatly reduced NS3 protein expression although more of the input plasmid remained for the samples in which NS3/4A was knocked down (Figure 24C, lanes 9 and 10). This suggests that even small amounts of NS3/4A were still able to elicit a clear proteolytic phenotype at least against MAVS.

4.0 Discussion

Hepatitis C virus frequently leads to serious liver disease in chronically infected patients, with one consequence being hepatocellular carcinoma. Although the mechanism likely depends on both host and viral factors, the respective roles for each of these components remains poorly defined. Prior studies have suggested that several of the HCV proteins may be responsible, including core, NS5A, and NS5B. In addition, NS3 genotype 1b has been implicated in oncogenesis; however the effect of the NS3/4A protein complex has not been well documented. I sought to replicate the advanced cellular transformation induced by NS3/4A genotype 1b and determine the host proteomic changes associated with this phenotype. However, I was unable to replicate this phenotype through cellular growth assays therefore the aim was shifted to evaluating the total host proteomic changes induced by NS3/4A genotype 1b. Using SILAC (stable isotopic labeling of amino acids in cell culture) with mass spectrometry I was able to identify 23 differentially regulated proteins upon NS3/4A 1b expression. While these candidates have yet to be confirmed by another method, the reasons for discrepancy between the mass spectrometry peptide and western blot protein data are explored below.

4.1. Production of stable cell lines expressing functional NS3/4A

The initial aim of this study was to replicate the advanced cellular transformation phenotype observed by NS3 expression in murine NIH 3T3 cell line upon HCV

NS3/4A expression then identify proteins showing quantitative changes which may have played a role in the altered phenotype (79, 80). We used stable cell lines which should allow for a more direct comparison of a polyclonal cell line expressing the NS3/4A or control GFP at a more moderate level compared to cells that were transiently transfected. Such overexpression can lead to cellular responses due more to the overexpression of a protein compared to what would happen at expression more resembling natural biological protein levels. Initially however, NS3/4A expression and function were evaluated by transient transfection and western blot analysis. NS3 was detected only in cells expressing NS3/4A, as seen by the 70kDa band in lanes 2, 5, and 6 of Figure 6A. Bands that appeared at ~44kDa may be internal cleavage products or degradation products of NS3. Infectious HCV virus JFH1 infection was carried out in Huh7.5 cells, therefore a mock-infected negative control was used to control for this cell line (Figure 6A). GFP was also used as a negative control in this and subsequent experiments for presence of the vector and protein expression.

Function was demonstrated by analysis of cleaved MAVS, 68kDa, which was seen only in those cell lines that expressed NS3/4A (Figure 6B, lanes 2, 5, and 6). JFH1 demonstrated complete cleavage of MAVS; whereas the NS3/4A expressing cells retained some full length MAVS as seen by the MAVS bands at both 70 and 68kDa in lanes 5 and 6. This is due to the nature of transient transfections as not all cells take up the NS3/4A plasmid and therefore MAVS is not cleaved in these cells. In the case of JFH1 infection, all cells are infected and

therefore full cleavage occurs. Bands between 48 and 51kDa may also be MAVS cleavage products as the smaller species (48kDa) was preferentially seen, presumably cleaved, in lysates expressing NS3/4A.

4.2. Phenotypic study of NS3/4A oncogenic potential

Despite NS3/4A 1b expression and function, increased cell growth, or transformation, was not observed in comparison to NIH 3T3 cells or vector controls. Cell viability, as measured by the Alamar blue assay, did not present increased growth (Figure 7). As well, the cell proliferation assay (Figure 8) showed no significant growth difference in cells expressing NS3/4A 1b. Several reasons may account for this; the NS3/4A protein complex was used in place of the NS3 protease alone, stable cell lines were created differently, differences in the NS3 1b amino acid sequences, or the time required to observe the phenotype is beyond what was measured.

Previous studies have only determined the oncogenic potential when expressing HCV NS3 or the NS3 protease domain alone (79-82, 114). These studies found that a functional protease domain was required to induce cellular transformation in NIH 3T3 cells, as mutating the active site or using serine protease inhibitors abrogated this effect. The main reason for using NS3/4A is that this is the natural protein complex found in HCV infected cells. The ability of NS4A to localize the complex to the membrane and to significantly increases the catalytic activity of the protease is very important (60, 61, 115). Therefore, the naturally occurring

NS3/4A complex should increase the catalytic activity and thus also increase the transforming effect, unless the transforming effect is independent of protease activity. However, the ability of NS4A to localize the protein to the membrane may provide an explanation as to why the transforming potential of NS3 was not observed. Previous studies have shown that NS3 can be found in the nucleus, and was also able to interact with the major tumour suppressor p53 (65, 85). However, if NS3 is complexed with NS4A, it becomes localized to cellular membranes and is no longer found in the nucleus (65). Interestingly, one study using NS3/4A claimed that the transformation potential of NS3/4A was higher than that of NS3 alone (114). The authors used genotype 2a NS3/4A, which has a slightly different sequence than the 1b genotype used in the previous and the present study (Figures 7 and 8), and may account for differences seen. They also used a soft agar assay to monitor anchorage independent growth of the NS3/4A expressing cells. However, the amount of growth increase cannot be properly evaluated because NS3 only expressing cells were used as the baseline control instead of the inclusion of a cell or vector only control.

It is important to note that most of these previous studies did not test for NS3 protease activity (79, 80, 82). Zemel et al concluded that protease activity was required by mutating amino acids in the active site catalytic triad, and through inclusion of protease inhibitors, at least in rat fibroblast cells (81). However, this does not ensure that protein stability and structure were not greatly affected or that the protease inhibitors were not also affecting a cellular protease that could

explain the transformed phenotype. It would be important to know if any of these constructs used were able to cleave endogenous cellular MAVS, although others and our unpublished data (Schaeffer, Rypien, and Carpenter) suggests that NS4A is essential for cleavage activity, at least against the NS5A/5B cleavage junction.

Another difference that may account for the discrepancy in transformation capacity is the manner in which stable cell lines were produced. Previous studies performed transient transfections and selected out colonies in which NS3 integrated into the genome, therefore the cell line is a clone containing this single integration site (79-82, 114). However, a retroviral expression system was used in the present study to stably integrate NS3/4A randomly into the genome, and the resulting cell line is composed of a heterogeneous mixture of integration sites. It is possible that in the course of making a stable cell line from a single clone, a specific integration of NS3 caused the observed phenotype. Moreover, generation of stable cell lines following transient transfection often leads to incorporation of a higher number of gene copies, whereas our method resulted in typically 1 copy per cell (as suggested by most of the cells dying under neomycin selection following plasmid integration).

Furthermore, sequence differences of the NS3 1b protein could account for the differences observed between studies. The high mutation rate of RNA viruses due to the lack of proof reading ability of the polymerase and high replication rate

leads to numerous subtypes of HCV (4, 114). There is an estimated 30% difference between in sequence between genotypes, with 25% variability in subtypes (116). These slight differences in sequence can have major functional effects on the proteins involved. In fact, when the NS3 sequence was evaluated from patients with the 1b genotype, sequences were found to be highly or weakly associated with hepatocellular carcinoma based on secondary structure (117). The present study used NS3/4A isolated from the 1b replicon sequence, whereas the sequences used in previous studies are largely unknown and may also attribute to differences in lack of an observed phenotype. Recently, polymorphisms in the N terminal protease domain of NS3 have been found to be associated with HCC (118). Tyrosine at amino acid 1082 and glutamine at position 1112 are more highly associated with the development of HCC, and may have been present in NS3 sequences used in studies that observe the transformation phenotype. However, both of these residues are also found in the NS3/4A 1b sequence used in the present study and therefore likely do not account for the differences observed. Also, previous publications did not provide the sequences and therefore could not be evaluated.

Lastly, it is also possible that the time for NS3/4A to induce transformation compared to NS3 or NS3 protease only differs. The Alamar blue results here indicated no change in cell viability between NS3/4A 1b and vector control after 5 days, suggesting no increase in cell proliferation in NS3/4A expressing cells (Figure 7). It is not clear why the NIH 3T3 control trended to grow faster than

NS3/4A expressing cells and the vector control. It suggests that in this case transducing the cells with NS3/4A actually decreases cell proliferation. This observation prompted us to conduct a growth assay over a longer period of time. However, cell proliferation was still not observed in the NS3/4A 1b expressing cells as compared to vector alone (Figure 8). These findings were taken from two replicates, so further replicates should be performed in future to determine significance. However, Zemel et al did a similar growth assay in which the cell cycle was increased in NS3 expressing cells after only 10 days (81). Since the previous study was using NS3 only, it may be possible that it takes longer for the transformation phenotype to be observed in NS3/4A expressing cells, if it is in fact able to induce this phenotype. Interestingly, NS3/4A 2a trended towards slightly increase cell proliferation as compared to 1b after 2 weeks (Figure 8), although further replicates are required for significance. A previous report also noticed this difference in genotypes when evaluated by soft agar assay (114). However, since genotype 1 is predominantly seen in HCV patients with hepatocellular carcinoma, this difference was not evaluated further.

In conclusion, I was not able to replicate the advanced cellular transformation in cells due to NS3/4A and was therefore this course of study abandoned in favour of observing global proteomic changes induced by NS3/4A 1b expression.

4.3. Stable isotopic labeling of amino acids in cell culture (SILAC)

The second aim of this project was to use SILAC in conjunction with mass spectrometry to measure the proteomic changes in GP2 293 cells upon NS3/4A 1b expression. Over 6000 SILAC paired proteins were identified when the four experiments were combined in NS3/4A expressing cells compared to GFP expressing cells. This is comparable to what others have seen in recent studies employing SILAC labeling with highly sensitive instruments and processing algorithms (93, 119).

The mere act of transducing a gene to generate a stable cell line creates changes in the cell. As such, overexpressing a protein induces cellular stress that would be mistaken as a functional change due specifically to the protein being overexpressed. We reasoned that expressing an 'irrelevant protein' such as GFP could account for cellular stress and that any effects due to GFP expression could be separated from NS3/4A during follow up analysis. The second level of control was to eliminate any bias in the selection media by growing NS3/4A expressing cells in both "light" SILAC media and in "heavy" SILAC media (Figure 9). This allowed common contaminants such as keratin to be easily eliminated, as they would always show as increase in the "light" samples as they were introduced during sample processing.

The cellular proteome of NS3/4A and GFP expression in GP2 293 cells (a derivative of HEK 293 cells) did not differ, as seen by the normal distribution of proteins from all experiments with few outliers (Figure 13). This was expected

since a mass change in the proteome could suggest major alterations within the cell most likely resulting in cell death, which was not observed during experimentation. Replicate experiments provided us with a list of 23 total deregulated proteins, 10 up and 13 down regulated (Figure 14, Table 2 and 3). For the scope of this project, only the top 2 up regulated, PTGR1 and PSMD5, and 1 down regulated protein, peripherin, were chosen for further study. Interestingly, although MAVS is clearly altered upon NS3/4A expression (Figure 6, lanes 2, 5, and 6), it was not found by mass spectrometry to be deregulated. This is due to the fact that the cleaved product remains stable in the cells, as it is detected by western blot, and the small clipped peptide was not detected by mass spectrometry.

Prostaglandin reductase 1 (PTGR1) was the most highly altered protein identified upon NS3/4A expression with a $\log_2$ ratio of 1.53 (p-value of 3.11×10^{-3}), and was identified in all four experiments (Table 2). It has been previously characterized as a leukotriene B4 dehydrogenase, which inactivates the proinflammatory factor leukotriene B4 (120). Since successful viruses are those that can remain undetected in the host cell, the up-regulation of PTGR1 upon NS3/4A expression may serve to inhibit the host inflammatory innate immune response. However, in the case of chronically infected patients that develop fibrosis, potentially via inflammation, this effect must somehow eventually be overcome. PTGR1 has also found to be strongly induced in rats by nuclear factor-like 2 (Nrf2) mediated gene activation, a central regulator in the cellular stress response, thus may be

similarly up-regulated by cellular stress induced by NS3/4A expression (121). Recently, PTGR1 over expression was discovered to activate antitumor chemotherapy agents *in vitro* (122), and was found to restrict mycobacterial infection in zebrafish (123). Interestingly, induction of PTGR1 has also been reported to suppress the oncogenic transformation of HepG2 cells *in vitro* as measured by focus formation and anchorage-independent growth (124). However, that study used extracted plant compounds to induce PTGR1 expression, which may have off-target effects resulting in oncogenic transformation suppression. Although more research needs to be performed to test the validity of these claims, it provides a potential clue as to why NS3/4A expression was not able to replicate the previous transforming ability of NS3.

The second most up-regulated protein upon NS3/4A expression was the 26S proteasome subunit 5SB (PSMD5, Table 2). The proteasome consists of a 20S proteolytic core particle and 19S regulatory particles subdivided into the lid and base (125). PSMD5 has been found to be a homologue to the yeast hsm3 protein, which acts as an assembly chaperone for the base of the proteasome, but is not present in the proteasome (126). While research has been heavily focused on the direct role of this protein in proteasome assembly, alternative roles have not been well documented. Interestingly, other proteasome subunits were identified by our mass spectrometry analysis; however none were differentially regulated upon NS3/4A expression. This suggests another role of this protein, potentially altering proteasome activity.

The most abundantly down regulated protein found upon NS3/4A expression was peripherin (PRPH), type III intermediate filament commonly found in neurons. This protein has been heavily studied in neuronal cells and self assembles into filamentous polymer networks. It is regulated in neuronal injury in response to proinflammatory cytokines (127). While studies involving peripherin in non-neuronal cells is severely limited, the protein vimentin (in the same group as peripherin) was shown to be elevated in HCV infected hepatoma cells and liver biopsies from chronically infected HCV patients (128). However, in the present study peripherin was down regulated and so the functional consequence of this protein abundance change remains unknown.

Studies on host proteomic changes induced by HCV NS3/4A are lacking and global changes due to NS3 are limited, with very little confirmation of protein deregulation. One study that found NS3 to induce transformation in human cells found several deregulated proteins, however only two were assessed by western blot (82). In this case, phosphorylated p44/42 and p38, which activate the ras/raf/MAPK cell cycle progression pathway, were significantly increased in cells expressing NS3 at both the peptide and protein level.

More research has been focused on proteomic changes upon HCV infection in cancer and non-cancerous liver biopsies. Several groups have identified elevated levels of heat shock stress response proteins in cancerous tissue through two-

dimensional electrophoresis (129, 130). Recently, a proteomic study looking at differentially regulated proteins in HCV infected patients with fibrosis documented elevations in proinflammatory response proteins, however these results were not confirmed by another method (119). Those previously documented proteomic changes were not observed in the present study, which may not be surprising. The lack of a transformation phenotype by NS3/4A expression may explain the lack of observed differentially regulated proteins involved in cell cycle progression.

Finally, most of the previous studies were performed with the full hepatitis C virus that will most likely generate different results than NS3/4A alone, as there are more host protein interactions and signaling involved with full virus. For instance, HCV was seen to elevate proteins involved in the proinflammatory response in liver fibrosis biopsies while NS3/4A in the present study was shown to up regulate PTGR1, which inhibits the proinflammatory LTB4. Other viral protein interactions may interfere with this signaling pathway, or since fibrosis occurs long after infection, it may be a time dependent effect. Care must be taken when making comparisons as neither of these protein abundance changes have been confirmed by a method other than mass spectrometry.

4.4. Confirmation of mass spectrometry data

Although the mass spectrometry data indicated that PTGR1, PSMD5, and peripherin were strongly deregulated upon NS3/4A expression, these effects

could not be confirmed by western blot. Given the low FDR value (0.01) at both peptide and protein levels; it is unlikely that the mass spectrometer misidentified each of these proteins. Several possible alternate explanations were explored. These included problems associated with the antibody, closer examination of the mass spectrometer data for poor data, and the detection by mass spectrometry of specific protein isoforms.

Because high-density mass spectrometry data works with only peptide data, western blot was chosen to confirm the mass spectrometry data by an alternate method. Although equal amounts of protein were loaded as determined by an actin control, several commercial antibodies were unable to detect the proteins in the cell lysates, as seen by lack of expected bands (arrows in Figures 15). It should be noted that several antibodies were used in an attempt to visualize protein abundance changes; however only one antibody to PTGR1 was found which exhibited reasonable specificity. This antibody was unable to detect the protein changes suggested by mass spectrometry when compared to actin load control (Figure 16). A dilution series of protein lysate was set up to ensure the antibody could detect various concentrations of protein. This experiment revealed that the PTGR1 and actin antibodies behaved linearly; however the efficiency of the PTGR1 antibody was less than that of actin meaning a change in PTGR1 protein concentration does not correspond to a large change in signal intensity (Figure 17). However, the amount of PTGR1 up regulation suggested by mass spectrometry suggests that the antibody efficiency is not likely the reason why

the western blot data did not correlate with the mass spectrometry data. In order to ensure the antibodies were detecting the correct protein, cells were made that over-expressed PTGR1 or peripherin. Figure 18 demonstrates that both PTGR1 and peripherin antibodies detected their respective proteins at the predicted molecular weights, and therefore rules out antibody specificity. PTGR1 was chosen as a model to explore these issues further as it was the most deregulated protein found by mass spectrometry and an appropriate antibody was available.

Further analysis of the mass spectrometry data for PTGR1 did not exhibit a bias as to which part of the protein was being detected (Figure 19). Importantly, as only certain peptides are detected by MS (so called signature peptides) we checked a study performed by Geiger et al who performed an analysis of eleven cell lines creating a database of common cellular MS peptides (131). All of our detected peptides were also considered signature peptides.

The distribution of each peptide seen in all four experiments was also further evaluated. When NS3/4A was “light” labeled, PTGR1 heavy/light peptide $\log_2$ ratios were all below zero and conversely when NS3/4A was “heavy” labeled, PTGR1 heavy/light peptide $\log_2$ ratios were all above zero (Figure 20). This indicated that each PTGR1 peptide detected was elevated when NS3/4A was expressed. The mass spectrometry traces of the PTGR1 peptides were of low intensity, which could bias the actual ratio, but is reproducible across experiments and with label swapping. To evaluate this issue further, targeted

multiple reaction monitoring (MRM) should be performed with differentially labeled synthetic peptides to PTGR1 to evaluate performance by MS.

It is important to keep in mind that the mass spectrometer identifies peptides, and not proteins. From these peptides, the MaxQuant software makes the best protein match and reports a list of proteins. In the case of PTGR1, there were 5 proteins listed, with PTGR1 listed as the top match (Figure 21). However, PTGR1 and PTGR1 isoform 2 contain the same identified peptides. This prompted us to examine whether PTGR1 isoform 2 was actually being up regulated upon NS3/4A expression, and not PTGR1. Immunoprecipitation (IP) was employed to enrich for PTGR1 isoforms as the antibody epitope was also found in PTGR1 isoform 2, however it was not successful as demonstrated by lack of discernible bands between 32 and 36kDa (Figure 22). It is likely that the signal from the antibody heavy and light chains masked the isoforms, and therefore separation by higher resolution techniques was not further addressed. Since isoforms could not be resolved, it cannot be ruled out that the mass spectrometer is identifying a PTGR1 isoform and this explains why it cannot be confirmed by western blot.

Quantitative real time reverse transcriptase PCR (RT^2-PCR) was used as another method to assess the mass spectrometry data by measuring the transcript levels of the major up and down regulated proteins. However, this method was used solely as a means to further evaluate the data, as it measures transcript levels rather than protein levels. Unfortunately, the mRNA levels did not

match the protein levels, and was therefore not useful in exploring the difference between MS and western blot data. When comparing the transcript levels from GFP expressing cells and NS3/4A expressing cells, the transcripts for PTGR1, peripherin, and PSMD5 show no difference in levels (Figure 23, dark pink and red bars). BNIP1 transcripts however, showed a slight increase upon NS3/4A expression, which is opposite to the peptide data. This is not surprising though, since there is often poor correlation between mRNA and protein levels (101-103). Variable stability of the transcript and proteins play a role in the differences between the two assays. For instance, plenty of transcripts may be made but if it not stable, little will be translated into protein, which may be the case for BNIP1.

An important point was discovered upon examination of the RT^2-PCR data, the proper use of controls. Comparing the transcript levels from NS3/4A expressing cells and untransfected cells, there were drastic changes (Figure 23, light pink and red bars). Peripherin transcript levels increased, BNIP1 transcript levels decreased, and transcript levels for PSMD5 and PTGR1 decreased. However, the same results are seen when comparing GFP to cells only. This clearly indicates that the mere act of over-expressing a protein can have an effect on transcript levels and would have wrongly been attributed to NS3/4A expression if untransfected cells were used as a control. While we would have liked to include a second control, untransfected cells, SILAC analysis is difficult with anything greater than two samples multiplexed.

While candidate confirmation was underway, shRNA targets to NS3 were constructed in preparation to test the candidate protein levels when NS3/4A expression was lost. NS3 expression was markedly reduced in NS3/4A expressing cells that contained these shRNA targets compared to controls (Figure 24A, lane 9 and 10 compared to lanes 6-8). Unexpectedly, these same cells still demonstrated comparable MAVS cleavage as those cells with full NS3 expression (Figure 24B, lanes 9 and 10 compared to lanes 6-8). This could not be due to slow protein turnover, as protein lysates were taken almost a month after the shRNA targets were introduced to the cells. To ensure MAVS cleavage was not due to irreversible cell alterations due to previous NS3/4A expression, an N-terminally GFP tagged NS5A/B junction sequence was transfected into the cells. NS5A/B is one of the natural viral substrates of the NS3/4A protease and therefore is indicative of direct NS3/4A activity. Indeed, cells with reduced NS3 expression were still able to cleave this sequence (Figure 24). The arrows in Figure 24C point to the suspected GFP tagged sequence, however the migration pattern deviates from the calculated molecular weights of 54kDa for full length and 44kDa for cleaved constructs. This may simply be due to the nature of this particular proteins migration in SDS-PAGE gels since both suspected full length and cleaved bands are the same ~3kDa larger than predicted. Mutating the cleavage site to become uncleavable could determine whether this is the correct protein species or not. GFP is seen in Figure 24C as a 27kDa band found in GFP cells and those containing the tagged construct (lanes 2 and 4-10, respectively).

These results reveal that MAVS is cleaved regardless of NS3/4A expression levels, as long as some NS3/4A is present.

5.0 Conclusion

NS3/4A 1b did not cause the previously reported cellular transformation of NS3 1b, as measured by Alamar blue cell viability and growth assay, and therefore may play a different and less direct role in hepatocellular carcinoma than previously thought. It may instead react or suppress reactions, such as the immune response, when placed in the context of the whole organism. This result is not surprising however, since HCV is a chronic infection and readily causing immediate cell cycle deregulation would most likely result in cell destruction before the virus has a chance to chronically infect additional cells and persist within the host. Also, studies using NS3 constructs without the NS4A cofactor are not so useful in determining effects on the host because it is not what is seen in a natural HCV infection. Perhaps not surprisingly, due to its chronic infection nature, NS3/4A 1b expression had only a modest effect on the host cell proteome however these protein abundance changes are yet to be confirmed by another method; highlighting caution when interpreting mass spectrometry data without confirmation. NS3/4A on its own may not cause large changes in the proteome in this cell line at this expression level.

The shRNA results in this study demonstrate that there is no doubt that NS3/4A was expressed at high enough levels in this study to induce a phenotype (cleavage of a known cellular target). Whether this was a high enough level to induce the transformation phenotype is not clear. Most other studies significantly over-express their proteins of interest and this may lead to a difference in what

we see compared to those studies. Over-expression of any protein could lead to erroneous interpretation of data.

As an aside, these results also provide grounds for caution when evaluating studies aimed at reducing HCV replication in cells through specific virally targeted shRNAs (132, 133). While shRNAs may reduce the amount of HCV to low levels, the small amount of NS3/4A that remains may retain full protease activity and continue to interfere with the innate immune response.

6.0 Future Work

This study presents the quantitative host proteomic changes detected upon NS3/4A expression. While the mass spectrometry data is of high quality and significantly deregulated proteins were seen in at least three replicates, the abundance changes could not be confirmed by western blot. A major hindrance for confirmation lied at the antibody level, as suitable antibodies were lacking, and may be overcome by producing antibodies of good quality. As well, the role of isoforms has yet to be determined as immunoprecipitation was unsuccessful with the only commercial PTGR1 antibody that was able to detect the protein by western blot.

The SILAC proteomic approach used in the present study generated relative peptide quantitation reported as a change in ratio between SILAC pairs and the amount of peptide seen is unknown. A method called selected reaction monitoring (SRM) could be used to measure specific significantly deregulated peptides, as known amounts of isotopically labeled peptide are spiked into the reaction mixture and precise quantitation is obtained (134). Providing PTGR1, PSMD5, and peripherin can be confirmed by another method, the role of these protein changes in viral infection should be determined. Additionally, this study did not evaluate proteolytic cleavage substrates or post translational modifications induced by NS3/4A expression, an area that could have important implications for HCV biology.

7.0. References

1. **Perz JF**, **Armstrong GL**, **Farrington LA**, **Hutin YJF**, **Bell BP**. 2006. The contributions of hepatitis B virus and hepatitis C virus infections to cirrhosis and primary liver cancer worldwide. J Hepatol **45**:529–538.
2. **Public Health Agency of Canada**. 2009. HCV canada 1–52.
3. **Poynard T**, **Yuen M-F**, **Ratziu V**, **Lai CL**. 2003. Viral hepatitis C. Lancet **362**:2095–2100.
4. **Le Guillou-Guillemette H**, **Vallet S**, **Gaudy-Graffin C**, **Payan C**, **Pivert A**, **Goudeau A**, **Lunel-Fabiani F**. 2007. Genetic diversity of the hepatitis C virus: impact and issues in the antiviral therapy. World J Gastroenterol **13**:2416–2426.
5. **Choo QL**, **Kuo G**, **Weiner AJ**, **Overby LR**, **Bradley DW**, **Houghton M**. 1989. Isolation of a cDNA clone derived from a blood-borne non-A, non-B viral hepatitis genome. Science **244**:359–362.
6. **Te HS**, **Jensen DM**. 2010. Epidemiology of hepatitis B and C viruses: a global overview. Clin Liver Dis **14**:1–21– vii.
7. **Hoofnagle JH**. 2002. Course and outcome of hepatitis C. Hepatology **36**:S21–9.
8. **Liang TJ**, **Rehermann B**, **Seeff LB**, **Hoofnagle JH**. 2000. Pathogenesis, natural history, treatment, and prevention of hepatitis C., pp. 296–305. *In*.
9. **Brown RS**. 2005. Hepatitis C and liver transplantation. Nature **436**:973–978.
10. **Willems M**, **Metselaar HJ**, **Tilanus HW**, **Schalm SW**, **de Man RA**. 2002. Liver transplantation and hepatitis C. Transpl. Int. **15**:61–72.
11. **Maag D**, **Castro C**, **Hong Z**, **Cameron CE**. 2001. Hepatitis C virus RNA-dependent RNA polymerase (NS5B) as a mediator of the antiviral activity of ribavirin. J Biol Chem **276**:46094–46098.
12. **Contreras AM**, **Hiasa Y**, **He W**, **Terella A**, **Schmidt EV**, **Chung RT**. 2002. Viral RNA mutations are region specific and increased by ribavirin in a full-length hepatitis C virus replication system. J Virol **76**:8505–8517.
13. **Fried MW**, **Shiffman ML**, **Reddy KR**, **Smith C**, **Marinos G**, **Gonçales FL**, **Häussinger D**, **Diago M**, **Carosi G**, **Dhumeaux D**, **Craxi A**, **Lin A**, **Hoffman J**, **Yu J**. 2002. Peginterferon alfa-2a plus ribavirin for chronic hepatitis C virus infection. N. Engl. J. Med. **347**:975–982.
14. **Hadziyannis SJ**, **Sette H**, **Morgan TR**, **Balan V**, **Diago M**, **Marcellin P**, **Ramadori G**, **Bodenheimer H**, **Bernstein D**, **Rizzetto M**, **Zeuzem S**, **Pockros PJ**, **Lin A**, **Ackrill AM**, **PEGASYS International Study Group**. 2004. Peginterferon-alpha2a and ribavirin combination therapy in chronic hepatitis C: a randomized study of treatment duration and ribavirin dose. Ann. Intern. Med. **140**:346–355.
15. **Feld JJ**, **Hoofnagle JH**. 2005. Mechanism of action of interferon and ribavirin in treatment of hepatitis C. Nature **436**:967–972.
16. **Simmonds P**, **Holmes EC**, **Cha TA**, **Chan SW**, **McOmish F**, **Irvine B**, **Beall E**, **Yap PL**, **Kolberg J**, **Urdea MS**. 1993. Classification of hepatitis

C virus into six major genotypes and a series of subtypes by phylogenetic analysis of the NS-5 region. J Gen Virol **74 (Pt 11)**:2391–2399.
17. **Nakano T**, **Lau GMG**, **Lau GML**, **Sugiyama M**, **Mizokami M**. 2012. An updated analysis of hepatitis C virus genotypes and subtypes based on the complete coding region. Liver Int **32**:339–345.
18. **Lau JY**, **Davis GL**, **Prescott LE**, **Maertens G**, **Lindsay KL**, **Qian K**, **Mizokami M**, **Simmonds P**. 1996. Distribution of hepatitis C virus genotypes determined by line probe assay in patients with chronic hepatitis C seen at tertiary referral centers in the United States. Hepatitis Interventional Therapy Group. Ann. Intern. Med. **124**:868–876.
19. **Garber K**. 2011. Hepatitis C: move over interferon. Nature Biotechnology **29**:963–966.
20. **Robertson B**, **Myers G**, **Howard C**, **Brettin T**, **Bukh J**, **Gaschen B**, **Gojobori T**, **Maertens G**, **Mizokami M**, **Nainan O**, **Netesov S**, **Nishioka K**, **Shin i T**, **Simmonds P**, **Smith D**, **Stuyver L**, **Weiner A**. 1998. Classification, nomenclature, and database development for hepatitis C virus (HCV) and related viruses: proposals for standardization. International Committee on Virus Taxonomy. Archives of Virology.
21. **Moradpour D**, **Penin F**, **Rice CM**. 2007. Replication of hepatitis C virus. Nat. Rev. Microbiol. **5**:453–463.
22. **Joyce MA**, **Tyrrell DLJ**. 2010. The cell biology of hepatitis C virus. Microbes Infect. **12**:263–271.
23. **Wang C**, **Sarnow P**, **Siddiqui A**. 1993. Translation of human hepatitis C virus RNA in cultured cells is mediated by an internal ribosome-binding mechanism. J Virol **67**:3338–3344.
24. **McLauchlan J**, **Lemberg MK**, **Hope G**, **Martoglio B**. 2002. Intramembrane proteolysis promotes trafficking of hepatitis C virus core protein to lipid droplets. EMBO J. **21**:3980–3988.
25. **Op De Beeck A**, **Cocquerel L**, **Dubuisson J**. 2001. Biogenesis of hepatitis C virus envelope glycoproteins. J Gen Virol **82**:2589–2595.
26. **Griffin SDC**, **Beales LP**, **Clarke DS**, **Worsfold O**, **Evans SD**, **Jaeger J**, **Harris MPG**, **Rowlands DJ**. 2003. The p7 protein of hepatitis C virus forms an ion channel that is blocked by the antiviral drug, Amantadine. FEBS Lett **535**:34–38.
27. **Grakoui A**, **McCourt DW**, **Wychowski C**, **Feinstone SM**, **Rice CM**. 1993. A second hepatitis C virus-encoded proteinase. Proc Natl Acad Sci USA **90**:10583–10587.
28. **Bartenschlager R**, **Ahlborn-Laake L**, **Mous J**, **Jacobsen H**. 1993. Nonstructural protein 3 of the hepatitis C virus encodes a serine-type proteinase required for cleavage at the NS3/4 and NS4/5 junctions. J Virol **67**:3835–3844.
29. **Kim DW**, **Gwack Y**, **Han JH**, **Choe J**. 1995. C-terminal domain of the hepatitis C virus NS3 protein contains an RNA helicase activity. Biochem Biophys Res Commun **215**:160–166.
30. **Wölk B**, **Sansonno D**, **Kräusslich HG**, **Dammacco F**, **Rice CM**, **Blum HE**, **Moradpour D**. 2000. Subcellular localization, stability, and trans-

cleavage competence of the hepatitis C virus NS3-NS4A complex expressed in tetracycline-regulated cell lines. J Virol **74**:2293–2304.

31. **Egger D**, **Wölk B**, **Gosert R**, **Bianchi L**, **Blum HE**, **Moradpour D**, **Bienz K**. 2002. Expression of hepatitis C virus proteins induces distinct membrane alterations including a candidate viral replication complex. J Virol **76**:5974–5984.
32. **Evans MJ**, **Rice CM**, **Goff SP**. 2004. Phosphorylation of hepatitis C virus nonstructural protein 5A modulates its protein interactions and viral RNA replication. Proc Natl Acad Sci USA **101**:13038–13043.
33. **Lesburg CA**, **Cable MB**, **Ferrari E**, **Hong Z**, **Mannarino AF**, **Weber PC**. 1999. Crystal structure of the RNA-dependent RNA polymerase from hepatitis C virus reveals a fully encircled active site. Nat. Struct. Biol. **6**:937–943.
34. **Pileri P**, **Uematsu Y**, **Campagnoli S**, **Galli G**, **Falugi F**, **Petracca R**, **Weiner AJ**, **Houghton M**, **Rosa D**, **Grandi G**, **Abrignani S**. 1998. Binding of hepatitis C virus to CD81. Science **282**:938–941.
35. **Scarselli E**, **Ansuini H**, **Cerino R**, **Roccasecca RM**, **Acali S**, **Filocamo G**, **Traboni C**, **Nicosia A**, **Cortese R**, **Vitelli A**. 2002. The human scavenger receptor class B type I is a novel candidate receptor for the hepatitis C virus. EMBO J. **21**:5017–5025.
36. **Barth H**, **Schafer C**, **Adah MI**, **Zhang F**, **Linhardt RJ**, **Toyoda H**, **Kinoshita-Toyoda A**, **Toida T**, **Van Kuppevelt TH**, **Depla E**, **Weizsacker Von F**, **Blum HE**, **Baumert TF**. 2003. Cellular binding of hepatitis C virus envelope glycoprotein E2 requires cell surface heparan sulfate. J Biol Chem **278**:41003–41012.
37. **Agnello V**, **Abel G**, **Elfahal M**, **Knight GB**, **Zhang QX**. 1999. Hepatitis C virus and other flaviviridae viruses enter cells via low density lipoprotein receptor. Proc Natl Acad Sci USA **96**:12766–12771.
38. **Evans MJ**, **Hahn von T**, **Tscherne DM**, **Syder AJ**, **Panis M**, **Wölk B**, **Hatziioannou T**, **McKeating JA**, **Bieniasz PD**, **Rice CM**. 2007. Claudin-1 is a hepatitis C virus co-receptor required for a late step in entry. Nature **446**:801–805.
39. **Ploss A**, **Evans MJ**, **Gaysinskaya VA**, **Panis M**, **You H**, **de Jong YP**, **Rice CM**. 2009. Human occludin is a hepatitis C virus entry factor required for infection of mouse cells. Nature **457**:882–886.
40. **Blanchard E**, **Belouzard S**, **Goueslain L**, **Wakita T**, **Dubuisson J**, **Wychowski C**, **Rouillé Y**. 2006. Hepatitis C virus entry depends on clathrin-mediated endocytosis. J Virol **80**:6964–6972.
41. **Tscherne DM**, **Jones CT**, **Evans MJ**, **Lindenbach BD**, **McKeating JA**, **Rice CM**. 2006. Time- and temperature-dependent activation of hepatitis C virus for low-pH-triggered entry. J Virol **80**:1734–1741.
42. **Otto GA**, **Puglisi JD**. 2004. The pathway of HCV IRES-mediated translation initiation. Cell **119**:369–380.
43. **Gosert R**, **Egger D**, **Lohmann V**, **Bartenschlager R**, **Blum HE**, **Bienz K**, **Moradpour D**. 2003. Identification of the hepatitis C virus RNA replication complex in Huh-7 cells harboring subgenomic replicons. J Virol **77**:5487–

5492.
44. **Gastaminza P**, **Cheng G**, **Wieland S**, **Zhong J**, **Liao W**, **Chisari FV**. 2008. Cellular determinants of hepatitis C virus assembly, maturation, degradation, and secretion. J Virol **82**:2120–2129.
45. **Valli MB**, **Crema A**, **Lanzilli G**, **Serafino A**, **Bertolini L**, **Ravagnan G**, **Ponzetto A**, **Menzo S**, **Clementi M**, **Carloni G**. 2007. Molecular and cellular determinants of cell-to-cell transmission of HCV in vitro. J. Med. Virol. **79**:1491–1499.
46. **Kim JL**, **Morgenstern KA**, **Griffith JP**, **Dwyer MD**, **Thomson JA**, **Murcko MA**, **Lin C**, **Caron PR**. 1998. Hepatitis C virus NS3 RNA helicase domain with a bound oligonucleotide: the crystal structure provides insights into the mode of unwinding. Structure **6**:89–100.
47. **Lam AMI**, **Frick DN**. 2006. Hepatitis C virus subgenomic replicon requires an active NS3 RNA helicase. J Virol **80**:404–411.
48. **Tai CL**, **Chi WK**, **Chen DS**, **Hwang LH**. 1996. The helicase activity associated with hepatitis C virus nonstructural protein 3 (NS3). J Virol **70**:8477–8484.
49. **Frick DN**, **Rypma RS**, **Lam AMI**, **Gu B**. 2004. The nonstructural protein 3 protease/helicase requires an intact protease domain to unwind duplex RNA efficiently. J Biol Chem **279**:1269–1280.
50. **Gu M**, **Rice CM**. 2010. Inaugural Article: Three conformational snapshots of the hepatitis C virus NS3 helicase reveal a ratchet translocation mechanism. Proc Natl Acad Sci USA **107**:521–528.
51. **Beran RKF**, **Lindenbach BD**, **Pyle AM**. 2009. The NS4A protein of hepatitis C virus promotes RNA-coupled ATP hydrolysis by the NS3 helicase **83**:3268–3275.
52. **Grakoui A**, **McCourt DW**, **Wychowski C**, **Feinstone SM**, **Rice CM**. 1993. Characterization of the hepatitis C virus-encoded serine proteinase: determination of proteinase-dependent polyprotein cleavage sites. J Virol **67**:2832–2843.
53. **Love RA**, **Parge HE**, **Wickersham JA**, **Hostomsky Z**, **Habuka N**, **Moomaw EW**, **Adachi T**, **Hostomska Z**. 1996. The crystal structure of hepatitis C virus NS3 proteinase reveals a trypsin-like fold and a structural zinc binding site. Cell **87**:331–342.
54. **Yao N**, **Reichert P**, **Taremi SS**, **Prosise WW**, **Weber PC**. 1999. Molecular views of viral polyprotein processing revealed by the crystal structure of the hepatitis C virus bifunctional protease-helicase. Structure **7**:1353–1363.
55. **Morikawa K**, **Lange CM**, **Gouttenoire J**, **Meylan E**, **Brass V**, **Penin F**, **Moradpour D**. 2011. Nonstructural protein 3-4A: the Swiss army knife of hepatitis C virus. Journal of Viral Hepatitis **18**:305–315.
56. **Brass V**, **Berke JM**, **Montserret R**, **Blum HE**, **Penin F**, **Moradpour D**. 2008. Structural determinants for membrane association and dynamic organization of the hepatitis C virus NS3-4A complex. Proc Natl Acad Sci USA **105**:14545–14550.
57. **Li X-D**, **Sun L**, **Seth RB**, **Pineda G**, **Chen ZJ**. 2005. Hepatitis C virus

protease NS3/4A cleaves mitochondrial antiviral signaling protein off the mitochondria to evade innate immunity. Proc Natl Acad Sci USA **102**:17717–17722.

58. **Li K**, **Foy E**, **Ferreon JC**, **Nakamura M**, **Ferreon ACM**, **Ikeda M**, **Ray SC**, **Gale M**, **Lemon SM**. 2005. Immune evasion by hepatitis C virus NS3/4A protease-mediated cleavage of the Toll-like receptor 3 adaptor protein TRIF. Proc Natl Acad Sci USA **102**:2992–2997.
59. **Brenndörfer ED**, **Karthe J**, **Frelin L**, **Cebula P**, **Erhardt A**, **Schulte am Esch J**, **Hengel H**, **Bartenschlager R**, **Sällberg M**, **Häussinger D**, **Bode JG**. 2009. Nonstructural 3/4A protease of hepatitis C virus activates epithelial growth factor-induced signal transduction by cleavage of the T-cell protein tyrosine phosphatase. Hepatology **49**:1810–1820.
60. **Failla C**, **Tomei L**, **De Francesco R**. 1994. Both NS3 and NS4A are required for proteolytic processing of hepatitis C virus nonstructural proteins. J Virol **68**:3753–3760.
61. **Tanji Y**, **Hijikata M**, **Satoh S**, **Kaneko T**, **Shimotohno K**. 1995. Hepatitis C virus-encoded nonstructural protein NS4A has versatile functions in viral protein processing. J Virol **69**:1575–1581.
62. **Kasprzak A**, **Seidel J**, **Biczysko W**, **Wysocki J**, **Spachacz R**, **Zabel M**. 2005. Intracellular localization of NS3 and C proteins in chronic hepatitis C. Liver Int **25**:896–903.
63. **Nomura-Takigawa Y**, **Nagano-Fujii M**, **Deng L**, **Kitazawa S**, **Ishido S**, **Sada K**, **Hotta H**. 2006. Non-structural protein 4A of Hepatitis C virus accumulates on mitochondria and renders the cells prone to undergoing mitochondria-mediated apoptosis. J Gen Virol **87**:1935–1945.
64. **Horner SM**, **Liu HM**, **Park HS**, **Briley J**, **Gale M**. 2011. Mitochondrial-associated endoplasmic reticulum membranes (MAM) form innate immune synapses and are targeted by hepatitis C virus. Proc Natl Acad Sci USA **108**:14590–14595.
65. **Muramatsu S**, **Ishido S**, **Fujita T**, **Itoh M**, **Hotta H**. 1997. Nuclear localization of the NS3 protein of hepatitis C virus and factors affecting the localization. J Virol **71**:4954–4961.
66. **Li K**, **Lemon SM**. 2013. Innate immune responses in hepatitis C virus infection. Semin Immunopathol **35**:53–72.
67. **Yoneyama M**, **Kikuchi M**, **Natsukawa T**, **Shinobu N**, **Imaizumi T**, **Miyagishi M**, **Taira K**, **Akira S**, **Fujita T**. 2004. The RNA helicase RIG-I has an essential function in double-stranded RNA-induced innate antiviral responses. Nat. Immunol. **5**:730–737.
68. **Alexopoulou L**, **Holt AC**, **Medzhitov R**, **Flavell RA**. 2001. Recognition of double-stranded RNA and activation of NF-kappaB by Toll-like receptor 3. Nature **413**:732–738.
69. **Foy E**, **Li K**, **Wang C**, **Sumpter R**, **Ikeda M**, **Lemon SM**, **Gale M**. 2003. Regulation of interferon regulatory factor-3 by the hepatitis C virus serine protease. Science **300**:1145–1148.
70. **Bellecave P**, **Sarasin-Filipowicz M**, **Donzé O**, **Kennel A**, **Gouttenoire J**, **Meylan E**, **Terracciano L**, **Tschopp J**, **Sarrazin C**, **Berg T**, **Moradpour**

D, **Heim MH**. 2010. Cleavage of mitochondrial antiviral signaling protein in the liver of patients with chronic hepatitis C correlates with a reduced activation of the endogenous interferon system. Hepatology **51**:1127–1136.

71. **McGivern DR**, **Lemon SM**. 2009. Tumor suppressors, chromosomal instability, and hepatitis C virus-associated liver cancer. Annu Rev Pathol **4**:399–415.
72. … http://www who int/mediacentre/factsheets/fs164/en.
73. **Brownell J**, **Polyak SJ**. 2013. Molecular pathways: hepatitis C virus, CXCL10, and the inflammatory road to liver cancer. Clin. Cancer Res. **19**:1347–1352.
74. **Choi J**, **Ou J-HJ**. 2006. Mechanisms of liver injury. III. Oxidative stress in the pathogenesis of hepatitis C virus. Am. J. Physiol. Gastrointest. Liver Physiol. **290**:G847–51.
75. **Thorén F**, **Romero A**, **Lindh M**, **Dahlgren C**, **Hellstrand K**. 2004. A hepatitis C virus-encoded, nonstructural protein (NS3) triggers dysfunction and apoptosis in lymphocytes: role of NADPH oxidase-derived oxygen radicals. J. Leukoc. Biol. **76**:1180–1186.
76. **Bureau C**, **Bernad J**, **Chaouche N**, **Orfila C**, **Béraud M**, **Gonindard C**, **Alric L**, **Vinel JP**, **Pipy B**. 2001. Nonstructural 3 protein of hepatitis C virus triggers an oxidative burst in human monocytes via activation of NADPH oxidase. J Biol Chem **276**:23077–23083.
77. **Poli G**. 2000. Pathogenesis of liver fibrosis: role of oxidative stress. Mol. Aspects Med. **21**:49–98.
78. **Kasprzak A**, **Adamek A**. 2008. Role of hepatitis C virus proteins (C, NS3, NS5A) in hepatic oncogenesis. Hepatol Res **38**:1–26.
79. **Smirnova IS**, **Aksenov ND**, **Vonsky MS**, **Isaguliants MG**. 2006. Different transformation pathways of murine fibroblast NIH 3T3 cells by hepatitis C virus core and NS3 proteins. Cell Biol. Int. **30**:915–919.
80. **Sakamuro D**, **Furukawa T**, **Takegami T**. 1995. Hepatitis C virus nonstructural protein NS3 transforms NIH 3T3 cells. J Virol **69**:3893–3896.
81. **Zemel R**, **Gerechet S**, **Greif H**, **Bachmatove L**, **Birk Y**, **Golan-Goldhirsh A**, **Kunin M**, **Berdichevsky Y**, **Benhar I**, **Tur-Kaspa R**. 2001. Cell transformation induced by hepatitis C virus NS3 serine protease. Journal of Viral Hepatitis **8**:96–102.
82. **He Q**, **Cheng R**, **Chen Z**, **Xiao X**, **Xiao Z**, **Li C**, **Li B**, **Zhang P**, **Zheng H**, **Feng D**. 2007. Cell transformation and proteome alteration in QSG7701 cells transfected with hepatitis C virus non-structural protein 3 **39**:751–762.
83. **Shoji I**, **Suzuki T**, **Sato M**, **Aizaki H**, **Chiba T**, **Matsuura Y**, **Miyamura T**. 1999. Internal processing of hepatitis C virus NS3 protein. Virology **254**:315–323.
84. **Yang SH**, **Lee CG**, **Song MK**, **Sung YC**. 2000. Internal cleavage of hepatitis C virus NS3 protein is dependent on the activity of NS34A protease. Virology **268**:132–140.
85. **Ishido S**, **Hotta H**. 1998. Complex formation of the nonstructural protein

3 of hepatitis C virus with the p53 tumor suppressor. FEBS Lett **438**:258–262.

86. **Kwun HJ**, **Jung EY**, **Ahn JY**, **Lee MN**, **Jang KL**. 2001. p53-dependent transcriptional repression of p21(waf1) by hepatitis C virus NS3. J Gen Virol **82**:2235–2241.
87. **Borowski P**, **Heiland M**, **Feucht H**, **Laufs R**. 1999. Characterisation of non-structural protein 3 of hepatitis C virus as modulator of protein phosphorylation mediated by PKA and PKC: evidences for action on the level of substrate and enzyme. Archives of Virology **144**:687–701.
88. **Borowski P**, **Schulze zur Wiesch J**, **Resch K**, **Feucht H**, **Laufs R**, **Schmitz H**. 1999. Protein kinase C recognizes the protein kinase A-binding motif of nonstructural protein 3 of hepatitis C virus. J Biol Chem **274**:30722–30728.
89. **Borowski P**, **Kühl R**, **Laufs R**, **Schulze zur Wiesch J**, **Heiland M**. 1999. Identification and characterization of a histone binding site of the non-structural protein 3 of hepatitis C virus. J. Clin. Virol. **13**:61–69.
90. **Kang X**, **Chen X**, **He Y**, **Guo D**, **Guo L**, **Zhong J**, **Shu H-B**. 2012. DDB1 is a cellular substrate of NS3/4A protease and required for hepatitis C virus replication. Virology.
91. **Li T**, **Chen X**, **Garbutt KC**, **Zhou P**, **Zheng N**. 2006. Structure of DDB1 in complex with a paramyxovirus V protein: viral hijack of a propeller cluster in ubiquitin ligase. Cell **124**:105–117.
92. **Yamaji S**, **Zhang M**, **Zhang J**, **Endo Y**, **Bibikova E**, **Goff SP**, **Cang Y**. 2010. Hepatocyte-specific deletion of DDB1 induces liver regeneration and tumorigenesis. Proc Natl Acad Sci USA **107**:22237–22242.
93. **Morikawa K**, **Gouttenoire J**, **Hernandez C**, **Thi VLD**, **Tran HTL**, **Lange CM**, **Dill MT**, **Heim MH**, **Donzé O**, **Penin F**, **Quadroni M**, **Moradpour D**. 2013. Quantitative proteomics identifies the membrane-associated peroxidase GPx8 as a cellular substrate of the hepatitis C virus NS3-4A protease. Hepatology.
94. **Nguyen VD**, **Saaranen MJ**, **Karala A-R**, **Lappi A-K**, **Wang L**, **Raykhel IB**, **Alanen HI**, **Salo KEH**, **Wang C-C**, **Ruddock LW**. 2011. Two endoplasmic reticulum PDI peroxidases increase the efficiency of the use of peroxide during disulfide bond formation. J Mol Biol **406**:503–515.
95. **Smith MW**, **Yue ZN**, **Korth MJ**, **Do HA**, **Boix L**, **Fausto N**, **Bruix J**, **Carithers RL**, **Katze MG**. 2003. Hepatitis C virus and liver disease: global transcriptional profiling and identification of potential markers. Hepatology **38**:1458–1467.
96. **Blackham S**, **Baillie A**, **Al-Hababi F**, **Remlinger K**, **You S**, **Hamatake R**, **McGarvey MJ**. 2010. Gene expression profiling indicates the roles of host oxidative stress, apoptosis, lipid metabolism, and intracellular transport genes in the replication of hepatitis C virus. J Virol **84**:5404–5414.
97. **Ciccaglione AR**, **Marcantonio C**, **Tritarelli E**, **Tataseo P**, **Ferraris A**, **Bruni R**, **Dallapiccola B**, **Gerosolimo G**, **Costantino A**, **Rapicetta M**. 2008. Microarray analysis identifies a common set of cellular genes

modulated by different HCV replicon clones. BMC Genomics **9**:309.
98. **Aizaki H**, **Harada T**, **Otsuka M**, **Seki N**, **Matsuda M**, **Li YW**, **Kawakami H**, **Matsuura Y**, **Miyamura T**, **Suzuki T**. 2002. Expression profiling of liver cell lines expressing entire or parts of hepatitis C virus open reading frame. Hepatology **36**:1431–1438.
99. **Walters K-A**, **Syder AJ**, **Lederer SL**, **Diamond DL**, **Paeper B**, **Rice CM**, **Katze MG**. 2009. Genomic analysis reveals a potential role for cell cycle perturbation in HCV-mediated apoptosis of cultured hepatocytes. PLoS Pathog. **5**:e1000269.
100. **Nishimura-Sakurai Y**, **Sakamoto N**, **Mogushi K**, **Nagaie S**, **Nakagawa M**, **Itsui Y**, **Tasaka-Fujita M**, **Onuki-Karakama Y**, **Suda G**, **Mishima K**, **Yamamoto M**, **Ueyama M**, **Funaoka Y**, **Watanabe T**, **Azuma S**, **Sekine-Osajima Y**, **Kakinuma S**, **Tsuchiya K**, **Enomoto N**, **Tanaka H**, **Watanabe M**. 2010. Comparison of HCV-associated gene expression and cell signaling pathways in cells with or without HCV replicon and in replicon-cured cells. J. Gastroenterol. **45**:523–536.
101. **Anderson L**, **Seilhamer J**. 1997. A comparison of selected mRNA and protein abundances in human liver. Electrophoresis **18**:533–537.
102. **Chen G**, **Gharib TG**, **Huang C-C**, **Taylor JMG**, **Misek DE**, **Kardia SLR**, **Giordano TJ**, **Iannettoni MD**, **Orringer MB**, **Hanash SM**, **Beer DG**. 2002. Discordant Protein and mRNA Expression in Lung Adenocarcinomas.
103. **Gygi SP**, **Rochon Y**, **Franza BR**, **Aebersold R**. 1999. Correlation between protein and mRNA abundance in yeast. Mol. Cell. Biol. **19**:1720–1730.
104. **Michalski A**, **Cox J**, **Mann M**. 2011. More than 100,000 detectable peptide species elute in single shotgun proteomics runs but the majority is inaccessible to data-dependent LC-MS/MS. J. Proteome Res. **10**:1785–1793.
105. **Ong SE**, **Mann M**. 2005. Mass spectrometry-based proteomics turns quantitative : Abstract : Nature Chemical Biology. Nature chemical biology.
106. **Neilson KA**, **Ali NA**, **Muralidharan S**, **Mirzaei M**, **Mariani M**, **Assadourian G**, **Lee A**, **van Sluyter SC**, **Haynes PA**. 2011. Less label, more free: approaches in label-free quantitative mass spectrometry. Proteomics **11**:535–553.
107. **Gygi SP**, **Rist B**, **Gerber SA**, **Turecek F**, **Gelb MH**, **Aebersold R**. 1999. Quantitative analysis of complex protein mixtures using isotope-coded affinity tags. Nature Biotechnology **17**:994–999.
108. **Ross PL**, **Huang YN**, **Marchese JN**, **Williamson B**, **Parker K**, **Hattan S**, **Khainovski N**, **Pillai S**, **Dey S**, **Daniels S**, **Purkayastha S**, **Juhasz P**, **Martin S**, **Bartlet-Jones M**, **He F**, **Jacobson A**, **Pappin DJ**. 2004. Multiplexed protein quantitation in Saccharomyces cerevisiae using amine-reactive isobaric tagging reagents. Mol Cell Proteomics **3**:1154–1169.
109. **Ong S-E**, **Blagoev B**, **Kratchmarova I**, **Kristensen DB**, **Steen H**, **Pandey A**, **Mann M**. 2002. Stable isotope labeling by amino acids in cell

culture, SILAC, as a simple and accurate approach to expression proteomics. Mol Cell Proteomics **1**:376–386.
110. **Cox J**, **Mann M**. 2008. MaxQuant enables high peptide identification rates, individualized p.p.b.-range mass accuracies and proteome-wide protein quantification. Nature Biotechnology **26**:1367–1372.
111. **Cox J**, **Matic I**, **Hilger M**, **Nagaraj N**, **Selbach M**, **Olsen JV**, **Mann M**. 2009. A practical guide to the MaxQuant computational platform for SILAC-based quantitative proteomics. Nat Protoc **4**:698–705.
112. **Stein DR**, **Hu X**, **McCorrister SJ**, **Westmacott GR**, **Plummer FA**, **Ball TB**, **Carpenter MS**. 2013. High pH Reversed-phase Chromatography as a Superior Fractionation Scheme Compared to Off-Gel Isoelectric Focusing for Complex Proteome Analysis. Proteomics.
113. **Cox J**, **Neuhauser N**, **Michalski A**, **Scheltema RA**, **Olsen JV**, **Mann M**. 2011. Andromeda: a peptide search engine integrated into the MaxQuant environment. J. Proteome Res. **10**:1794–1805.
114. **Kou Y-H**, **Chang M-F**, **Wang Y-M**, **Hung T-M**, **Chang SC**. 2007. Differential requirements of NS4A for internal NS3 cleavage and polyprotein processing of hepatitis C virus. J Virol **81**:7999–8008.
115. **Lin C**, **Thomson JA**, **Rice CM**. 1995. A central region in the hepatitis C virus NS4A protein allows formation of an active NS3-NS4A serine proteinase complex in vivo and in vitro. J Virol **69**:4373–4380.
116. **Simmonds P**, **Bukh J**, **Combet C**, **Deléage G**, **Enomoto N**, **Feinstone S**, **Halfon P**, **Inchauspé G**, **Kuiken C**, **Maertens G**, **Mizokami M**, **Murphy DG**, **Okamoto H**, **Pawlotsky J-M**, **Penin F**, **Sablon E**, **Shin-I T**, **Stuyver LJ**, **Thiel H-J**, **Viazov S**, **Weiner AJ**, **Widell A**. 2005. Consensus proposals for a unified system of nomenclature of hepatitis C virus genotypes., pp. 962–973. *In*.
117. **Ogata S**, **Florese RH**, **Nagano-Fujii M**, **Hidajat R**, **Deng L**, **Ku Y**, **Yoon S**, **Saito T**, **Kawata S**, **Hotta H**. 2003. Identification of hepatitis C virus (HCV) subtype 1b strains that are highly, or only weakly, associated with hepatocellular carcinoma on the basis of the secondary structure of an amino-terminal portion of the HCV NS3 protein. J Clin Microbiol **41**:2835–2841.
118. **El-Shamy A**, **Shindo M**, **Shoji I**, **Deng L**, **Okuno T**, **Hotta H**. 2013. Polymorphisms of the core, NS3, and NS5A proteins of hepatitis C virus genotype 1b associate With development of hepatocellular carcinoma. Hepatology **58**:555–563.
119. **Diamond DL**, **Krasnoselsky AL**, **Burnum KE**, **Monroe ME**, **Webb-Robertson B-J**, **McDermott JE**, **Yeh MM**, **Dzib JFG**, **Susnow N**, **Strom S**, **Proll SC**, **Belisle SE**, **Purdy DE**, **Rasmussen AL**, **Walters K-A**, **Jacobs JM**, **Gritsenko MA**, **Camp DG**, **Bhattacharya R**, **Perkins JD**, **Carithers RL**, **Liou IW**, **Larson AM**, **Benecke A**, **Waters KM**, **Smith RD**, **Katze MG**. 2012. Proteome and computational analyses reveal new insights into the mechanisms of hepatitis C virus-mediated liver disease posttransplantation. Hepatology **56**:28–38.
120. **Yokomizo T**, **Izumi T**, **Takahashi T**, **Kasama T**, **Kobayashi Y**, **Sato F**,

Taketani Y, **Shimizu T**. 1993. Enzymatic inactivation of leukotriene B4 by a novel enzyme found in the porcine kidney. Purification and properties of leukotriene B4 12-hydroxydehydrogenase. J Biol Chem **268**:18128–18135.

121. **Dick RA**, **Kwak MK**, **Sutter TR**, **Kensler TW**. 2001. Antioxidative function and substrate specificity of NAD(P)H-dependent alkenal/one oxidoreductase. A new role for leukotriene B4 12-hydroxydehydrogenase/15-oxoprostaglandin 13-reductase. J Biol Chem **276**:40803–40810.
122. **Yu X**, **Erzinger MM**, **Pietsch KE**, **Cervoni-Curet FN**, **Whang J**, **Niederhuber J**, **Sturla SJ**. 2012. Up-regulation of human prostaglandin reductase 1 improves the efficacy of hydroxymethylacylfulvene, an antitumor chemotherapeutic agent. J. Pharmacol. Exp. Ther. **343**:426–433.
123. **Tobin DM**, **Roca FJ**, **Ray JP**, **Ko DC**, **Ramakrishnan L**. 2013. An enzyme that inactivates the inflammatory mediator leukotriene b4 restricts mycobacterial infection. PLoS ONE **8**:e67828.
124. **Wei L**, **Liu J**, **Le XC**, **Han Y**, **Tong Y**, **Lau ASY**, **Rong J**. 2011. Pharmacological induction of leukotriene B4-12-hydroxydehydrogenase suppresses the oncogenic transformation of human hepatoma HepG2 cells. Int. J. Oncol. **39**:735–745.
125. **Barrault M-B**, **Richet N**, **Godard C**, **Murciano B**, **Le Tallec B**, **Rousseau E**, **Legrand P**, **Charbonnier J-B**, **Le Du M-H**, **Guérois R**, **Ochsenbein F**, **Peyroche A**. 2012. Dual functions of the Hsm3 protein in chaperoning and scaffolding regulatory particle subunits during the proteasome assembly.
126. **Le Tallec B**, **Barrault M-B**, **Guérois R**, **Carré T**, **Peyroche A**. 2009. Hsm3/S5b participates in the assembly pathway of the 19S regulatory particle of the proteasome. Mol Cell **33**:389–399.
127. **Xiao S**, **McLean J**, **Robertson J**. 2006. Neuronal intermediate filaments and ALS: a new look at an old question. Biochim. Biophys. Acta **1762**:1001–1012.
128. **Ghosh S**, **Ahrens WA**, **Phatak SU**, **Hwang S**, **Schrum LW**, **Bonkovsky HL**. 2011. Association of filamin A and vimentin with hepatitis C virus proteins in infected human hepatocytes. Journal of Viral Hepatitis **18**:e568–77.
129. **Takashima M**, **Kuramitsu Y**, **Yokoyama Y**, **Iizuka N**, **Toda T**, **Sakaida I**, **Okita K**, **Oka M**, **Nakamura K**. 2003. Proteomic profiling of heat shock protein 70 family members as biomarkers for hepatitis C virus-related hepatocellular carcinoma. Proteomics **3**:2487–2493.
130. **Yokoyama Y**, **Kuramitsu Y**, **Takashima M**, **Iizuka N**, **Toda T**, **Terai S**, **Sakaida I**, **Oka M**, **Nakamura K**, **Okita K**. 2004. Proteomic profiling of proteins decreased in hepatocellular carcinoma from patients infected with hepatitis C virus. Proteomics **4**:2111–2116.
131. **Geiger T**, **Wehner A**, **Schaab C**, **Cox J**, **Mann M**. 2012. Comparative proteomic analysis of eleven common cell lines reveals ubiquitous but

varying expression of most proteins. Mol Cell Proteomics **11**:M111.014050.
132. **Motavaf M**, **Safari S**, **Alavian SM**. 2012. Therapeutic potential of RNA interference: a new molecular approach to antiviral treatment for hepatitis C. Journal of Viral Hepatitis **19**:757–765.
133. **Imran M**, **Manzoor S**, **Khattak NM**, **Khalid M**, **Ahmed QL**, **Parvaiz F**, **Tariq M**, **Ashraf J**, **Ashraf W**, **Azam S**, **Ashraf M**. 2013. Current and future therapies for hepatitis C virus infection: from viral proteins to host targets. Archives of Virology.
134. **Wolf-Yadlin A**, **Hautaniemi S**, **Lauffenburger DA**, **White FM**. 2007. Multiple reaction monitoring for robust quantitative proteomic analysis of cellular signaling networks. Proc Natl Acad Sci USA **104**:5860–5865.

Appendix

Table A1. List of primers used in this study. Included are the targets, primer names, primer sequences, and contained restriction sites.

Target	Primer name	Primer sequence	Restriction site
NS3/4A 1b	726F	ATCACGTACGCATGGCGCCTATTACGGC	BsiWI
	725R	TGTAGGATCCTAGCACTCTTCCATCTCATCG	BamHI
NS3/4A 2a	722F	ATCACGTACGCATGGCTCCCATCACTGCTTAT	BsiWI
	723R	TGTAGGATCCTAGCATTCCTCCATCTCATCA	BamHI
PTGR1	772F	ACTAGCGGCCGCCATGGTTCGTACTAAGACATG	NotI
	780R	ACTACGTACGTCATGCTTTCACTATTGTCTTC	BsiWI
PRPH	775R	ATGTGGATCCTCAGTAACTGTGGGCAGAAG	BamHI
	776F	ACTAGCGGCCGCCATGAGCCACCACCCGTC	NotI
sh785 (NS3)	785F	CCGGGTATGCAGCCCAAGGGTATAACTCGAGTTATACCCTTGGGCTGCATACTTTTTG	N/A
	786R	AATTCAAAAAGTATGCAGCCCAAGGGTATAACTCGAGTTATACCCTTGGGCTGCATAC	N/A
sh789 (NS3)	789F	CCGGTCTGCCATTCCAAGAAGAAATCTCGAGATTTCTTCTTGGAATGGCAGATTTTTG	N/A
	790R	AATTCAAAAATCTGCCATTCCAAGAAGAAATCTCGAGATTTCTTCTTGGAATGGCAGA	N/A
shGFP	801F	CCGGACAACAGCCACAACGTCTATACTCGAGTATAGACGTTGTGGCTGTTGTTTTTTG	N/A
	802R	AATTCAAAAAACAACAGCCACAACGTCTATACTCGAGTATAGACGTTGTGGCTGTTGT	N/A
pLKO	791F	TGGACTATCATATGCTTACCGTAAC	N/A
	792R	GTATGTCTGTTGCTATTATGTCTA	N/A

Table A2. Comprehensive list of antibodies used in this study. Listed are the antibody targets, animal sources, dilutions used, and catalogue numbers.

Target	Source	Dilution	Company, cat#
NS3	Mouse	1/1000	Millipore, MAB8691
MAVS (Cardif)	Rabbit	1/2000	Assay Designs, ALX-210-929-C100
PTGR1 (good)	Rabbit	1/1000	Abcam, ab107005
PTGR1	Rabbit	1/1000	Abcam, ab105530
PRPH	Rabbit	1/500	Abcam, ab4666
PSMD5	Rabbit	1/1000	Epitomics, 53163
GFP	Mouse	1/500	Santa Cruz, sc-9996
Actin	Rabbit	1/2000	Abcam, ab46805
Rabbit	Goat	1/10000	Epitomics, 3053-1
Mouse (LiCor)	Goat	1/2500	Mandel Scientific, 926-68020
Rabbit (LiCor)	goat	1/2500	Mandel Scientific, 926-32211

Table A3. Differentially regulated protein list. List of the 23 deregulated proteins taken from the statistical software Perseus, displaying log_2 ratios of proteins inverted to show NS3/4A/GFP ratios instead of "H"/"L" ratio for each replicate, gene name, and protein names.

GFP-H2	GFP-H4	NS3/4A-H1	NS3/4A-H3	Gene Name	Protein Names
-0.611	-0.624	-0.638	-0.514	GOLGA3	Golgi complex-associated protein of 170 kDa;Golgin subfamily A member 3;Golgin-160
-0.584		-0.606	-0.568	MID1	Midin;Midline 1 RING finger protein;Midline-1;Putative transcription factor XPRF;RING finger protein 59;Tripartite motif-containing protein 18;cDNA FLJ76288, highly similar to Homo sapiens midline 1 (Opitz/BBB syndrome) (MID1), transcript variant 1, mRNA;cDNA FLJ57031, highly similar to Midline-1 (EC 6.3.2.-);Putative uncharacterized protein MID1;cDNA FLJ58683, highly similar to Midline-1 (EC 6.3.2.-)
-0.473	-0.305	-0.394	-0.507	PSPH	L-3-phosphoserine phosphatase;O-phosphoserine phosphohydrolase;Phosphoserine phosphatase;Phosphoserine phosphatase variant;Putative uncharacterized protein PSPH
-0.514	-0.510	-0.310	-0.438	DNAJC3	DnaJ homolog subfamily C member 3;Interferon-induced, double-stranded RNA-activated protein kinase inhibitor;Protein kinase inhibitor of 58 kDa;cDNA FLJ77657, highly similar to Homo sapiens DnaJ (Hsp40) homolog, subfamily C, member 3 (DNAJC3), mRNA;cDNA, FLJ93304, Homo sapiens DnaJ (Hsp40) homolog, subfamily C, member 3 (DNAJC3),mRNA;DnaJ (Hsp40) homolog, subfamily C, member 3
-0.707		-0.537	-0.669	DHCR24	24-dehydrocholesterol reductase;3-beta-hydroxysterol delta-24-reductase;Diminuto/dwarf1 homolog;Seladin-1;cDNA FLJ53870, highly similar to 24-dehydrocholesterol reductase (EC1.3.1.-);cDNA, FLJ79318, highly similar to 24-dehydrocholesterol reductase (EC 1.3.1.-);cDNA FLJ55321, highly similar to 24-dehydrocholesterol reductase (EC 1.3.1.-);cDNA, FLJ79326, highly similar to 24-dehydrocholesterol reductase (EC 1.3.1.-);Putative uncharacterized protein Nbla03646;cDNA FLJ58891, highly similar to 24-dehydrocholesterol reductase (EC 1.3.1.-);cDNA FLJ52052, highly similar to 24-dehydrocholesterol

					reductase (EC 1.3.1.-)
-0.462	-0.416		-0.334	NEK1	Never in mitosis A-related kinase 1;Renal carcinoma antigen NY-REN-55;Serine/threonine-protein kinase Nek1;Putative uncharacterized protein DKFZp564L2416
-0.954	-0.901	-0.390	-0.962	BNIP1	BCL2/adenovirus E1B 19 kDa protein-interacting protein 1;Transformation-related gene 8 protein;Vesicle transport protein SEC20
-0.569	-0.285	-0.644	-0.527	HSPA2	Heat shock-related 70 kDa protein 2;cDNA FLJ40505 fis, clone TESTI2045562, highly similar to HEAT SHOCK-RELATED 70 kDa PROTEIN 2
-0.445	-0.241	-0.490	-0.578	CPVL	Carboxypeptidase, vitellogenic-like;Probable serine carboxypeptidase CPVL;Vitellogenic carboxypeptidase-like protein;cDNA FLJ42481 fis, clone BRACE2032090, highly similar to Probable serine carboxypeptidase CPVL (EC 3.4.16.-);Putative uncharacterized protein CPVL;Uncharacterized bone marrow protein BM031
-0.378	-0.647	-0.295	-0.288	EMD	Emerin;EMD protein;Emerin (Emery-Dreifuss muscular dystrophy), isoform CRA_a;Emerin (Emery-Dreifuss muscular dystrophy), isoform CRA_b
-1.255	-0.366	-0.974	-0.860	PRPH	Neurofilament 4;Peripherin;cDNA FLJ43599 fis, clone SMINT2017781, highly similar to PERIPHERIN
-0.610	-0.660	-0.553	-0.168	PFET1	BTB/POZ domain-containing protein KCTD12;Pfetin;Predomitly fetal expressed T1 domain;cDNA FLJ46506 fis, clone THYMU3030752, highly similar to BTB/POZ domain-containing protein KCTD12
-0.304	-0.511		-0.341	DER2	Degradation in endoplasmic reticulum protein 2;Der1-like protein 2;Derlin-2;F-LAN-1;F-LANa
0.453		0.448	0.454	DC12	UPF0361 protein C3orf37;cDNA FLJ57398
1.078	0.938	0.873	1.024	OXCT	3-oxoacid-CoA transferase 1;Somatic-type succinyl-CoA:3-oxoacid-CoA-transferase;Succinyl-CoA:3-ketoacid-coenzyme A transferase 1, mitochondrial;Succinyl-CoA:3-ketoacid CoA transferase;cDNA, FLJ92639, highly similar to Homo sapiens 3-oxoacid CoA transferase (OXCT), nuclear geneencoding mitochondrial protein, mRNA;cDNA FLJ51747, highly similar to Succinyl-CoA:3-ketoacid-coenzyme A transferase1, mitochondrial (EC 2.8.3.5);OXCT protein;cDNA FLJ51924, highly similar to Succinyl-CoA:3-

					ketoacid-coenzyme A transferase1, mitochondrial (EC 2.8.3.5);cDNA, FLJ78801, highly similar to Succinyl-CoA:3-ketoacid-coenzyme A transferase1, mitochondrial (EC 2.8.3.5)
	1.230	1.129	1.298	PSMD5	26S protease subunit S5 basic;26S proteasome non-ATPase regulatory subunit 5;26S proteasome subunit S5B;cDNA FLJ76282, highly similar to Homo sapiens proteasome (prosome, macropain) 26S subunit, non-ATPase, 5 (PSMD5), mRNA;cDNA FLJ52877, highly similar to 26S proteasome non-ATPase regulatory subunit 5
1.779	1.400	1.752	1.179	PTGR1	15-oxoprostaglandin 13-reductase;NADP-dependent leukotriene B4 12-hydroxydehydrogenase;Prostaglandin reductase 1;cDNA FLJ59730, highly similar to NADP-dependent leukotriene B412-hydroxydehydrogenase (EC 1.3.1.74);Leukotriene B4 12-hydroxydehydrogenase, isoform CRA_d
0.471	0.614	0.487	0.398	C8orf55	Mesenchymal stem cell protein DSCD75;UPF0670 protein C8orf55;cDNA FLJ54968
0.602	0.678	0.527	0.395	CRYZ	NADPH:quinone reductase;Quinone oxidoreductase;Zeta-crystallin;Putative uncharacterized protein CRYZ
0.393	0.205	0.502	0.491	FAIM	Fas apoptotic inhibitory molecule 1;Putative uncharacterized protein FAIM
0.687	0.487	0.301	0.559	H1F1	Histone H1.1
0.402	0.261	0.581	0.721	FLC3A	GABA(A) receptor-associated protein-like 2;Gamma-aminobutyric acid receptor-associated protein-like 2;Ganglioside expression factor 2;General protein transport factor p16;Golgi-associated ATPase enhancer of 16 kDa;MAP1 light chain 3-related protein;cDNA FLJ76520, highly similar to Homo sapiens GABA(A) receptor-associated protein-like 2 (GABARAPL2), mRNA;GABA(A) receptor-associated protein-like 2, isoform CRA_b;GABARAPL2 protein
0.585	0.501	0.192	0.433	CPSF7	Cleavage and polyadenylation specificity factor 59 kDa subunit;Cleavage and polyadenylation specificity factor subunit 7;Pre-mRNA cleavage factor Im 59 kDa subunit;cDNA FLJ57877, highly similar to Cleavage and polyadenylation specificity factor 7